[redacted]

Copy No.
RM No. L9C04

NACA RM No. L9C04

1104
~~Douglas~~
~~558-2~~

NACA

RESEARCH MEMORANDUM

HIGH-SPEED WIND-TUNNEL INVESTIGATION OF THE LONGITUDINAL STABILITY AND CONTROL CHARACTERISTICS OF A $\frac{1}{16}$-SCALE MODEL OF THE D-558-2 RESEARCH AIRPLANE AT HIGH SUBSONIC MACH NUMBERS AND AT A MACH NUMBER OF 1.2

By

Robert S. Osborne

Langley Aeronautical Laboratory
Langley Air Force Base, Va.

NATIONAL ADVISORY COMMITTEE
FOR AERONAUTICS
WASHINGTON
April 5, 1949

[redacted]

[redacted]

[redacted]

ERRATA NO. 1

NACA RM L9C04

HIGH-SPEED WIND-TUNNEL INVESTIGATION OF THE LONGITUDINAL STABILITY AND CONTROL CHARACTERISTICS OF A $\frac{1}{16}$-SCALE MODEL OF THE D-558-2 RESEARCH AIRPLANE AT HIGH SUBSONIC MACH NUMBERS AND AT A MACH NUMBER OF 1.2

By Robert S. Osborne

April 5, 1949

Page 4, paragraph 2: The fifth sentence should be changed to read as follows:

> The model differs from a true-scale model in that no inlet flow or jet was simulated, no pitot-head extension exists, the thickness of the wing-tip airfoil section is 10 percent instead of 12 percent and the aft end of the fuselage, or model base, is enlarged 0.31 inches in diameter (25 percent of original diameter) to provide clearance about the available sting support.

Page 16, second line of table I: Change "NACA 63_1-012" to "NACA 63_1-010."

[redacted]

NACA-Langley - 5-16-52 - 225

NATIONAL ADVISORY COMMITTEE FOR AERONAUTICS

RESEARCH MEMORANDUM

HIGH-SPEED WIND-TUNNEL INVESTIGATION OF THE LONGITUDINAL STABILITY AND CONTROL CHARACTERISTICS OF A $\frac{1}{16}$-SCALE MODEL OF THE D-558-2 RESEARCH AIRPLANE AT HIGH SUBSONIC MACH NUMBERS AND AT A MACH NUMBER OF 1.2

By Robert S. Osborne

SUMMARY

Presented in this report are the results of lift, drag, and pitching-moment measurements made on a $\frac{1}{16}$-scale model of the Douglas D-558-2 high-speed research airplane. The model was tested at various angles of attack through a subsonic Mach number range from 0.6 to 0.95 and at the supersonic Mach number of 1.2. The data have been corrected for the interference effect of the sting support on the model and, therefore, represent the model in the power-off condition.

A small lift force break occurs at a Mach number of approximately 0.9. The drag rise at an angle of attack of 0° occurs at a Mach number of approximately 0.86, with the drag coefficient at a Mach number of 1.2 being slightly higher than at 0.95.

The addition of chordwise fences to the upper wing surfaces has little effect on the force and moment characteristics of the model at the Mach numbers and angles of attack tested.

Static longitudinal stability is indicated for the model at all lift coefficients and Mach numbers tested. The rate of change of pitching-moment coefficient with lift coefficient at constant Mach number for the complete model is -0.2 at subcritical speeds, and between the Mach numbers of 0.85 and 0.95 the value increases in magnitude to -0.4. It is indicated that this is due to wing-fuselage characteristics and a decrease in the rate of change of effective downwash angle with lift coefficient. The degree of stability at a Mach number of 1.2 is approximately equal to that at a Mach number of 0.95.

Horizontal stabilizer and elevator effectiveness is satisfactory at all Mach numbers tested, although a rapid decrease evident in the Mach number range from 0.9 to 0.95 indicates that substantial losses in horizontal stabilizer effectiveness and serious losses or reversal of elevator effectiveness occur in the untested Mach number range between 0.95 and 1.2. With increasing speed, rapid changes in elevator setting required for trimmed level flight appear necessary in the Mach number range from 0.9 to 1.2, while variations in horizontal stabilizer setting required are small and gradual through the Mach number range tested.

INTRODUCTION

The D-558-2 is a research airplane designed to investigate aerodynamic phenomena at low supersonic Mach numbers. It has a sweptback wing located vertically in a midposition on the fuselage and a sweptback horizontal and vertical tail. It is powered by a turbojet engine and a rocket engine which produce approximately 7500 pounds of thrust.

A $\frac{1}{16}$-scale model of the D-558-2 was tested in the Langley 8-foot high-speed tunnel at high subsonic Mach numbers and at a Mach number of 1.2. Force and moment characteristics for several configurations at various angles of attack were measured by an internal strain-gage balance system. The results, corrected for the interference effect of the sting support on the model (representing the model in a power-off condition), are presented herein. The effects of two different sets of chordwise fences on the force and moment characteristics of the model at high speeds were also investigated.

SYMBOLS

V free-stream velocity, feet per second

ρ free-stream density, slugs per cubic foot

q dynamic pressure, pounds per square foot $\left(\frac{1}{2}\rho V^2\right)$

a velocity of sound, feet per second

M free-stream Mach number $\left(\frac{V}{a}\right)$

L lift, pounds

D drag, pounds

M pitching moment about center of gravity, inch-pounds (20.2 percent $\bar{c}$)

S_w wing area, square feet

$\bar{c}$ wing mean aerodynamic chord, inches

C_L lift coefficient $\left(\frac{L}{qS_w}\right)$

C_D drag coefficient $\left(\frac{D}{qS_w}\right)$

C_m pitching-moment coefficient $\left(\frac{M}{qS_w\bar{c}}\right)$

α angle of attack of fuselage center line, degrees

i_t angle of incidence of the horizontal stabilizer with respect to fuselage center line, degrees

δ_e elevator angle with respect to horizontal stabilizer chord line measured in plane perpendicular to hinge line, degrees

ϵ effective downwash angle, degrees

A_s area of sting support at model base, square inches

A_b area of model base, square inches

P_b static pressure at the model base, pounds per square foot

P_s free-stream static pressure, pounds per square foot

APPARATUS AND METHODS

Tunnel

The tests were conducted in the Langley 8-foot high-speed tunnel, which is of the closed-throat single-return type. A plaster liner was installed in the tunnel at the minimum section, extending upstream to form the subsonic test section and downstream to form the supersonic test section. The Mach number was uniform in the subsonic test section and varied only by a maximum of 0.02 from the design Mach number of 1.2 in the supersonic test section.

Model

The all-metal $\frac{1}{16}$-scale model of the D-558-2 was constructed by the NACA. It has a hollow fuselage to accommodate the internal strain-gage balance system. Figure 1 provides a general view of the model mounted in the supersonic test section. Figure 2 is a three-view drawing of the model, and table I lists its dimensions. The model differs from a true-scale model in that no inlet flow or jet was simulated, no pitot-head extension exists, and the aft end of the fuselage, or model base, is enlarged 0.31 inches in diameter (25 percent of original diameter) to provide clearance about the available sting support.

Two different sets of chordwise fences were tested. They are designated in this report by the ratio of their lengths to the length of the wing chord in the plane of the fences. The 0.68c fences were designed by the Douglas Aircraft Company as a component part of the complete airplane, although they have been treated as a separate configuration in these tests. The 0.95c fences were constructed from a design in reference 1. Both sets of fences were located in the spanwise positions specified for the 0.68c fences. The over-all dimensions and location of the fences on the wing are shown in figure 3, and table II lists the ordinates of the fences and the airfoil section in the plane of the fences.

Model Support System

The model was attached to a strain-gage balance which was enclosed within the hollow fuselage. The downstream end of the balance formed a tapered sting that was attached to a telescoping support tube through couplings used to vary the angle of attack. The support tube was fixed axially in the center of the tunnel by two sets of support struts projecting from the tunnel walls.

The model was located in either the subsonic or supersonic test sections by extending or retracting the sliding portion of the telescoping support tube. Guy wires located 21 inches downstream of the model base and swept back to the tunnel walls were used to steady the support system in the subsonic test section. Figure 4 shows the model support system and model locations in the subsonic and supersonic test sections.

Test Conditions

The tests were run at angles of attack of -2°, 0°, 2°, and 4° through a Mach number range from 0.6 to 0.95 with the model in the subsonic test section, and at a Mach number of 1.2 in the supersonic test section. The Reynolds number based on a model mean aerodynamic chord of 5.46 inches ranged from 1.55×10^{6} at a Mach number of 0.6 to 1.80×10^{6} at a Mach number of 0.95. The Reynolds number was 1.73×10^{6} at a Mach number of 1.2.

During the subsonic runs tunnel-wall pressures were observed to insure that data were not obtained with the tunnel choked. Observations of static pressures along the upper and lower surfaces of the sting support, tunnel-wall pressures, and shadowgraph images showed that in all supersonic runs the normal shock was at least 6 inches downstream of the trailing edges of the horizontal tail. The local Mach numbers along the upper and lower surfaces of the sting support at various distances downstream of the model base are presented for representative configurations in figures 5 and 6. Tunnel-wall pressures indicated that in the supersonic runs the shock disturbance from the nose of the model was transmitted to the wall at a distance of approximately 26 inches downstream of the nose. This precluded the possibility of the reflected disturbance acting on the model.

Measurements

Lift, drag, and pitching-moment measurements were made by means of an internal strain-gage balance system. The pitching moment was measured about the center of gravity of the airplane with wheels retracted (20.2 percent of the wing mean aerodynamic chord). The following configurations were tested:

(a) Fuselage and fin

(b) Fuselage, fin, and wing

(c) Complete model with:

$$i_t = 4^\circ,\ \delta_e = 0^\circ$$

$$i_t = 1.9^\circ,\ \delta_e = 0^\circ$$

$$i_t = 0^\circ,\ \delta_e = 0^\circ$$

$$i_t = 1.9^\circ,\ \delta_e = 6^\circ$$

$$i_t = 1.9^\circ,\ \delta_e = 4^\circ$$

$$i_t = 1.9^\circ,\ \delta_e = 2^\circ$$

$$i_t = 1.9^\circ,\ \delta_e = -2^\circ$$

$$i_t = 1.9^\circ,\ \delta_e = -4^\circ$$

$$i_t = 1.9^\circ,\ \delta_e = -6^\circ$$

(d) Complete model, $i_t = 1.9^\circ$, $\delta_e = 0^\circ$ with:

0.68c fences

0.95c fences

Corrections

Due to the flexibility of the sting support system and the large aerodynamic loads on the model, the angle of attack varied with Mach number during a run. The change in angle at each test point was calculated from the movement on a ground glass of the reflection of a fixed point source of light from a small mirror attached to the fuselage of the model. With these data the results presented herein have been corrected to constant angles of attack.

No accurate expressions are available for evaluating the effects of model and wake constriction on Mach number and dynamic pressure for sweptback wings at high subsonic Mach numbers, and therefore no such corrections have been applied to these data. However, the use of expressions available for straight-wing configurations indicates that the corrections are only between 1 and 2 percent at a Mach number of 0.95 and are much less than 1 percent at a Mach number of 0.9. The corrections should be less for the sweptback configuration. The correction to angle of attack due to boundary-induced upwash was found from reference 2 to be negligible and, therefore, has not been applied to these data.

Because the balance system was an internal one, no forces on the sting support were measured, and the only tare was the interference effect of the sting support on the model. This tare was evaluated by testing the same configuration on each of four sting supports, each with a successively smaller diameter at the model base, and extrapolating the data to a sting-support diameter of zero, which is assumed to represent the model without sting-support interference. The sting supports are shown in figure 7. The diameters of the four sting supports at the model-base location were 1.44, 1.16, 0.84, and 0.67 inches. The 1.44-inch sting support was used for testing all the configurations through the Mach number and angle-of-attack ranges in order to obtain the uncorrected data. The fuselage and fin, the fuselage, fin, and wing, and the complete model with two horizontal stabilizer and two elevator settings were tested through the Mach number range on the smaller supports. Because of strength limitations, the latter tests, with the exception of the fuselage and fin configuration, were made at an angle of attack of -2° only and because of dangerous oscillatory tendencies, tests using the 0.67-inch sting support could not be continued above a Mach number of 0.8. However, sufficient data were obtained to result in good approximations of the tare values. The force and moment coefficients obtained with the various sized sting supports were plotted against the ratio of the sting-support area at the model base to the area of the model base. Curves faired through the data points were extrapolated to the ratio representing a sting-support diameter of zero. An example of this procedure for one configuration at several representative Mach numbers is presented in figure 8(a). The difference between the value of the coefficient for the 1.44-inch sting support and a sting-support diameter of zero is the tare. Tare values for the different tail settings tested were interpolated and extrapolated to obtain values for all tail settings. The tares were assumed to be constant through the small angle-of-attack range of these tests. All configurations had drag tares, while only those with the horizontal tail had pitching-moment tares. None of the configurations had lift tares. All data used for analysis in this paper have been corrected for tares and, therefore, represent the model in a power-off condition with no jet or sting support present.

Model base pressures were obtained for all configurations by means of a static-pressure orifice in the lower surface of the 1.44-inch sting support located 3/4 inch upstream of the model base inside the fuselage. Base pressures were obtained for the configurations tested on the smaller sting supports in a similar manner. With the smaller sting supports, the base pressures have been corrected for the interference effect of the sting support in the manner previously described for the force and moment data. An example for one configuration at several representative Mach numbers is shown in figure 8(b). The variations of the ratio of model base pressure to free-stream static pressure with Mach number are presented in figure 9. These values represent the model with power off and no sting support present and may be used to reduce the corrected drag data of figure 10 to free-stream static-pressure conditions at the model base. This correction has not been applied in this paper.

RESULTS AND DISCUSSION

An index of the figures presenting the results is given as follows:

Because of the lack of sufficient data no attempt is made in this report to interpolate data between the Mach numbers of 0.95 and 1.2 although trends may be indicated.

Force and Moment Characteristics

Force and moment data corrected and uncorrected for tares are presented in figure 10. Uncorrected values are included to indicate the magnitude of the tares for the various configurations and tail settings. The wing-alone data are the difference between fuselage, fin, and wing, and fuselage and fin corrected data, and, therefore, include wing-fuselage interference.

At an angle of attack of 0°, a small lift force break occurs for all complete model configurations at a Mach number of approximately 0.9. The angle of attack for zero lift is essentially constant through the subsonic Mach number range but increases slightly at a Mach number of 1.2. The variation of pitching-moment coefficient with Mach number is small up to a Mach number of 0.85, after which large changes occur with small increases in Mach number up to a Mach number of 1.2.

A drag force break occurs for the fuselage and fin configuration between the Mach numbers of 0.925 and 0.95. For the complete-model configurations at an angle of attack of 0° a drag force break is indicated at a Mach number of approximately 0.86, with the drag coefficient at a Mach number of 1.2 being slightly larger than at 0.95.

In figure 11 is presented the variation of lift coefficient required for level flight with Mach number for sea-level and 35,000-foot altitudes for the D-558-2 airplane with a wing loading of 65 pounds per square foot. This loading represents the airplane with approximately 60 percent of its fuel expended. Based on a drag coefficient of 0.08, the total drag of the airplane in level flight at 35,000 feet and at a Mach number of 1.2 would be approximately 7000 pounds. The thrust available is 7500 pounds, which indicates that flight at a Mach number of 1.2 at high altitudes is possible. However, it may be that the drag coefficient between the Mach numbers of 0.95 and 1.2 is higher than the value at 1.2 and that the critical condition is in this region.

The slope of the lift curve at a given Mach number was essentially constant through the small angle-of-attack range of these tests. For the complete model (fig. 12(a)) the value of $\frac{\partial C_L}{\partial \alpha}$ increases from 0.07 at a Mach number of 0.6 to its maximum value of 0.09 at a Mach number of 0.9. At a Mach number of 0.95 it has decreased slightly to 0.085 with a further small reduction to 0.075 being indicated at a Mach number of 1.2. The wing-alone configuration (fig. 12(b)) shows a similar small variation of slope of the lift curve with Mach number. From the variations of lift coefficient with drag coefficient for the complete model and wing-alone configurations (figs. 13 and 14), the variations of lift-drag ratio with lift coefficient were obtained (figs. 15 and 16). The maximum complete model lift-drag ratio occurs at a lift coefficient of 0.35, at a Mach number of 0.85, and is approximately 12. At the lift coefficient required for level flight at 35,000 feet at a Mach number of 1.2, the complete model lift-drag ratio is 1.6. The values of the lift-drag ratio for the wing-alone configuration are higher due to the exclusion of the drag of the fuselage and fin.

The effects of adding the 0.68c and 0.95c fences to the complete model are shown in figures 17 and 18. The incremental lift and drag coefficients are negligible throughout the Mach number and angle-of-attack ranges tested. The incremental pitching-moment coefficients are also negligible except at angles of attack of 0° and -2° at high subsonic Mach numbers, where increments approach a value of 0.01. This value is small, and it is, therefore, concluded that the addition of the fences has little effect on the force and moment characteristics of the model at the Mach numbers and angles of attack tested.

Comparison of the results of these tests at a Mach number of 0.6 has been made with the results of tests on a $\frac{1}{4}$-scale model of the D-558-2 at a Mach number of approximately 0.2 with a Reynolds number of approximately 2×10^6 (reference 3). Lift-curve slope agreement is excellent, while variations of lift coefficient with drag coefficient indicate that values of the drag coefficient for the $\frac{1}{4}$-scale model are approximately 0.008 higher at lift coefficients below 0.4.

Longitudinal Stability

The variations of pitching-moment coefficient with lift coefficient for various horizontal stabilizer settings (fig. 19) indicate that the complete-model configuration is longitudinally stable at all lift coefficients and Mach numbers for all horizontal stabilizer angles tested. The fuselage, fin, and wing configuration shows a stabilizing tendency at all lift coefficients at Mach numbers of 0.85 and above. The complete model with various elevator angles (fig. 20) is also longitudinally stable at all lift coefficients and Mach numbers tested. The variation of the static-longitudinal-stability parameter $\frac{\partial C_m}{\partial C_L}$ with Mach number for level-flight trim conditions at two altitudes for the complete-model configuration is presented in figure 21(a). The value of $\frac{\partial C_m}{\partial C_L}$ is approximately −0.2 at low Mach numbers and, above a Mach number of 0.85, increases in magnitude until it reaches a value of approximately −0.4 at a Mach number of 0.95. The value is approximately −0.42 at a Mach number of 1.2. In figure 21(b) is presented the variation of the static-longitudinal-stability parameter $\frac{\partial C_m}{\partial C_L}$ with Mach number for level flight at two altitudes for the fuselage, fin, and wing configuration. It is evident that the aerodynamic center of the tailless configuration moves rearward of the center-of-gravity position at a Mach number of approximately 0.85, with the rearward movement continuing up to a Mach number of 0.95. This indicates that the increase in stability above a Mach number of 0.85 evident with the complete-model configuration is due in part to wing fuselage characteristics which in turn are due to a rearward center-of-pressure movement on the sweptback wing. The degree of stability at a Mach number of 0.6 agrees closely with the values obtained from low-speed tests of a $\frac{1}{4}$-scale model. (See reference 3.)

Control

Horizontal-stabilizer effectiveness (fig. 22(a)) increases steadily up to a Mach number of 0.9, after which there is an abrupt 25-percent decrease up to a Mach number of 0.95. The effectiveness at a Mach number of 1.2 is equal to that at 0.95. It is indicated that a substantial loss of effectiveness occurs between these Mach numbers. Elevator effectiveness (fig. 22(b)), especially for the sea-level condition, also decreases rapidly between the Mach numbers of 0.9 and 0.95, with a further decrease being indicated at a Mach number of 1.2. It is indicated that serious loss or reversal of effectiveness may occur between the Mach numbers of 0.95 and 1.2.

In figures 23(a) and 23(b) are presented the variations of horizontal stabilizer and elevator angles required with Mach number for level-flight trim conditions at two altitudes for the complete model. The variation in horizontal stabilizer angle required is only 2° through the Mach number range tested, and no rapid changes with Mach number are indicated. A change in elevator angle of approximately 8° is required. For the sea-level case, rapid changes with Mach number occur after a Mach number of 0.9 is reached; whereas, at 35,000 feet, it is evident that rapid changes with Mach number must occur between the Mach numbers of 0.95 and 1.2. The variations of horizontal stabilizer and elevator angle required with Mach number for trimmed level flight at sea level are stable, whereas those at 35,000 feet are both stable and unstable, depending on the Mach number range considered. The preceding data indicate that the critical Mach number range with regard to control is between the Mach numbers of 0.9 and 1.2, the greater part of which is not covered by this investigation.

Very good agreement is indicated between the values of horizontal-stabilizer effectiveness for these tests at a Mach number of 0.6 and the values from the low-speed tests of the $\frac{1}{4}$-scale model (reference 3).

Downwash

The horizontal-tail airfoil section being symmetrical, the effective downwash angles may be found where the pitching-moment increment due to the tail ΔC_m is zero. Under these conditions it is assumed that the flow is lined up with the chord line of the tail and it becomes necessary only to find the angle between free-stream direction and the chord line of the tail. The drag of the tail is neglected. The effective downwash angle was determined by adding the angle of attack where $\Delta C_m = 0$ to the horizontal tail angle. Additional values of effective downwash angles were found by using data where ΔC_m did not equal zero. In these cases the values of additional horizontal stabilizer angle needed to bring ΔC_m to zero were calculated using the applicable values of $\frac{\partial C_m}{\partial i_t}$. The results of these calculations are presented in figure 24 as the variation of effective downwash angle with lift coefficient.

The variation of effective downwash angle with Mach number for level flight at two altitudes is presented in figure 25. The values decrease with increase in Mach number up to a Mach number of 0.9, after which they increase rapidly up to a Mach number of 0.95. At a Mach number of 1.2 the values are slightly higher than at 0.95. In figure 26 are presented the variations with Mach number of the rate of change of effective downwash angle with lift coefficient for level flight at two altitudes. The abrupt decrease in $\frac{\partial \epsilon}{\partial C_L}$ at a Mach number of 0.85 is an additional contributing factor to the increase in static longitudinal stability of the model at that Mach number. The value of $\frac{\partial \epsilon}{\partial C_L}$ increases between the Mach numbers of 0.95 and 1.2, with the occurrence of rapid changes with increasing Mach number being indicated. Although this is a destabilizing effect, there is no indication that it has reduced the stability of the model between these Mach numbers. Other effects apparently counteract the effect of the increase in $\frac{\partial \epsilon}{\partial C_L}$. The tail has greater sweepback than the wing and, therefore, would be expected to have suffered a smaller loss in value of the lift-curve slope at Mach numbers above 0.95. This effect is stabilizing and may be the reason that the high degree of stability is maintained at a Mach number of 1.2, although the value of $\frac{\partial \epsilon}{\partial C_L}$ has increased.

Comparison at a Mach number of 0.6 with the low-speed data from the $\frac{1}{4}$-scale model tests (reference 3) indicates excellent agreement between the respective values of $\frac{\partial \epsilon}{\partial C_L}$.

CONCLUSIONS

The following conclusions may be drawn from tests of a $\frac{1}{16}$-scale model of the D-558-2 in a simulated power-off condition at Mach numbers from 0.6 to 0.95 and at a Mach number of 1.2:

1. A small lift force break occurs at a Mach number of approximately 0.9. At an angle of attack of 0° the drag rise occurs at a Mach number of approximately 0.86. The airplane appears to have enough thrust available to fly at a Mach number of 1.2, at an altitude of 35,000 feet although the range between the Mach numbers of 0.95 and 1.2 may be the critical one in this respect.

2. It is indicated that the model is longitudinally stable at all lift coefficients and Mach numbers tested. The rate of change of pitching-moment coefficient with lift coefficient at constant Mach number for the complete model is −0.2 at subcritical Mach numbers, and between the Mach number of 0.85 and 0.95, the value increases in magnitude to −0.4 because of wing-fuselage characteristics and a decrease in the rate of change of effective downwash angle with lift coefficient. The degree of stability at a Mach number of 1.2 is approximately equal to that of 0.95.

3. Control effectiveness is satisfactory at the Mach numbers tested, although a rapid decrease is evident in the Mach number range from 0.9 to 0.95. This indicates the possibility of substantial losses of horizontal-stabilizer effectiveness and serious losses or reversal of elevator effectiveness occurring in the untested Mach number range between 0.95 and 1.2.

4. Changes in horizontal stabilizer setting required for trimmed level flight through the Mach number range are small and occur gradually. Changes in elevator deflection required are small and gradual up to a Mach number of approximately 0.9, after which it is indicated that rapid increases are necessary up to a Mach number of 1.2.

5. The addition of chordwise fences to the upper wing surfaces has little effect on the force and moment characteristics of the model.

Langley Aeronautical Laboratory
National Advisory Committee for Aeronautics
Langley Air Force Base, Va.

REFERENCES

1. Graham, Robert R., and Conner, D. William: Investigation of High-Lift and Stall-Control Devices on an NACA 64-Series 42° Sweptback Wing with and without Fuselage. NACA RM No. L7G09, 1947.

2. Eisenstadt, Bertram J.: Boundary-Induced Upwash for Yawed and Swept-Back Wings in Closed Circular Wind Tunnels. NACA TN No. 1265, 1947.

3. Kerker, R., and Miller, C. E.: Summary Report of Model D-558-2 Tests at Cooperative Wind Tunnel. Rep. No. ES-20648, Douglas Aircraft Co., Inc., Oct. 1, 1946.

TABLE I

DIMENSIONS OF THE $\frac{1}{16}$-SCALE MODEL OF THE D-558-2

010

Wing root section (normal to 30-percent normal chord line)	NACA 63_1-010
Wing tip section (normal to 30-percent normal chord line)	NACA 63_1-~~0~~
Wing area, sq ft	0.684
Wing span, in.	18.72
Wing mean aerodynamic chord, in.	5.46
Location of center of gravity, percent of M.A.C.	20.2
Wing root chord, in. (parallel to plane of symmetry)	6.78
Wing tip chord, in. (parallel to plane of symmetry)	3.83
Wing taper ratio	0.565
Wing aspect ratio	3.57
Wing sweep angle, deg (30-percent normal chord line)	35
Wing incidence, deg	3
Wing dihedral, deg	-3
Wing geometric twist, deg	0
Tail root section (normal to 30-percent normal chord line)	NACA 63_1-010
Tail tip section (normal to 30-percent normal chord line)	NACA 63_1-010
Tail area, sq ft	0.156
Tail span, in.	8.98
Tail mean aerodynamic chord, in.	2.61
Tail root chord, in. (parallel to plane of symmetry)	3.35
Tail tip chord, in. (parallel to plane of symmetry)	1.68
Tail taper ratio	0.5
Tail aspect ratio	3.59
Tail sweep angle, deg (30-percent normal chord line)	40
Tail dihedral, deg	0
Elevator area, percent of tail area	25
Fuselage length, in.	31.5
Fuselage maximum diameter, in.	3.75
Fuselage fineness ratio	8.40
Fuselage base diameter of model used in Langley 8-foot high-speed tunnel, in.	1.56
Tail height, wing root chords above the root chord extended, measured at the elevator hinge line	0.54
Tail length, in., measured between the 1/4 M.A.C. locations on the wing and tail in horizontal and vertical planes parallel to the fuselage center line	14.62

NACA

TABLE II

ORDINATES MEASURED FROM THE LEADING EDGE OF THE AIRFOIL SECTION IN THE PLANE OF THE FENCES, OF THE AIRFOIL SECTION, 0.68c FENCE, AND 0.95c FENCE FOR THE $\frac{1}{16}$-SCALE MODEL OF THE D-558-2

[All dimensions are in inches]

Airfoil section		0.68c fence		0.95c fence	
x	y	x	y	x	y
0	0	0.334	0.128	0.310	0.120
.334	.128	.955	.585	.480	.450
.955	.207	1.672	.746	.955	.518
1.672	.249	2.259	.766	1.672	.560
2.259	.259	3.073	.687	2.259	.570
3.073	.219	4.155	.125	3.073	.530
4.155	.125			4.155	.436
5.590	0			5.410	.320
				5.590	0

NACA

[redacted]

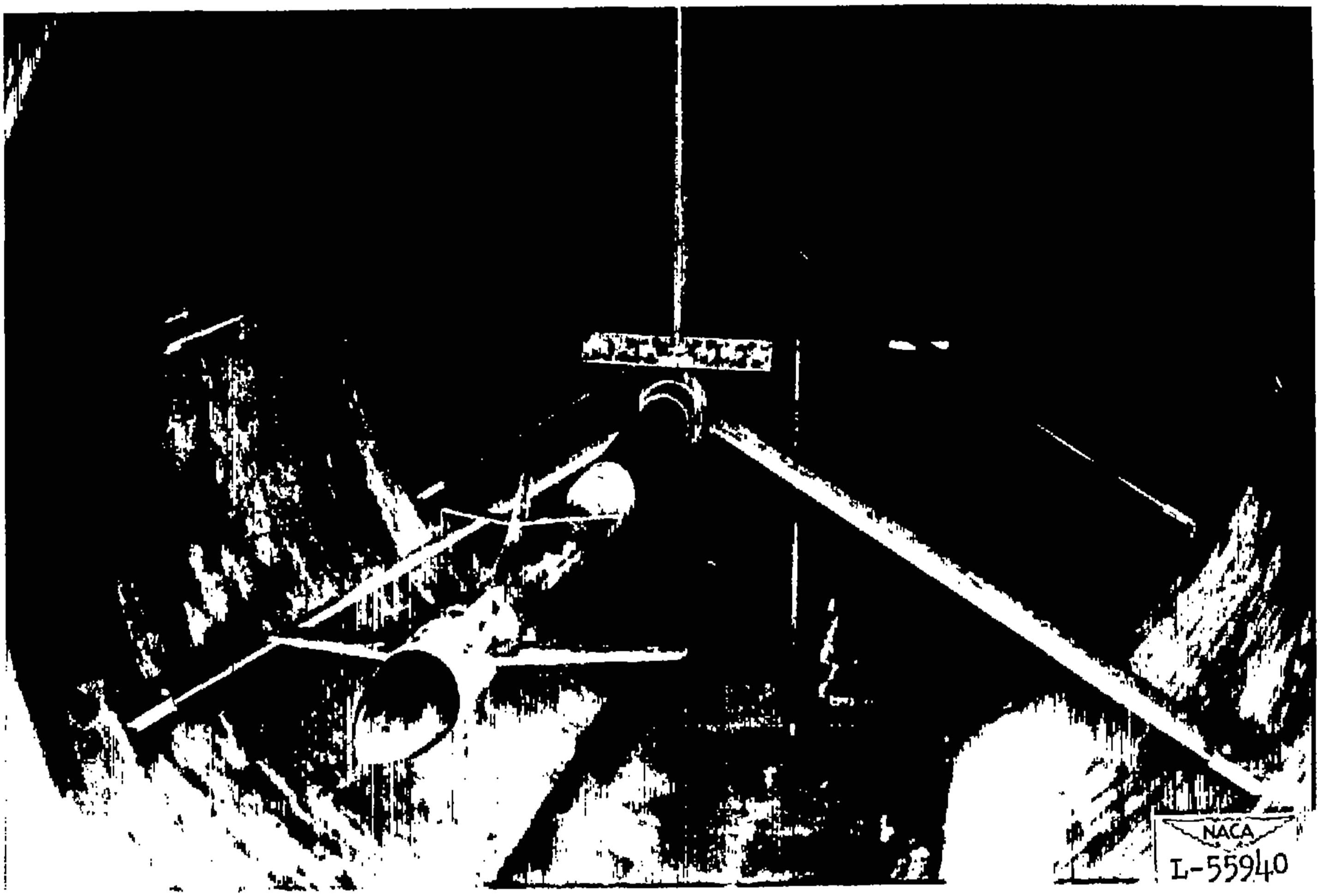

Figure 1.– The $\frac{1}{16}$–scale model of the D-558-2 mounted in the supersonic test section of the Langley 8-foot high-speed tunnel.

[redacted]

[redacted]

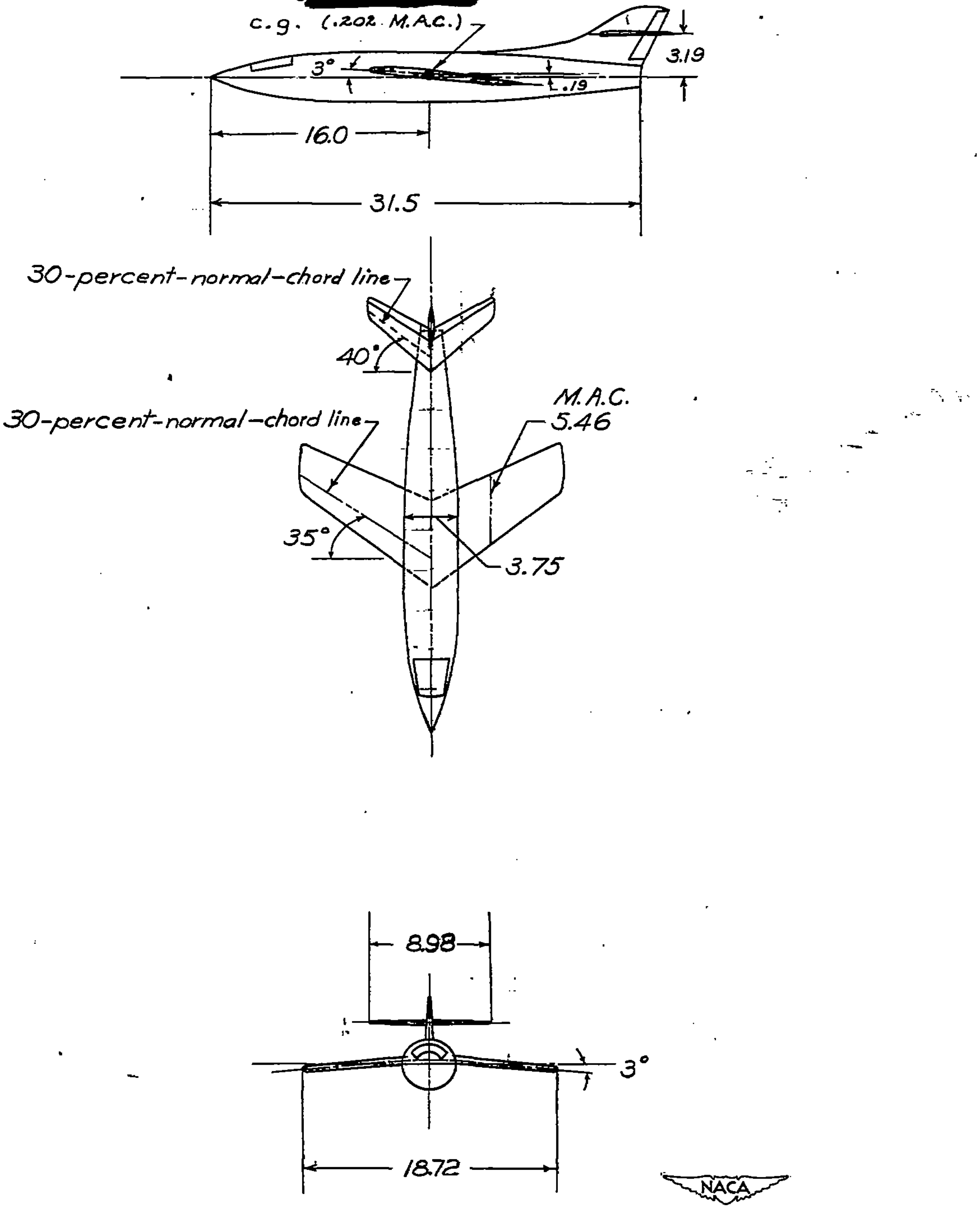

Figure 2.– Drawing of the $\frac{1}{16}$-scale model of the D-558-2 as tested in the Langley 8-foot high-speed tunnel. (All dimensions are in inches.)

[redacted]

[redacted]

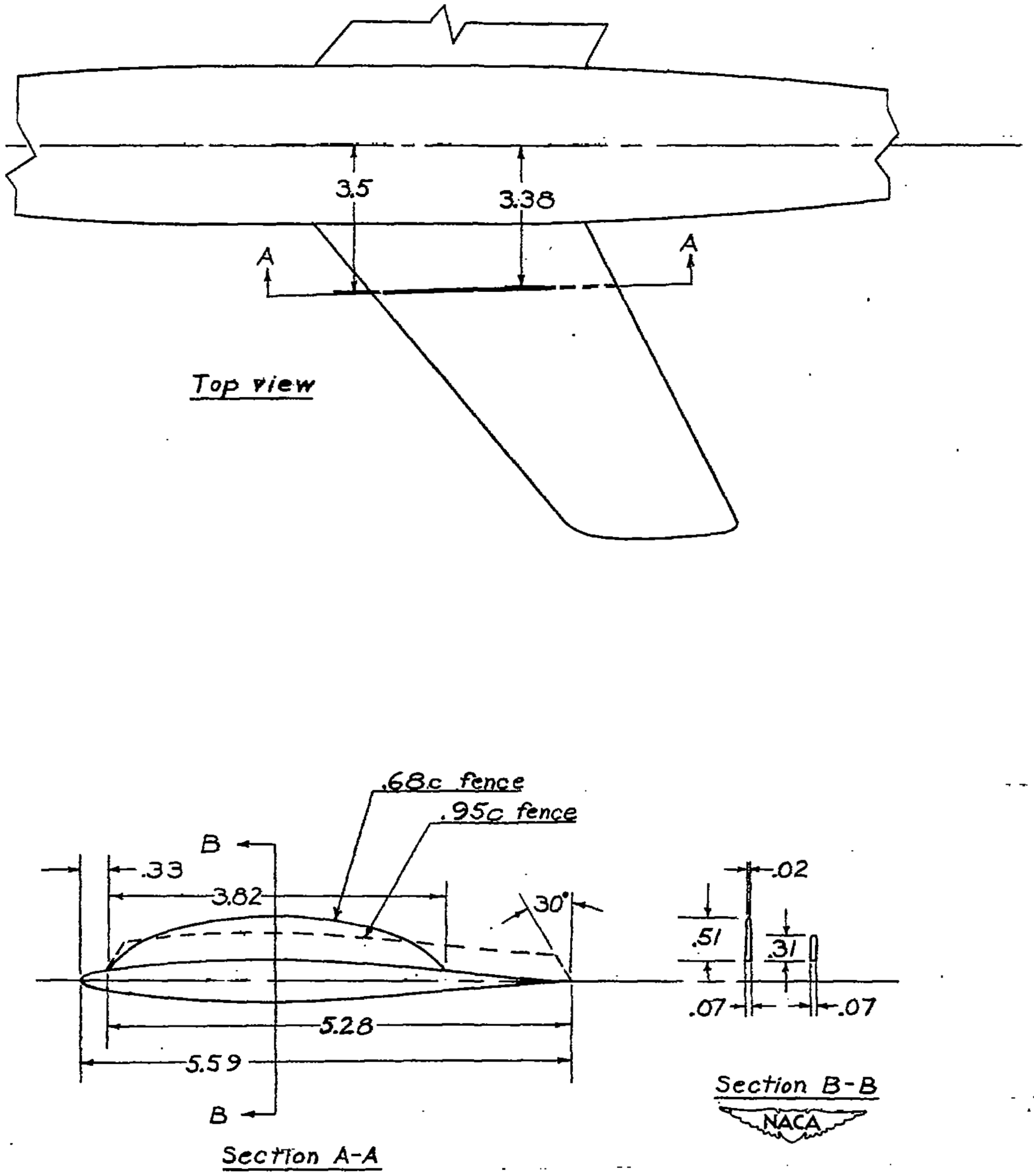

Figure 3.— Location and dimensions in inches of fences tested on the $\frac{1}{16}$-scale model of the D-558-2 in the Langley 8-foot high-speed tunnel.

[redacted]

[redacted]

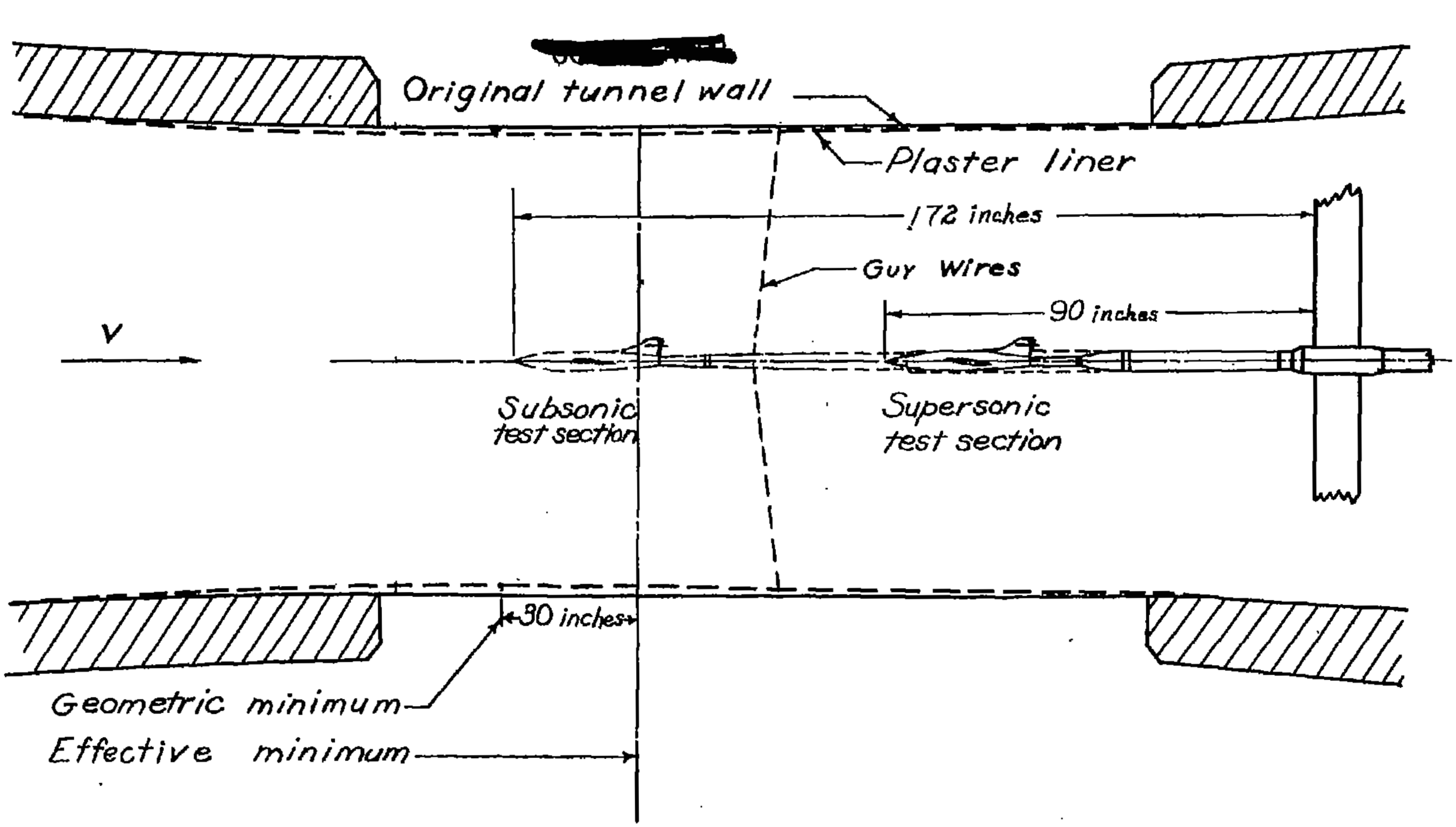

Figure 4.– Location of the $\frac{1}{16}$–scale model of the D-558-2 in the Langley 8-foot high-speed tunnel.

[redacted]

[redacted]

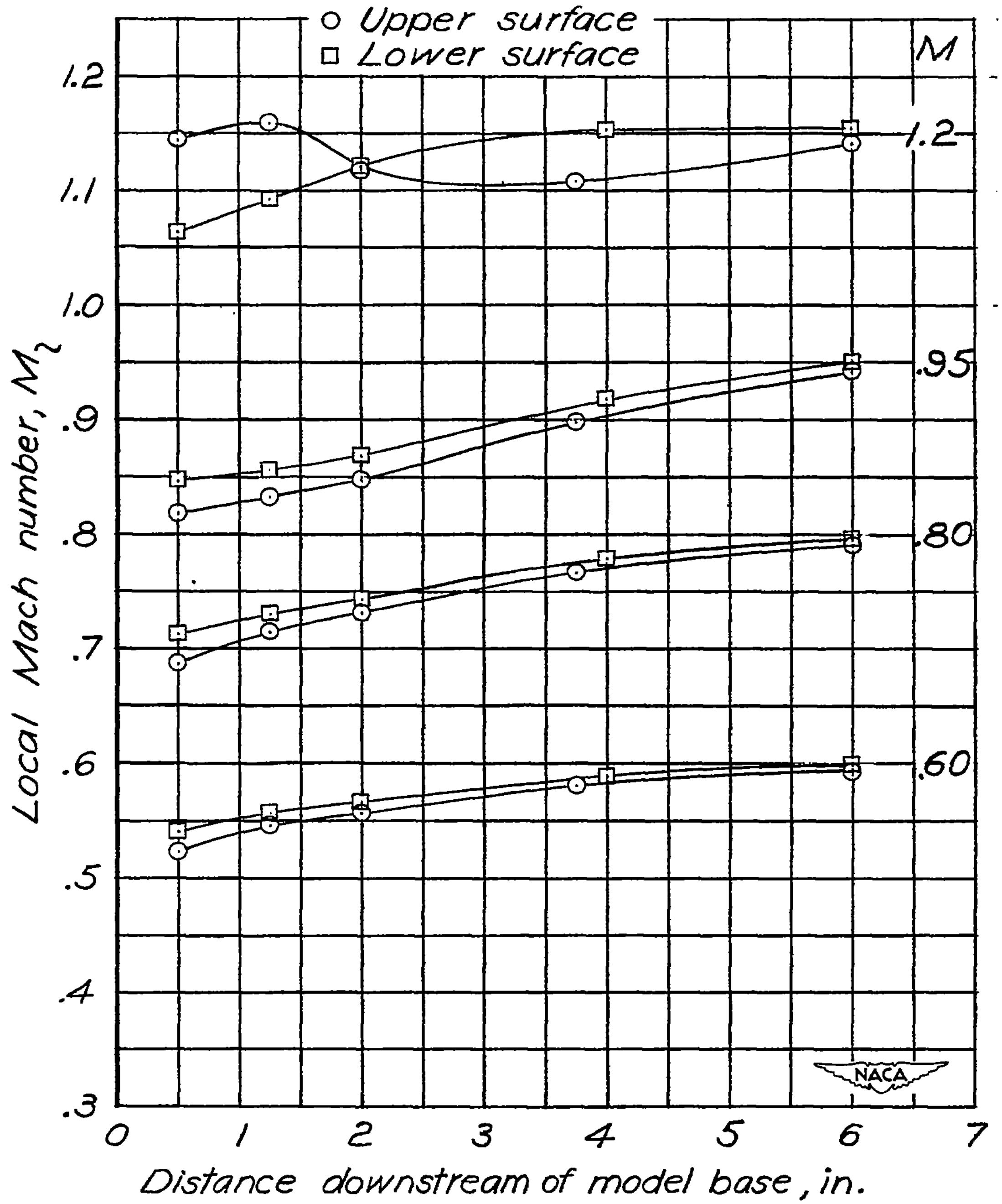

Figure 5.- Mach number distribution along upper and lower surfaces of 1.44-inch sting support at various stream Mach numbers. Complete model with 0.68c fences; $i_t = 1.9^\circ$; $\delta_e = 0^\circ$; $\alpha = -2^\circ$.

[redacted]

~~CONFIDENTIAL~~

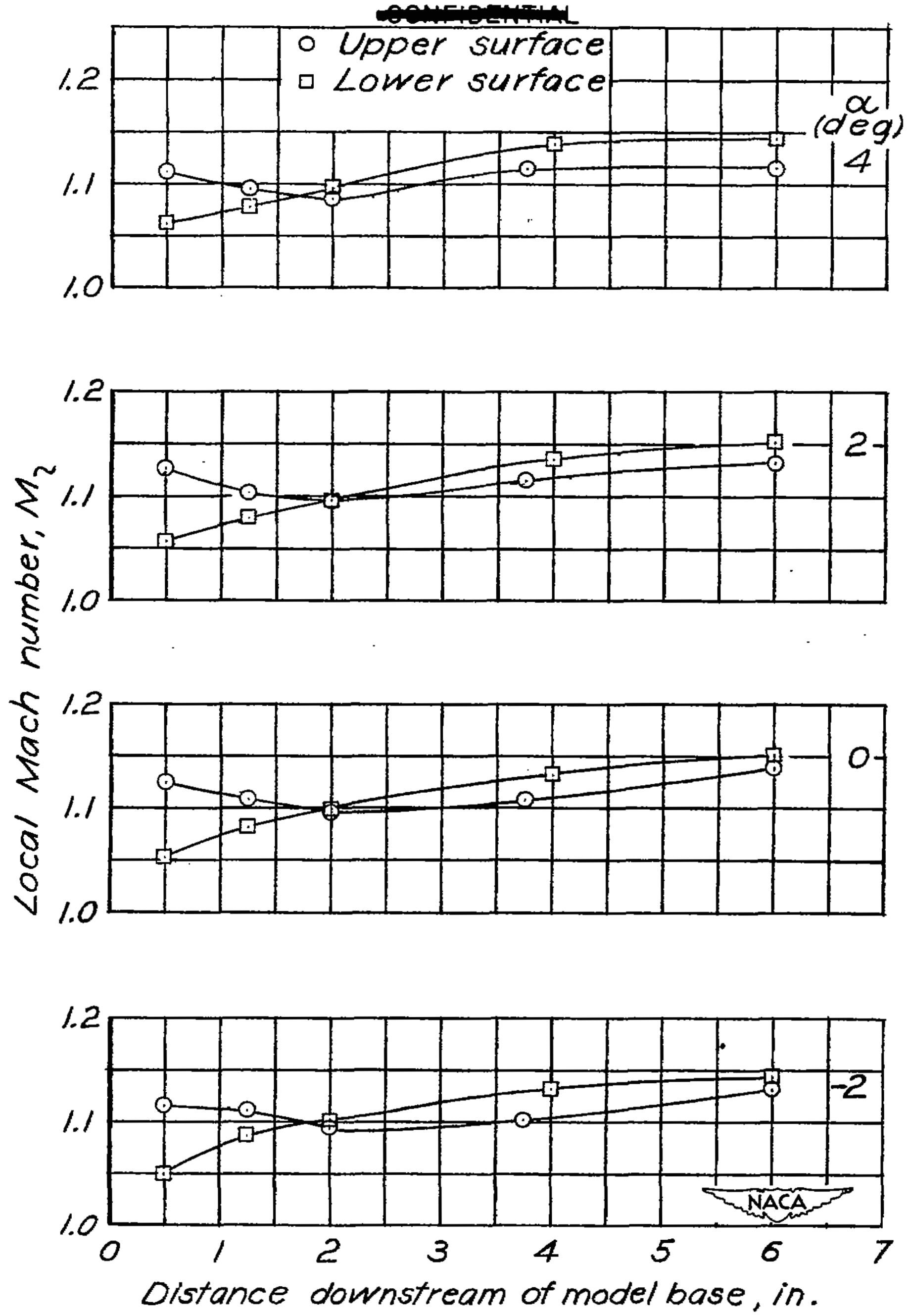

(a) Complete model; $i_t = 4^\circ$; $\delta_e = 0^\circ$.

Figure 6.– Mach number distribution along upper and lower surfaces of 1.44–inch sting support for various angles of attack at a stream Mach number of 1.2.

[redacted]

[redacted]

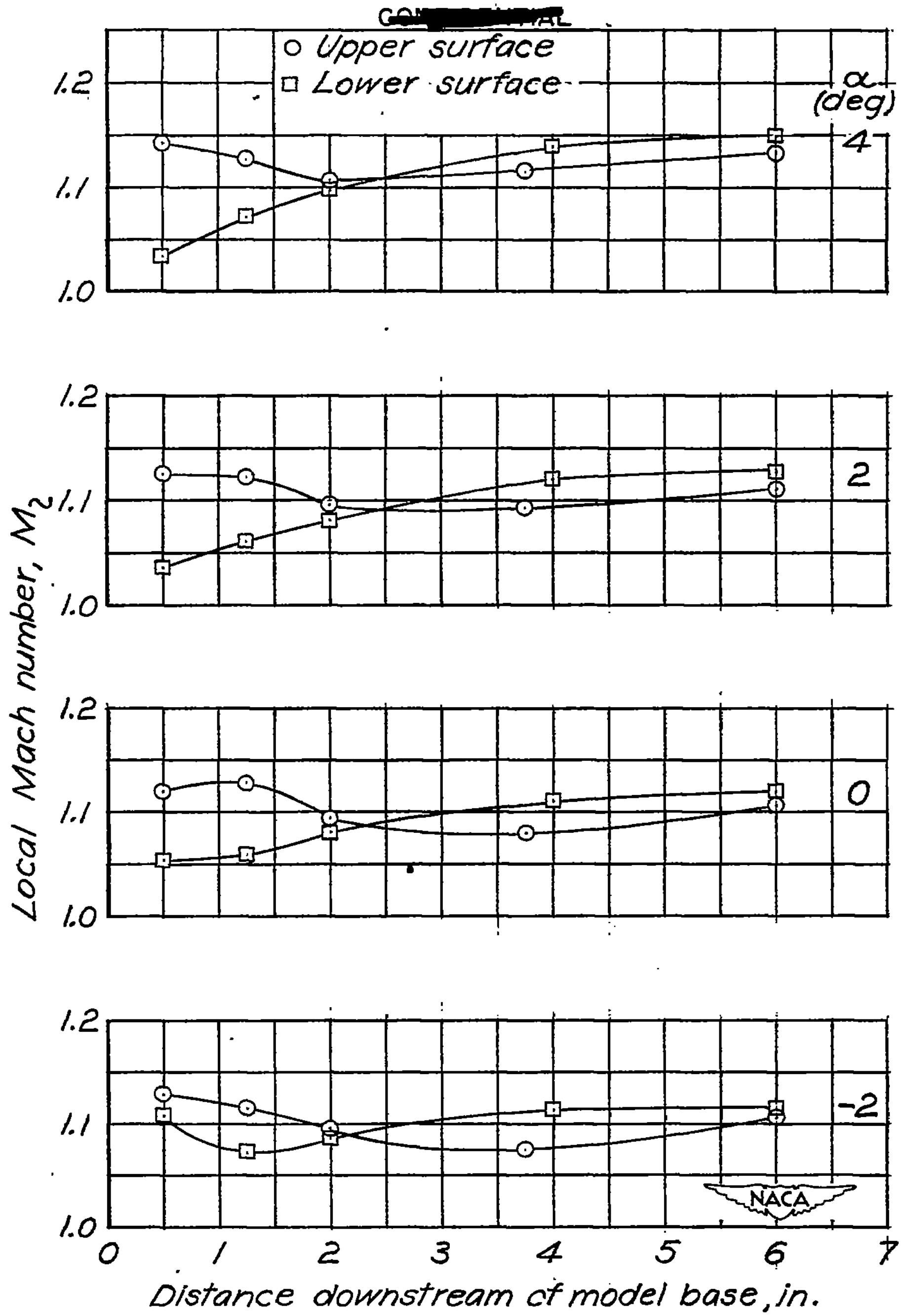

(b) Complete model; $i_t = 0^{\circ}$; $\delta_e = 0^{\circ}$.

Figure 6.– Concluded.

[redacted]

~~CONFIDENTIAL~~

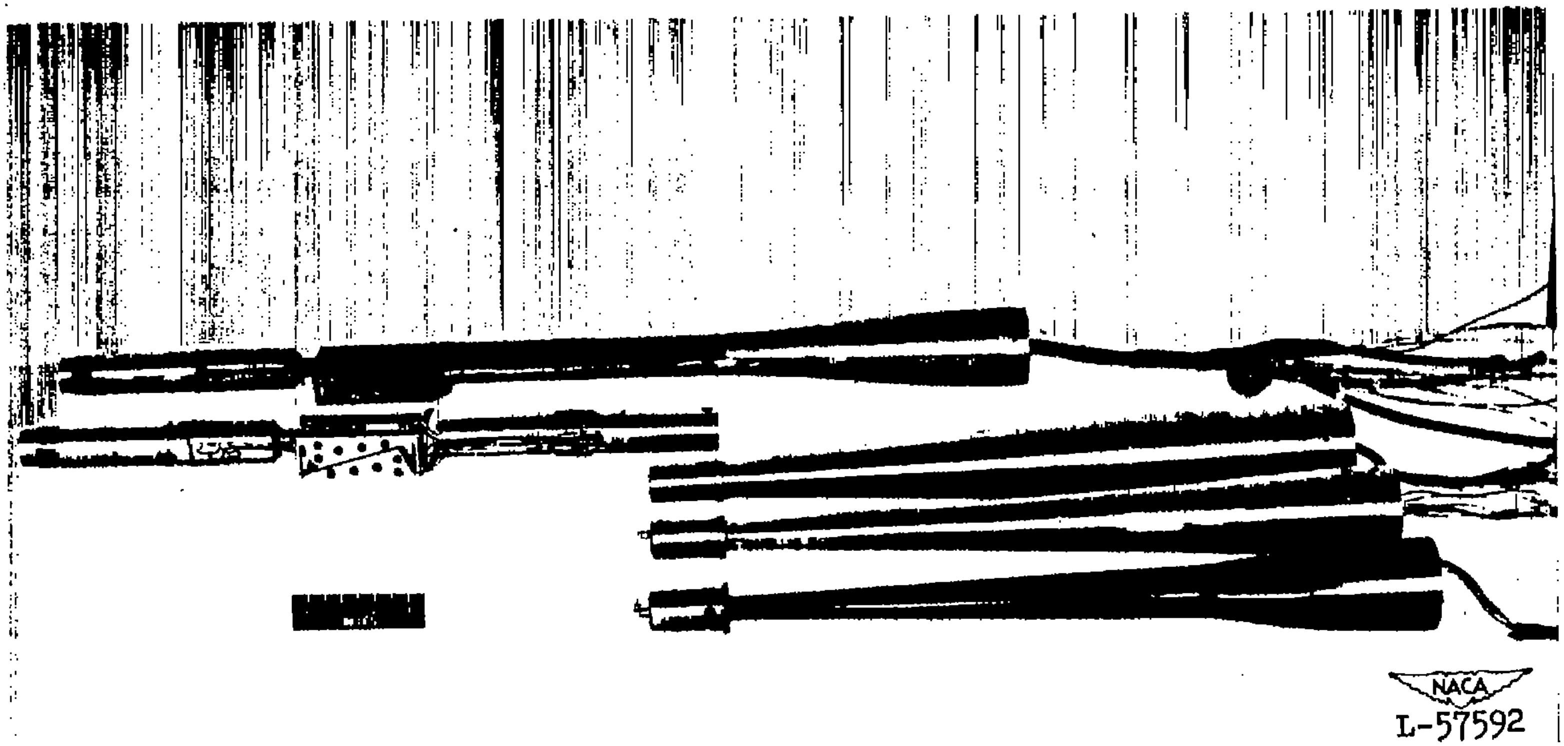

Figure 7.- Strain-gage balances and sting supports used in testing the D-558-2 model in the Langley 8-foot high-speed tunnel.

~~CONFIDENTIAL~~

[redacted]

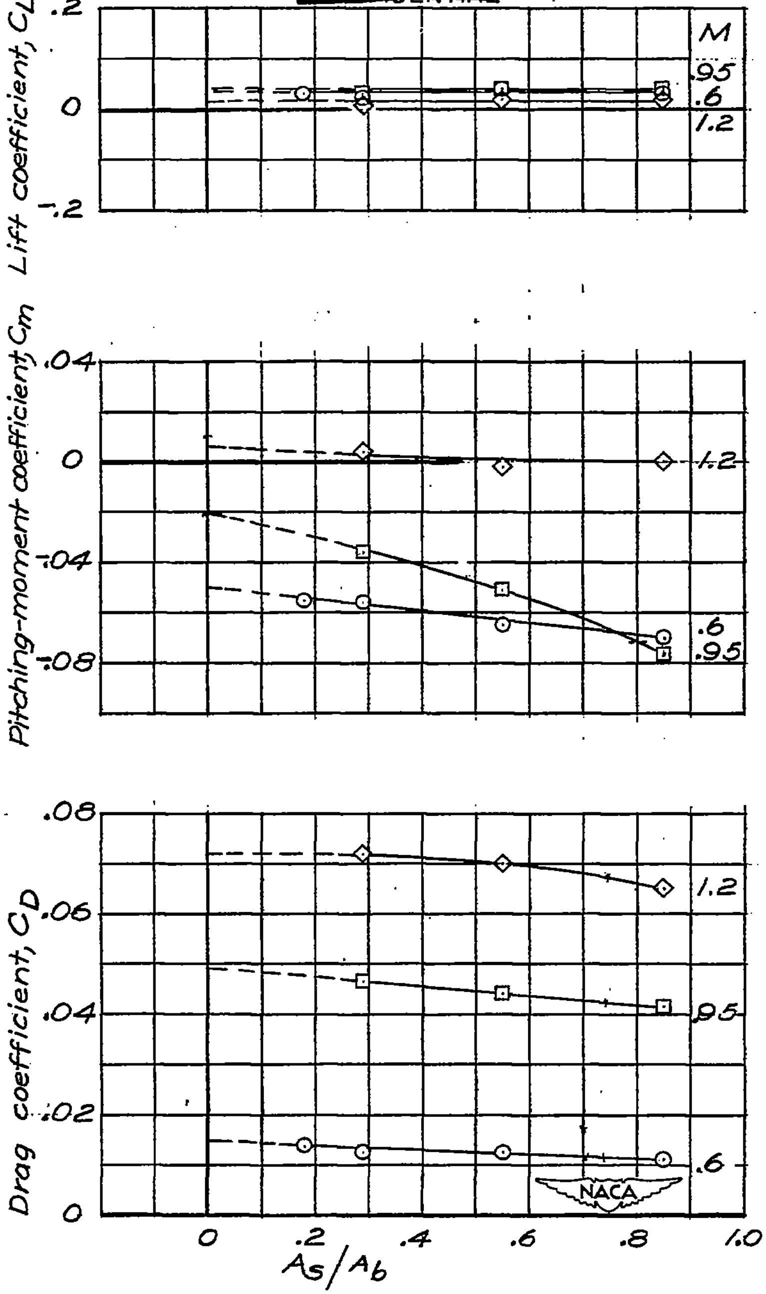

(a) C_L, C_m, and C_D plotted against A_s/A_b. $i_t = 4^\circ$; $\delta_e = 0^\circ$.

Figure 8.– Variation of force and base–pressure measurements with the ratio of sting area to model base area A_s/A_b at various Mach numbers. Complete model; $\alpha = -2^\circ$.

[redacted]

[redacted]

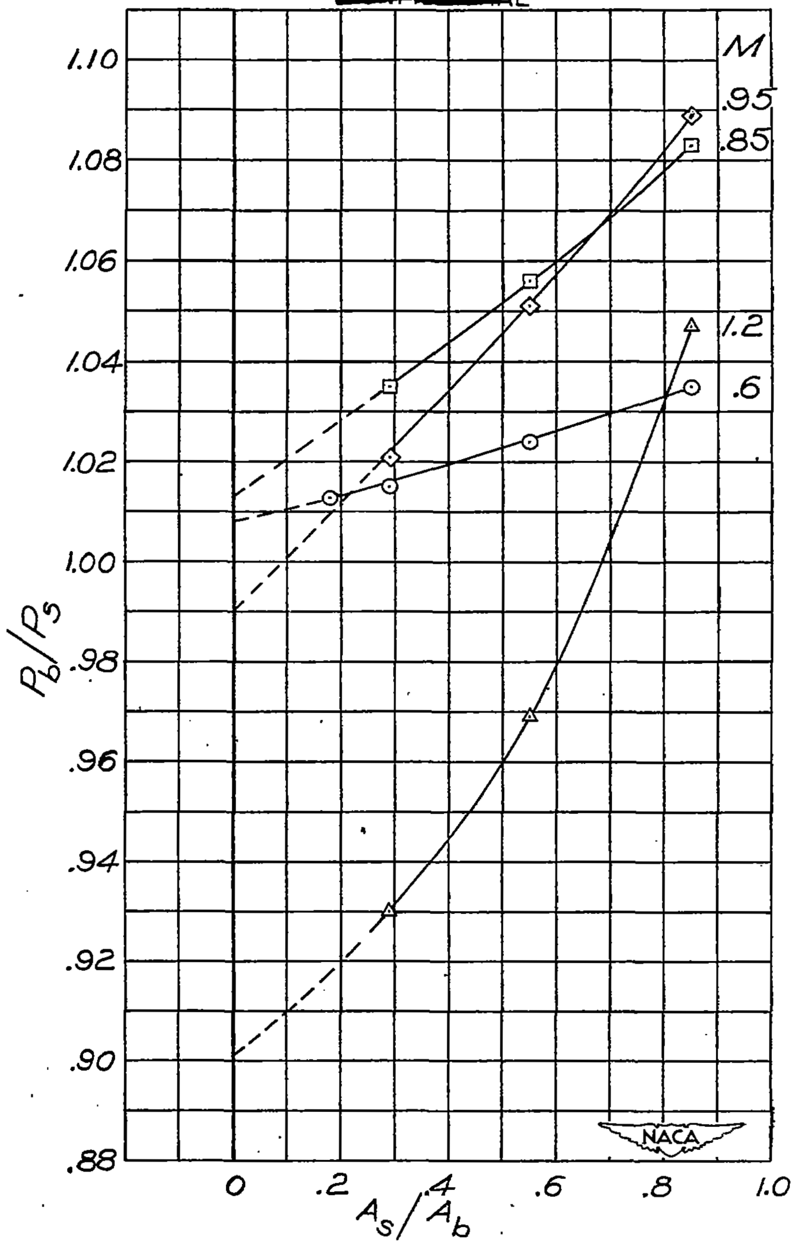

(b) P_b/P_s plotted against A_s/A_b. $i_t = 1.9^{\circ}$; $\delta_e = 6^{\circ}$.

Figure 8.– Concluded.

[redacted]

[redacted]

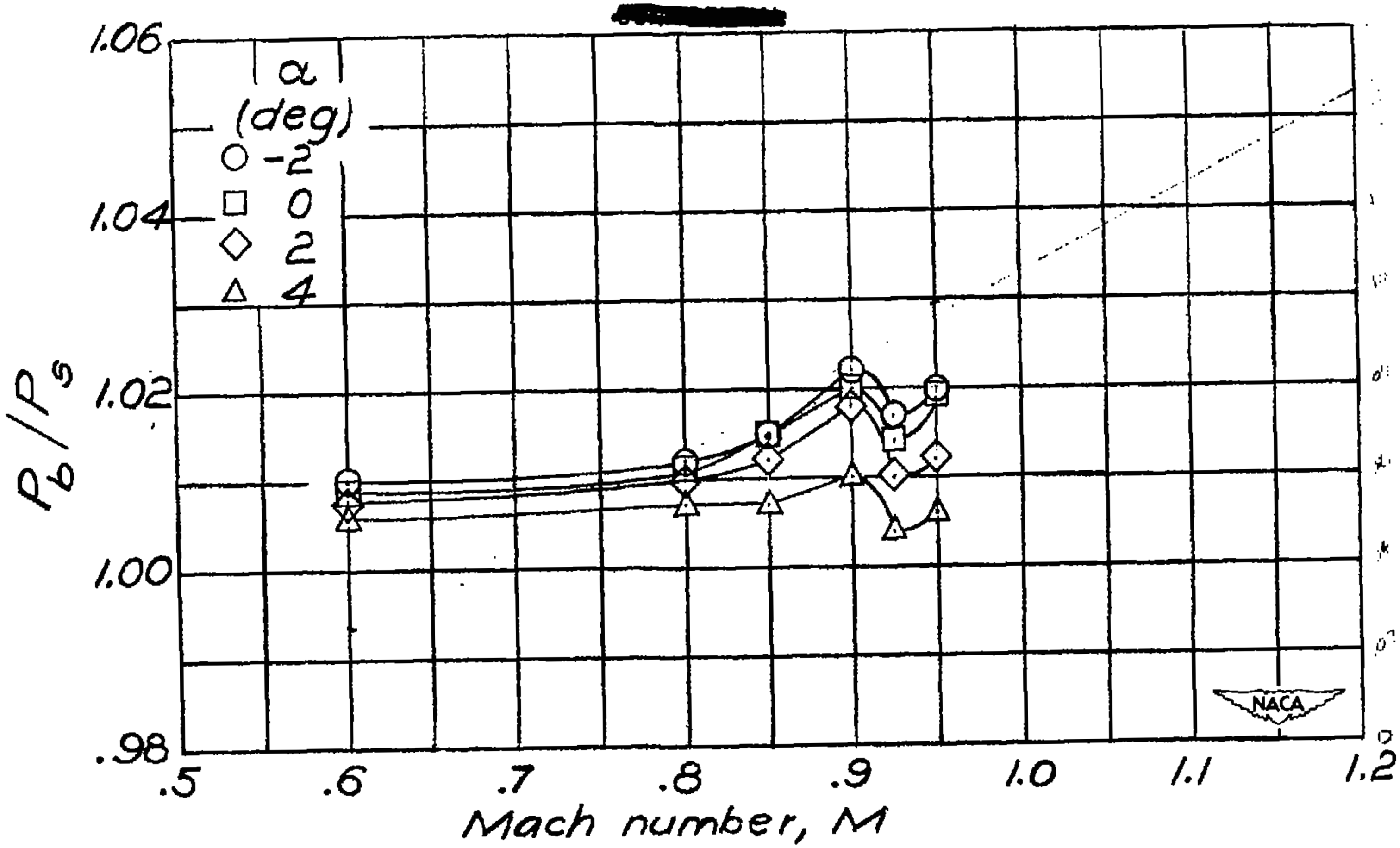

(a) Fuselage and fin.

Figure 9.- Variation of the ratio of model base pressure to free-stream static pressure P_b/P_s with Mach number for various configurations.

[redacted]

[redacted]

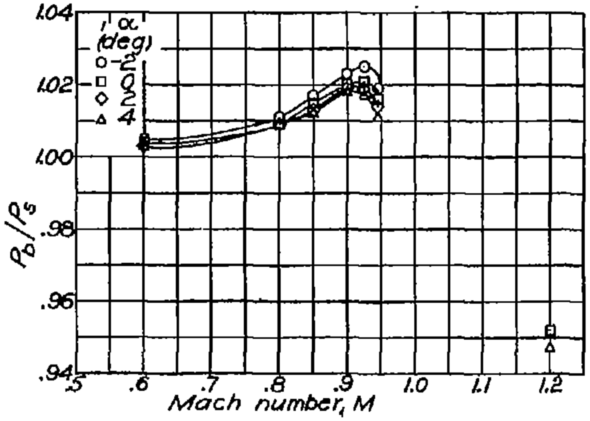

(b) Fuselage, fin and wing.

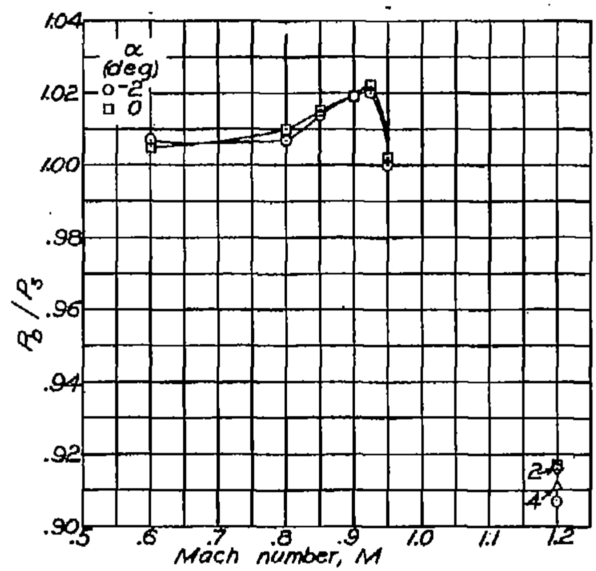

(c) Complete model; $i_t = 4^{\circ}$; $\delta_e = 0^{\circ}$.

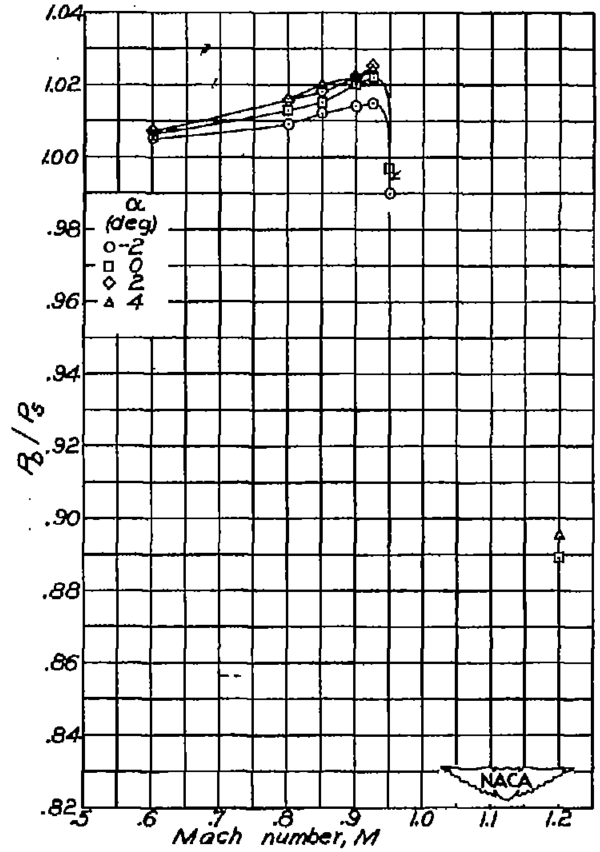

(d) Complete model; $i_t = 1.9^{\circ}$; $\delta_e = 0^{\circ}$.

Figure 9.– Continued.

[redacted]

[redacted]L

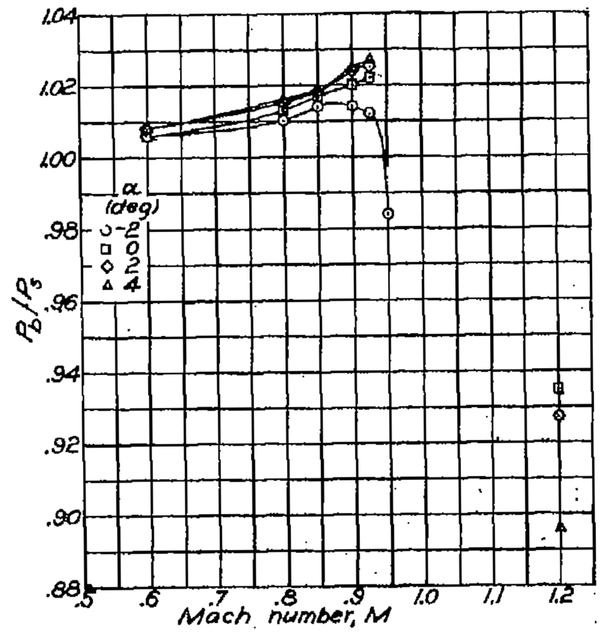

(e) Complete model; $i_t = 0^\circ$; $\delta_e = 0^\circ$.

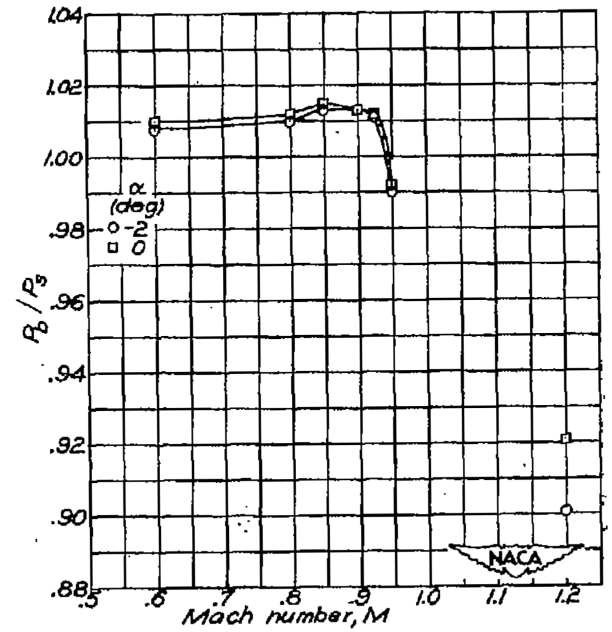

(f) Complete model; $i_t = 1.9^\circ$; $\delta_e = 6^\circ$.

Figure 9.– Continued.

[redacted]

[redacted]

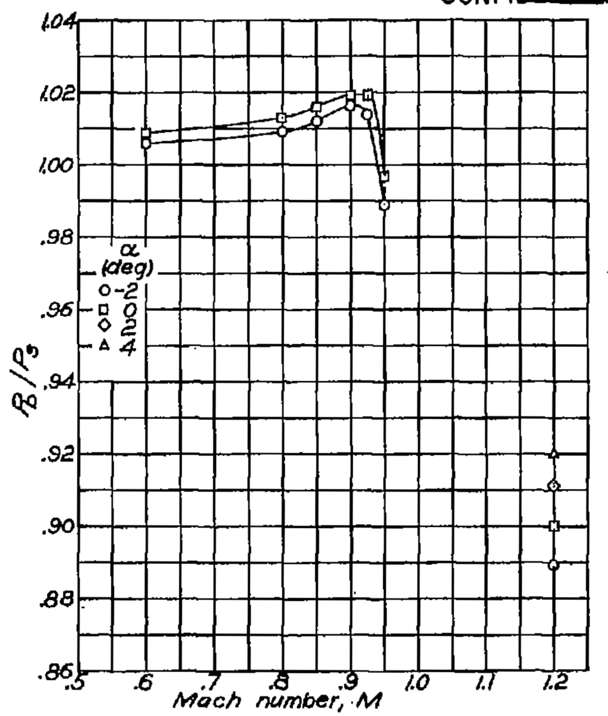

(g) Complete model; $i_t = 1.9^{\circ}$; $\delta_e = 4^{\circ}$.

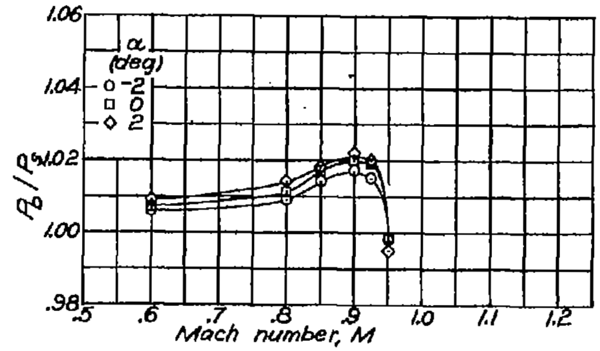

(h) Complete model; $i_t = 1.9^{\circ}$; $\delta_e = 2^{\circ}$.

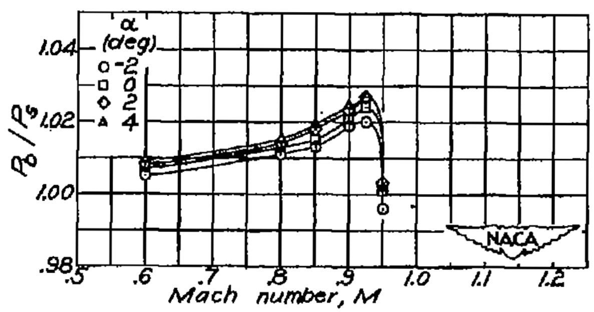

(i) Complete model; $i_t = 1.9^{\circ}$; $\delta_e = -2^{\circ}$.

Figure 9.– Continued.

[redacted]

[redacted]

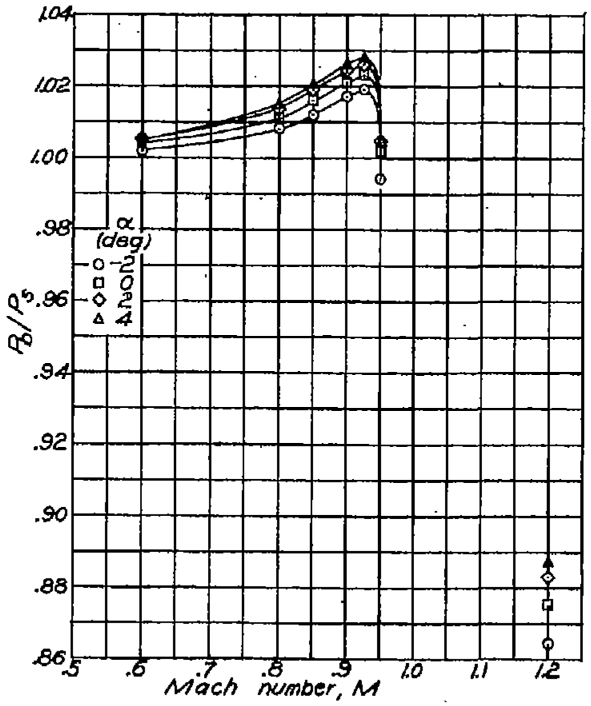

(j) Complete model; $i_t = 1.9^\circ$; $\delta_e = -4^\circ$.

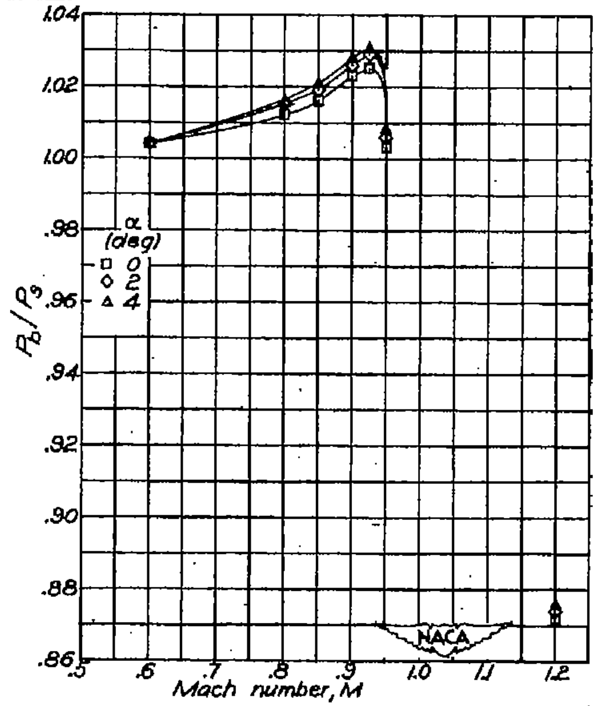

(k) Complete model; $i_t = 1.9^\circ$; $\delta_e = -6^\circ$.

Figure 9.– Continued.

[redacted]

[redacted]

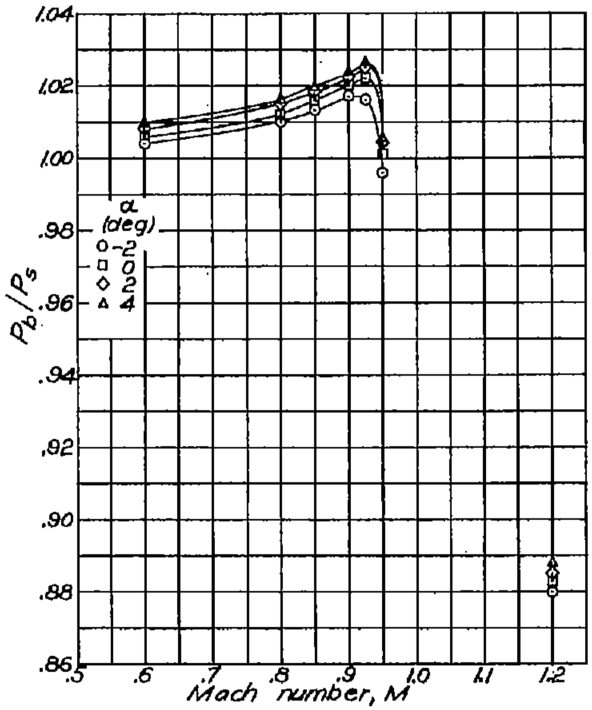

(l) Complete model and 0.68c fences; $i_t = 1.9^\circ$; $\delta_e = 0^\circ$.

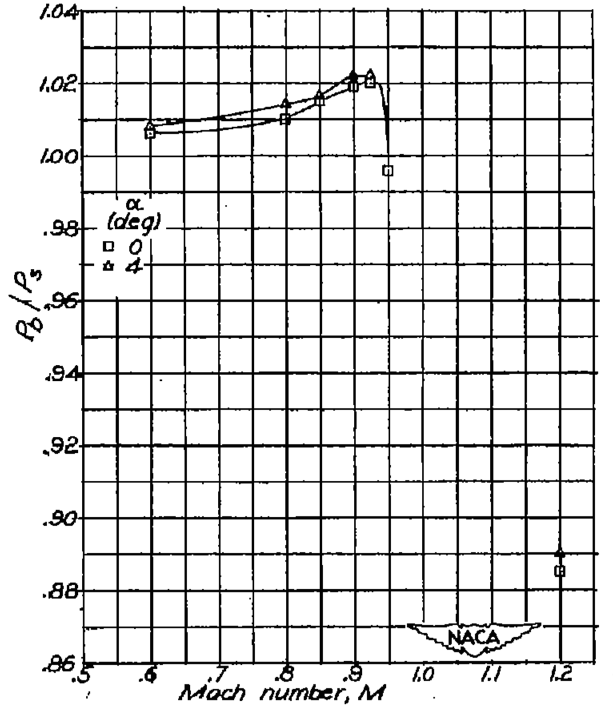

(m) Complete model and 0.95c fences; $i_t = 1.9^\circ$; $\delta_e = 0^\circ$

Figure 9.– Concluded.

[redacted]

[redacted]

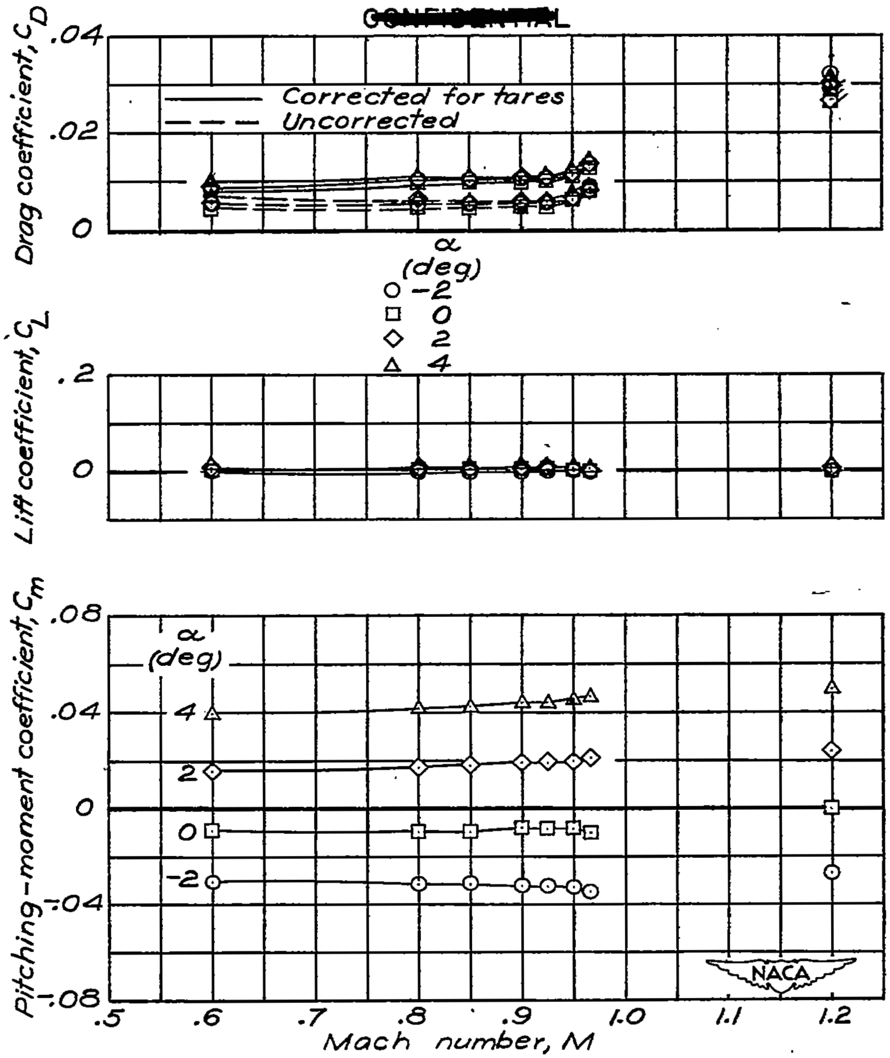

(a) Fuselage and fin.

Figure 10.– Variation of lift coefficient, pitching–moment coefficient, and drag coefficient with Mach number for several angles of attack for various configurations. (Plain symbols at M = 1.2 refer to data corrected for tares, and flagged symbols refer to uncorrected data.)

[redacted]

[redacted]

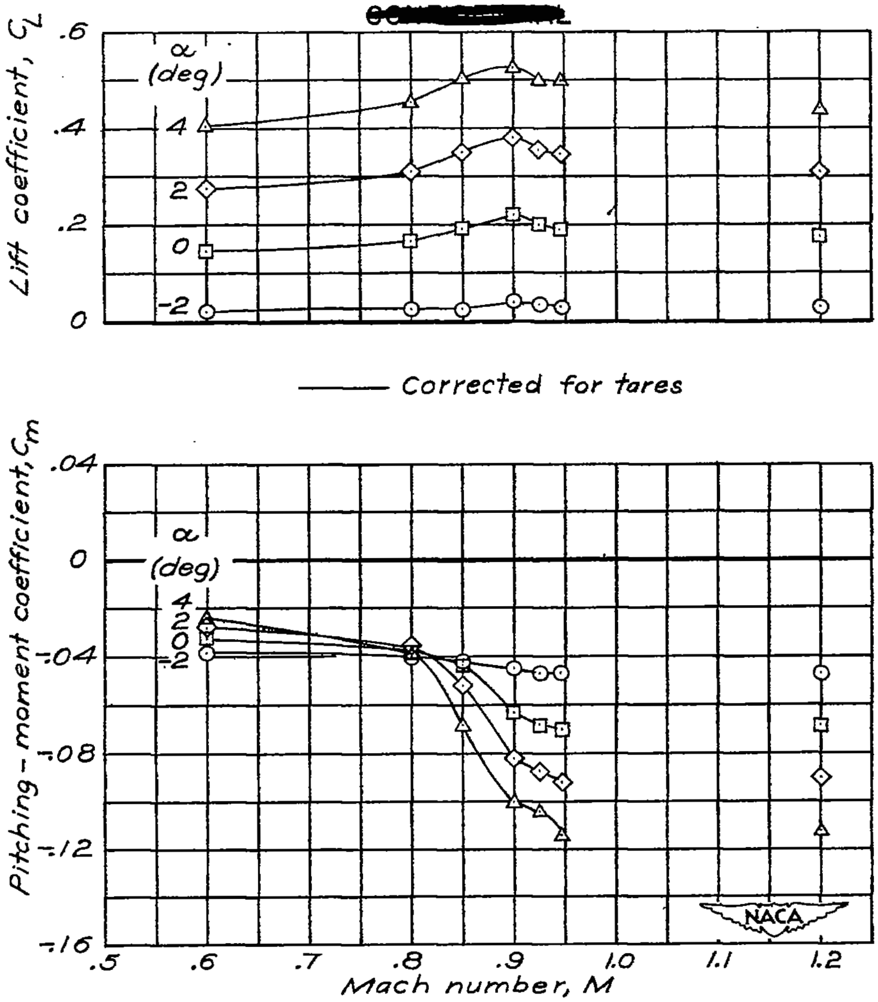

(b) Fuselage, fin, and wing.

Figure 10.– Continued.

[redacted]

CO[redacted]AL

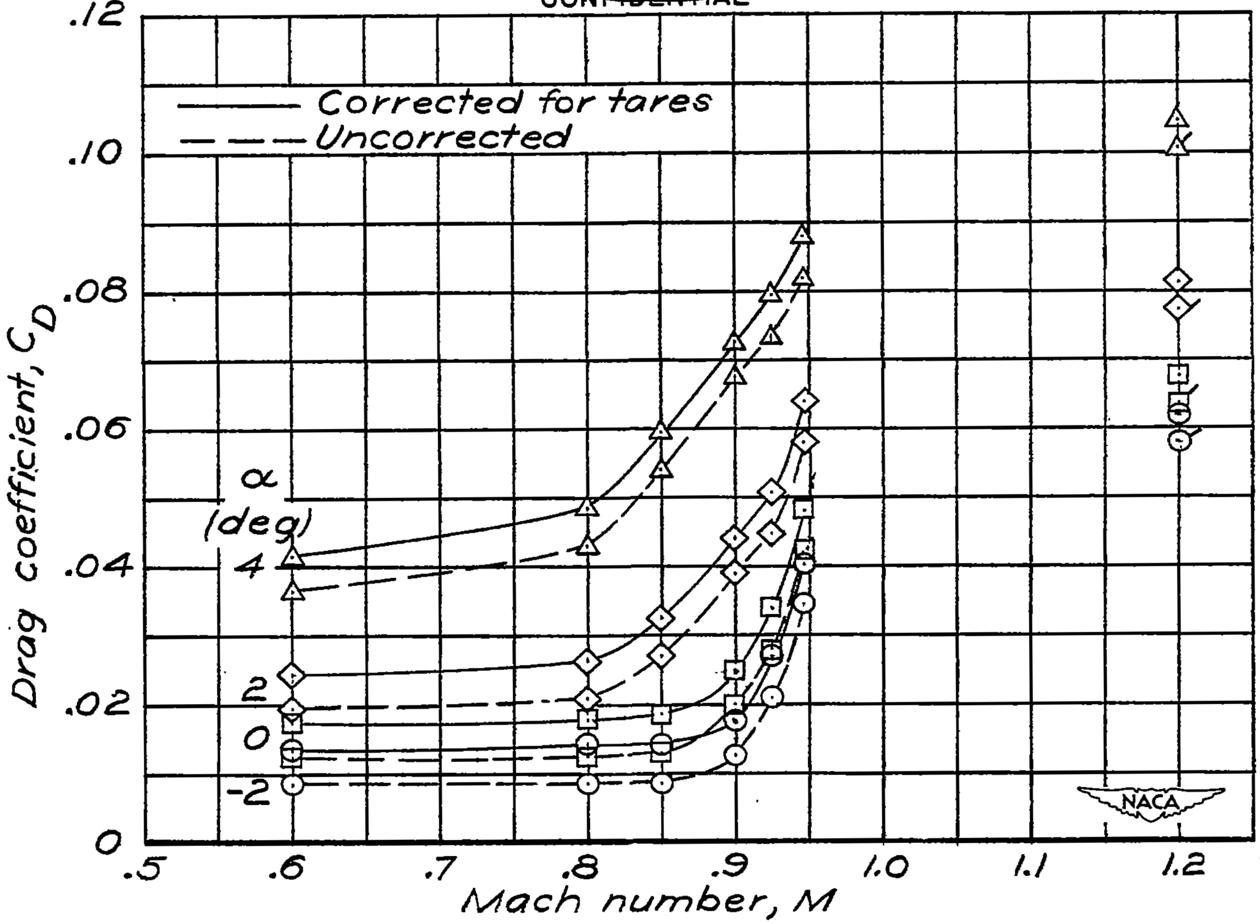

(b) Fuselage, fin, and wing. Concluded.

Figure 10.- Continued.

[redacted]L

[redacted]

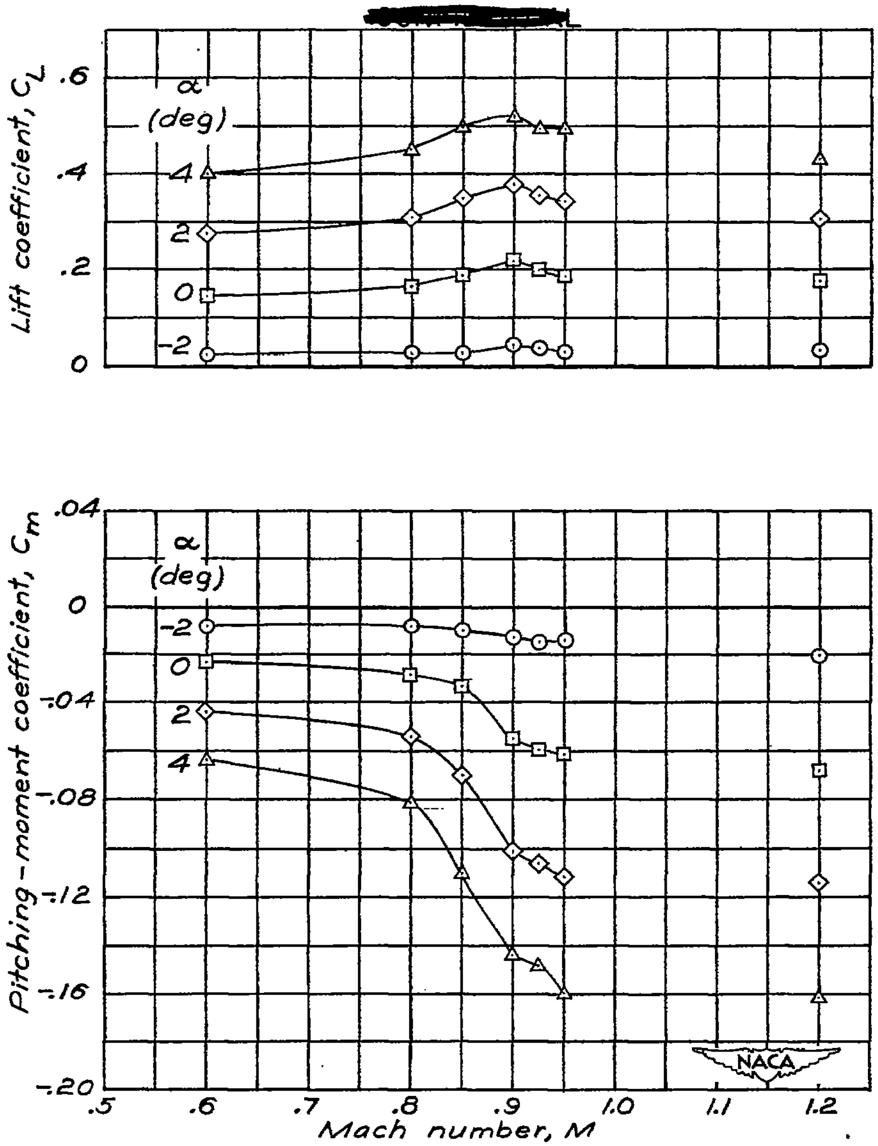

(c) Wing alone.

Figure 10.– Continued.

[redacted]

[redacted]

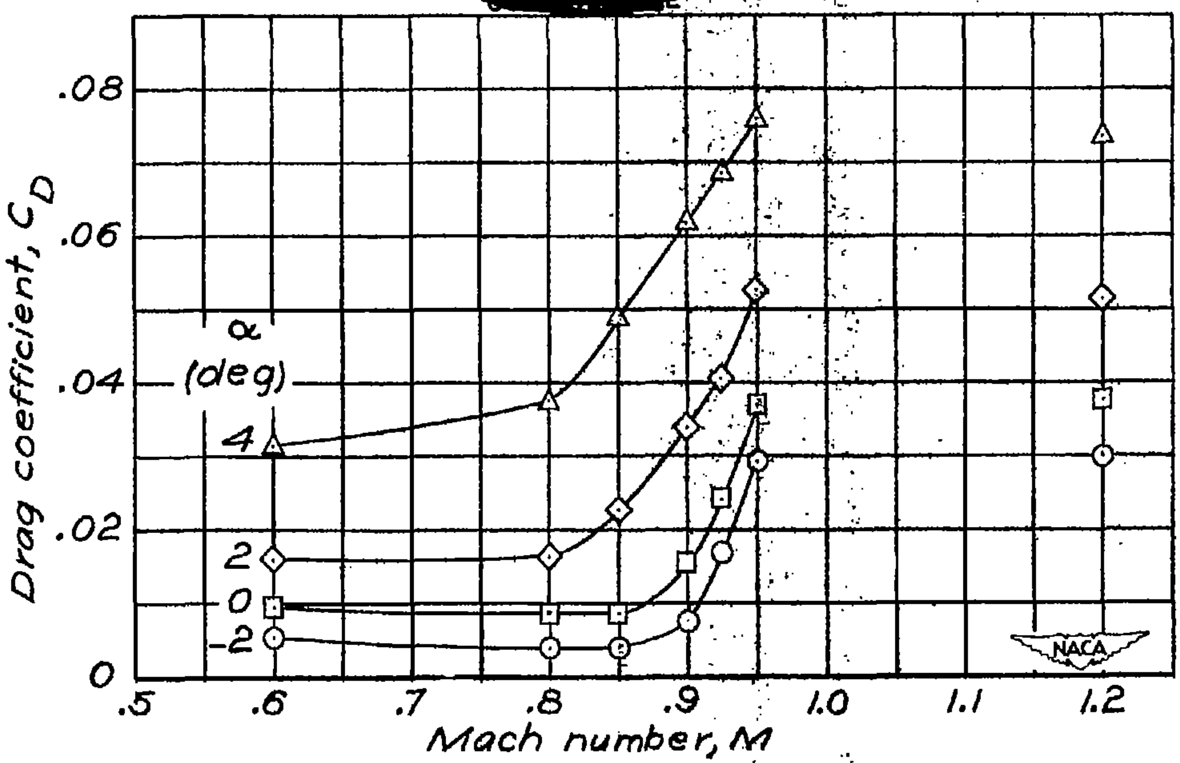

(c) Wing alone. Concluded.

Figure 10.– Continued.

[redacted]

[redacted]

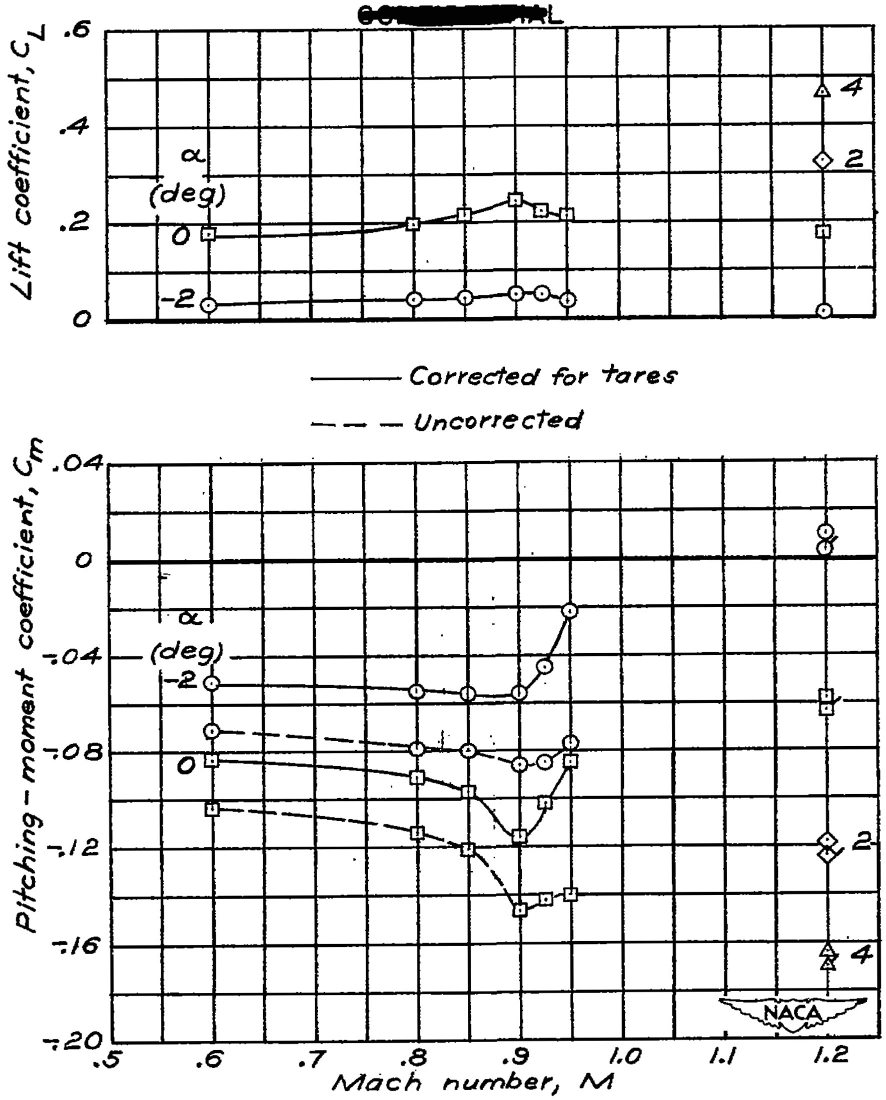

(d) Complete model; $i_t = 4^\circ$; $\delta_e = 0^\circ$.

Figure 10.– Continued.

[redacted]

[redacted]

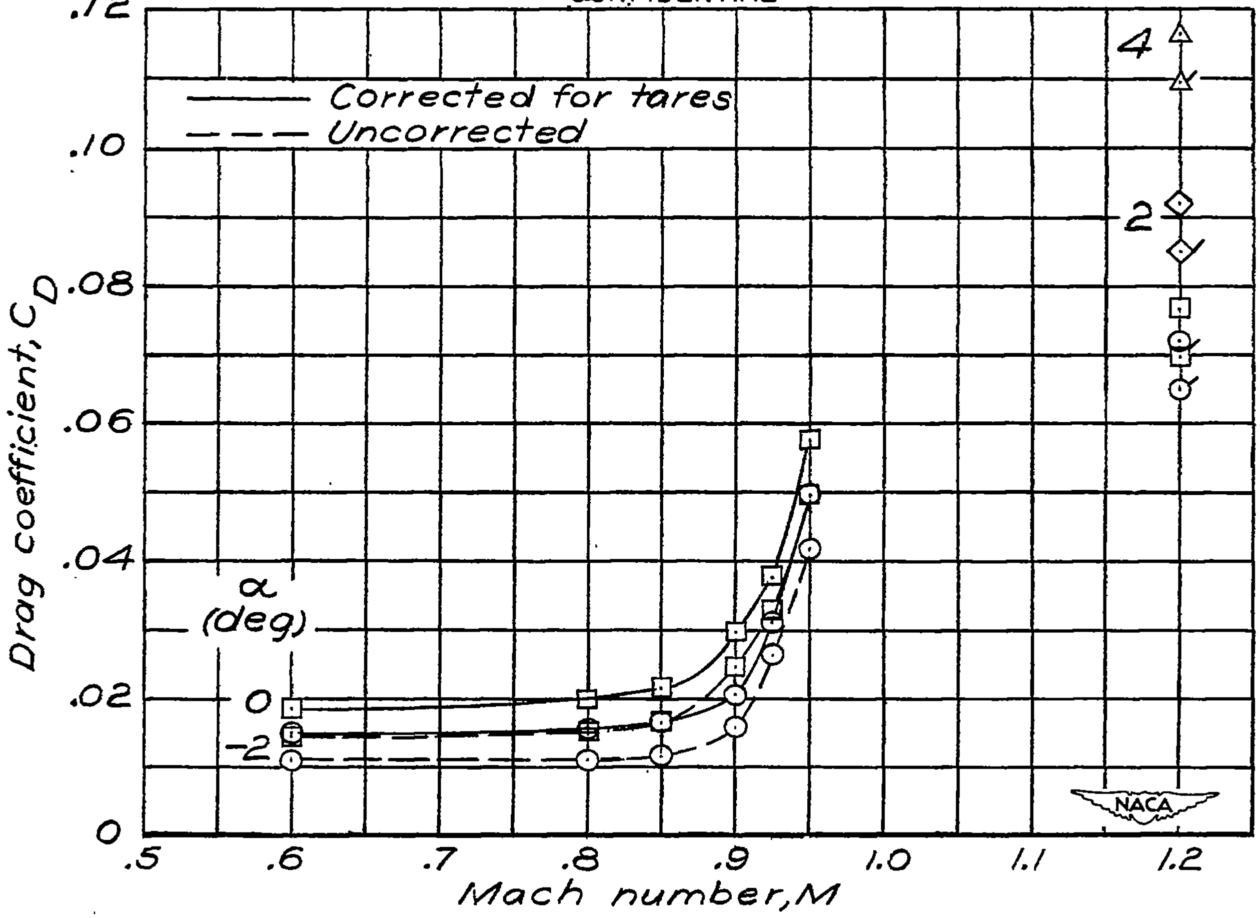

(d) Complete model; $i_t = 4^{\circ}$; $\delta_e = 0^{\circ}$. Concluded.

Figure 10.– Continued.

[redacted]

[redacted]

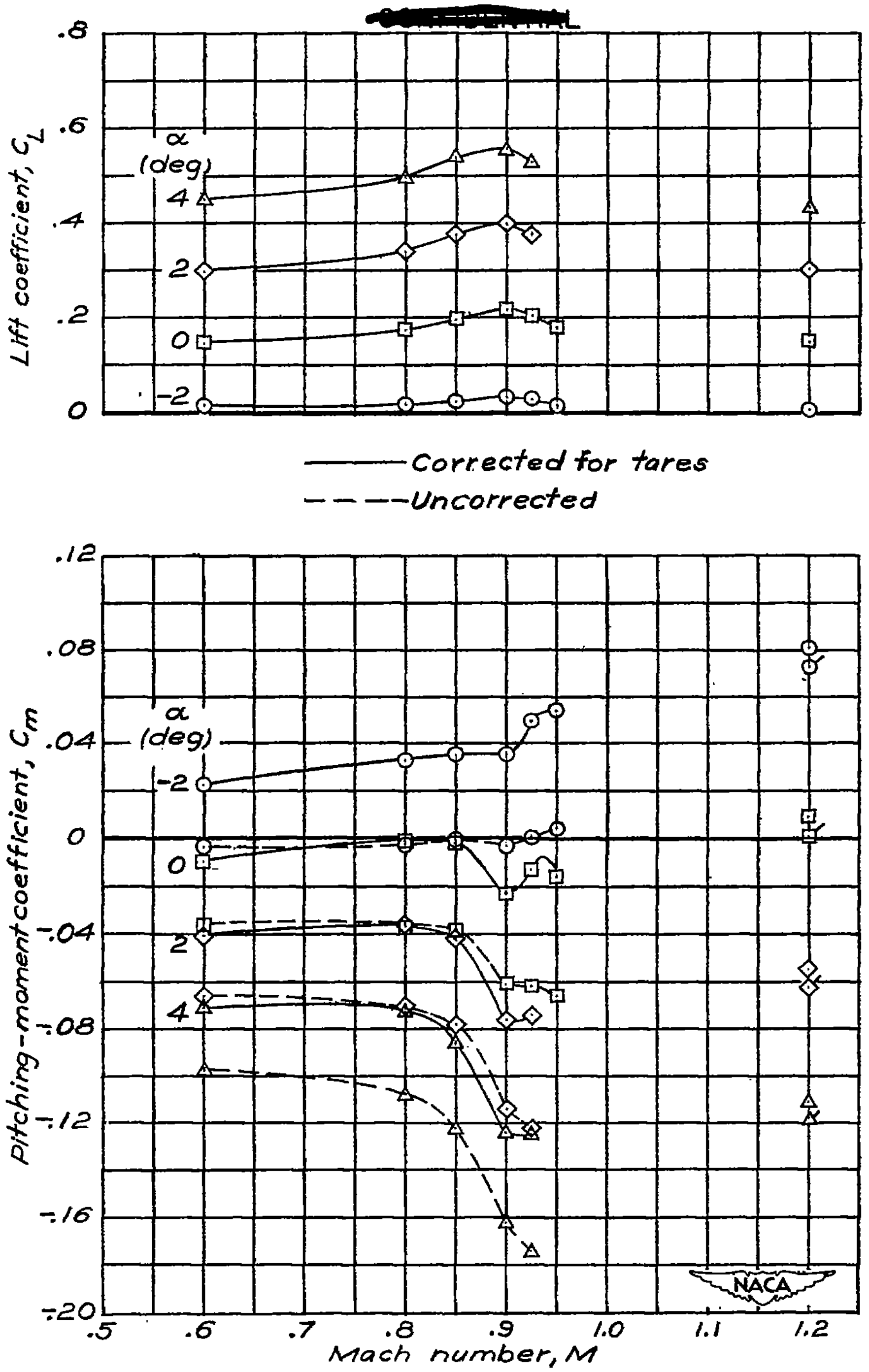

(e) Complete model; $i_t = 1.9^\circ$; $\delta_e = 0^\circ$.

Figure 10.– Continued.

[redacted]

[redacted]

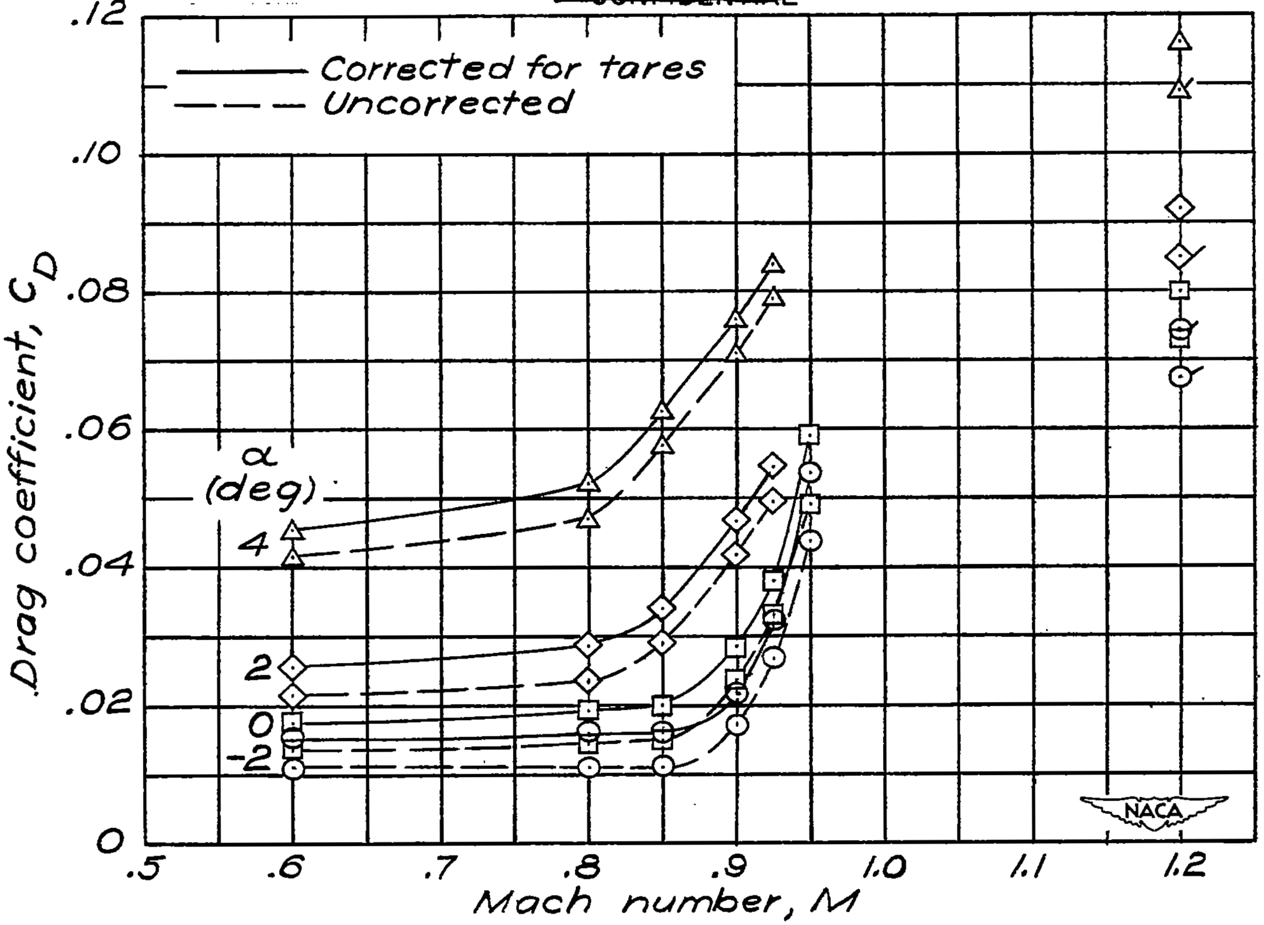

(e) Complete model; $i_t = 1.9^\circ$; $\delta_e = 0^\circ$. Concluded.

Figure 10.– Continued.

[redacted]

[redacted]

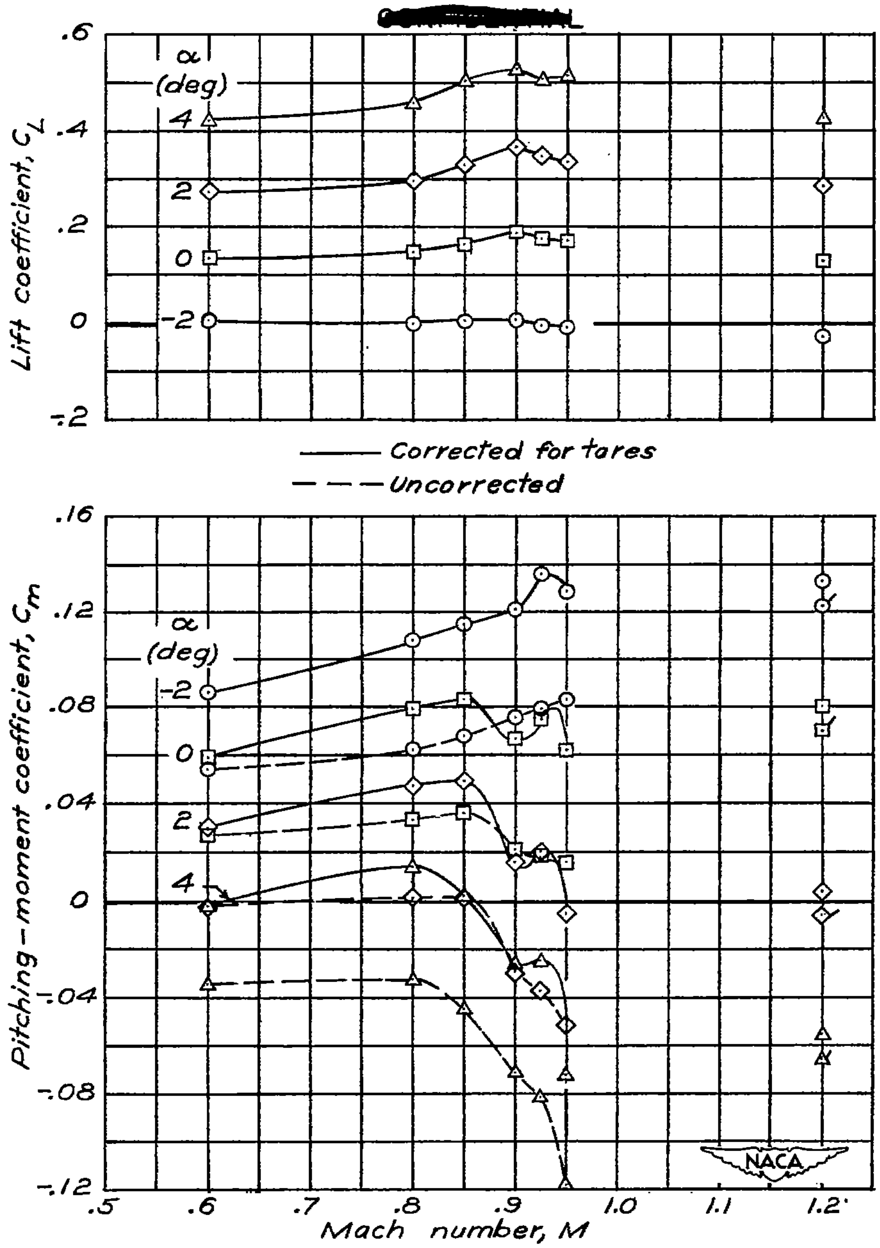

(f) Complete model; $i_t = 0^{\circ}$; $\delta_e = 0^{\circ}$.

Figure 10.– Continued.

[redacted]

[redacted]

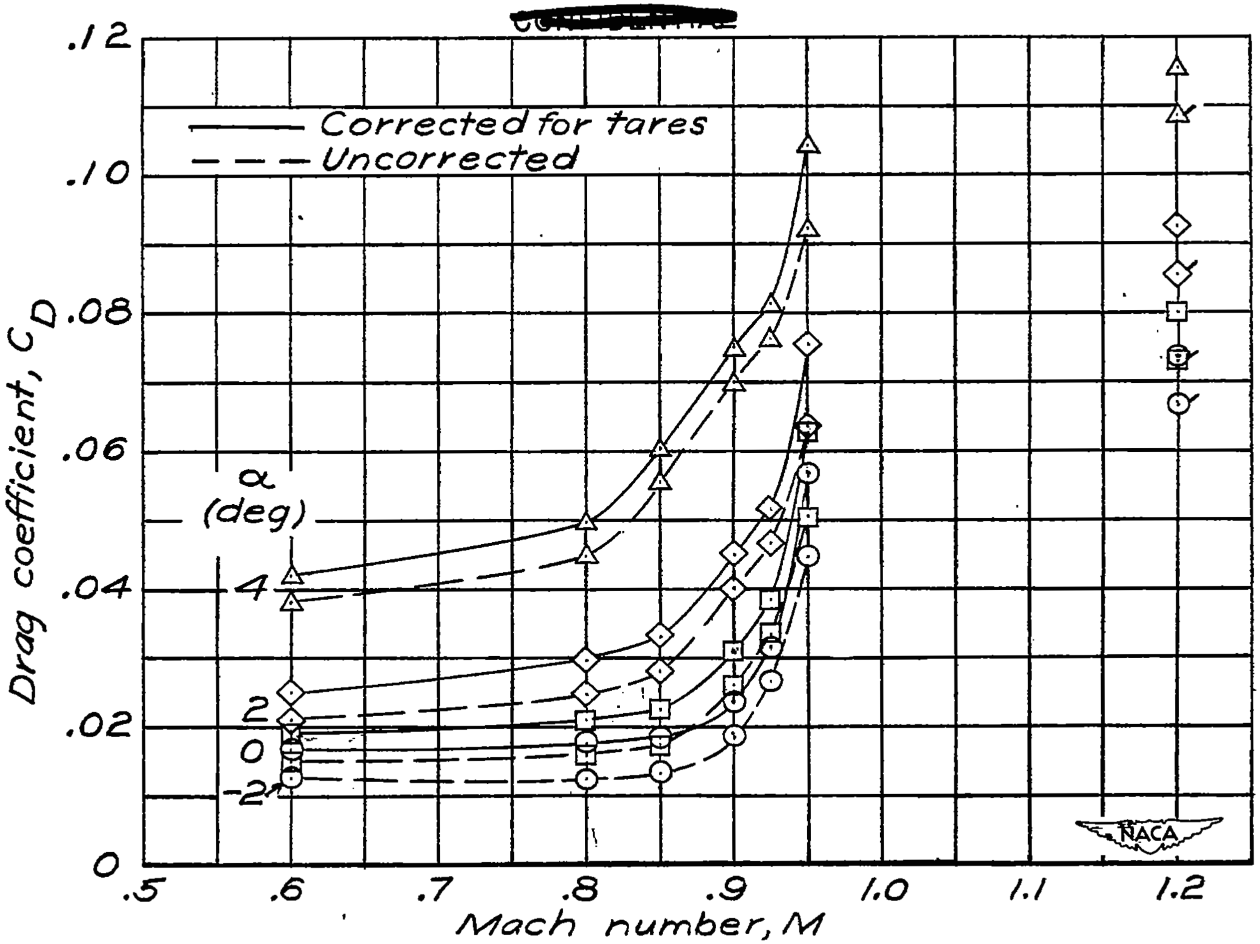

(f) Complete model; $i_t = 0^\circ$; $\delta_e' = 0^\circ$. Concluded.

Figure 10.– Continued.

[redacted]

[redacted]

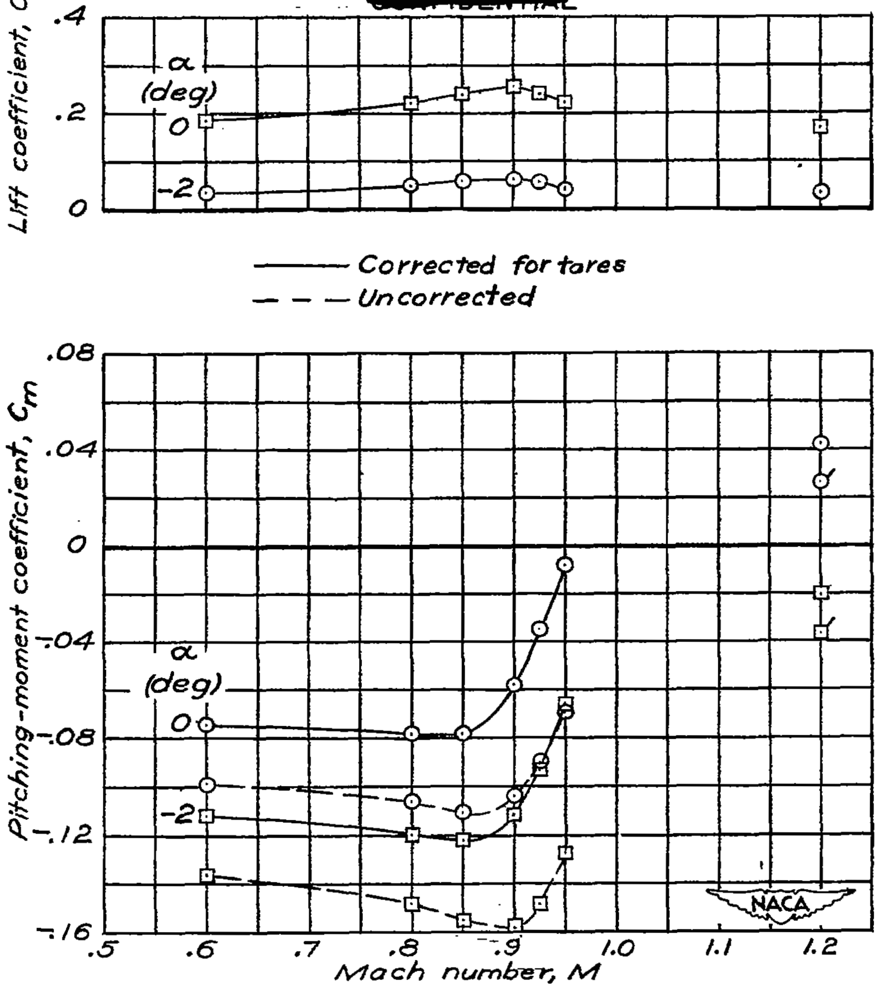

(g) Complete model; $i_t = 1.9^{\circ}$; $\delta_e = 6^{\circ}$.

Figure 10.– Continued.

[redacted]

[redacted]

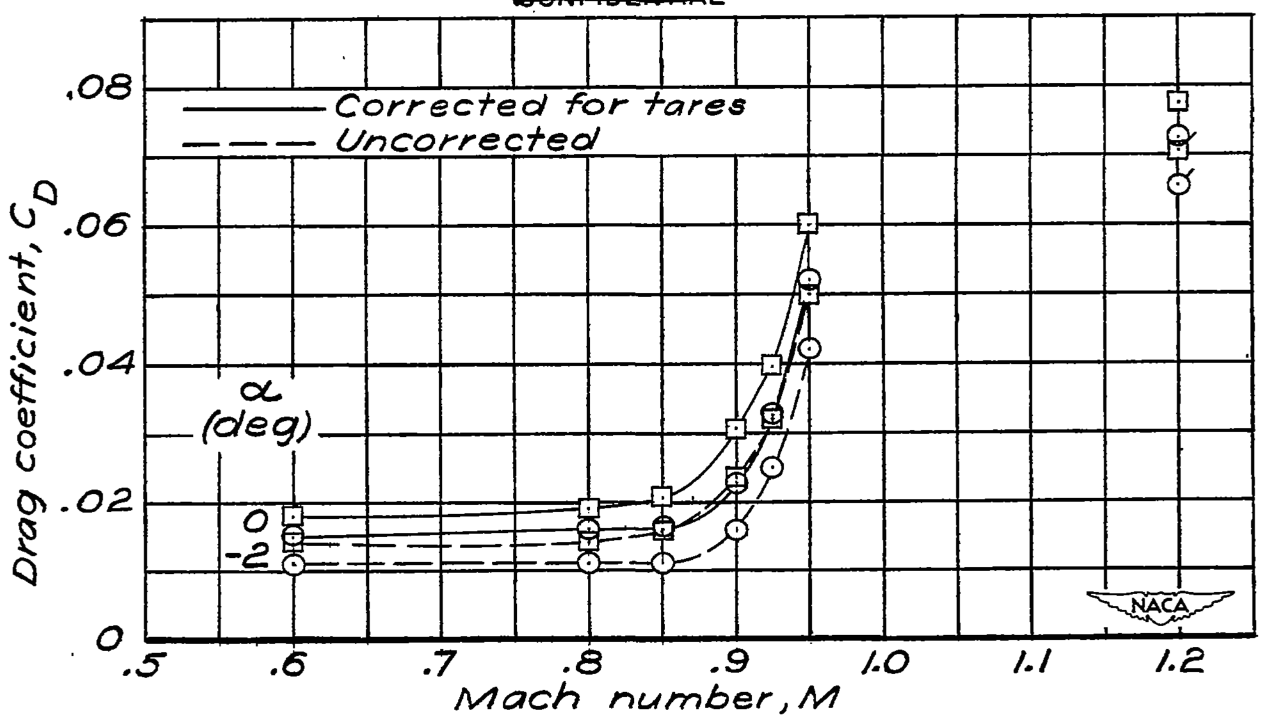

(g) Complete model; $i_t = 1.9^{\circ}$; $\delta_e = 6^{\circ}$. Concluded.

Figure 10.– Continued.

[redacted]

[redacted]

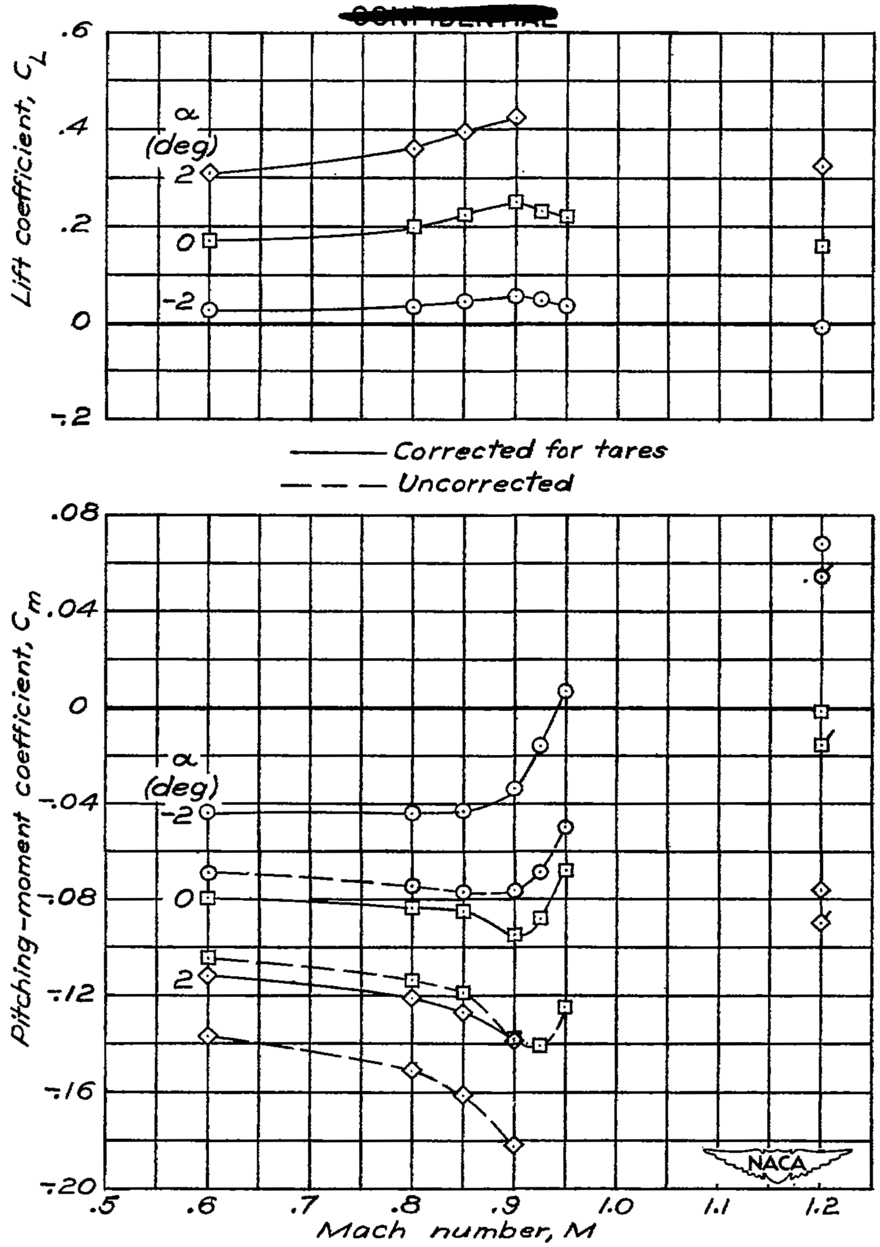

(h) Complete model; $i_t = 1.9^\circ$; $\delta_e = 4^\circ$.

Figure 10.– Continued.

[redacted]

[redacted]

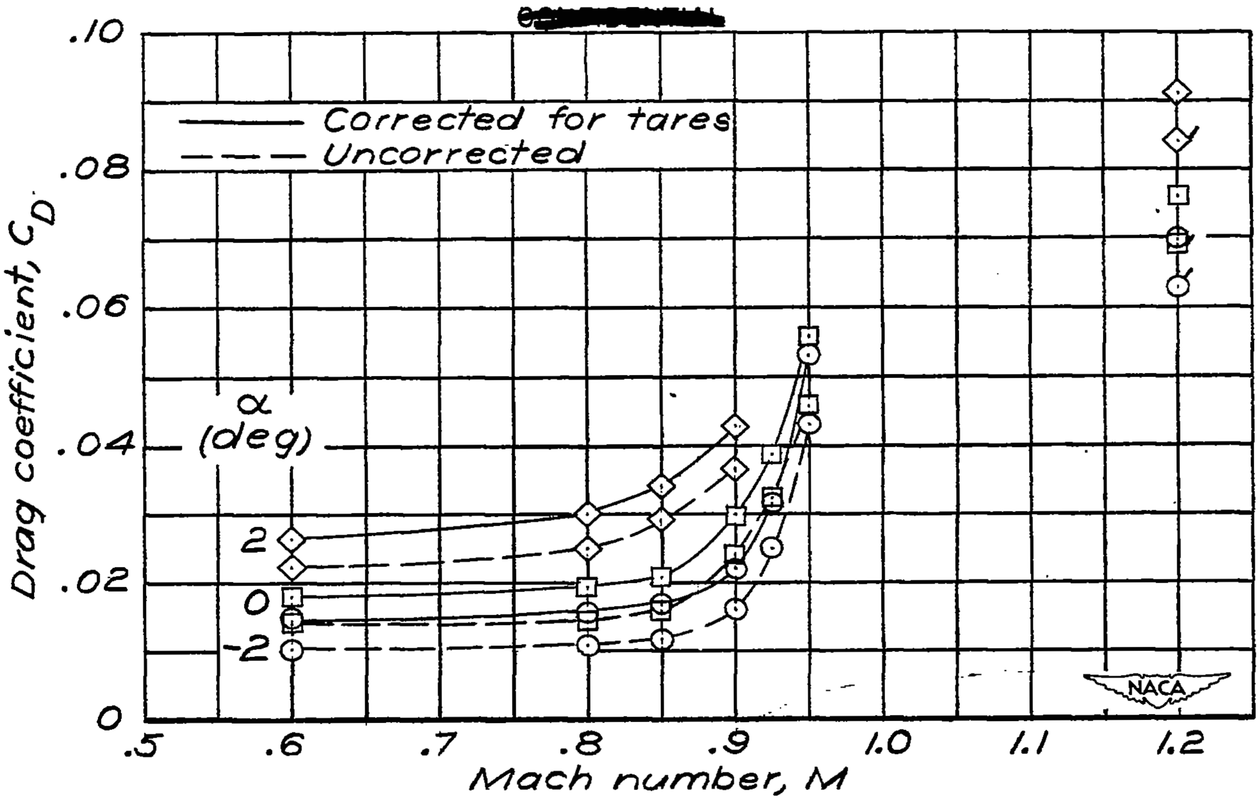

(h) Complete model; i_t = 1.9°; δ_e = 4°. Concluded.

Figure 10.– Continued.

[redacted]

[redacted]

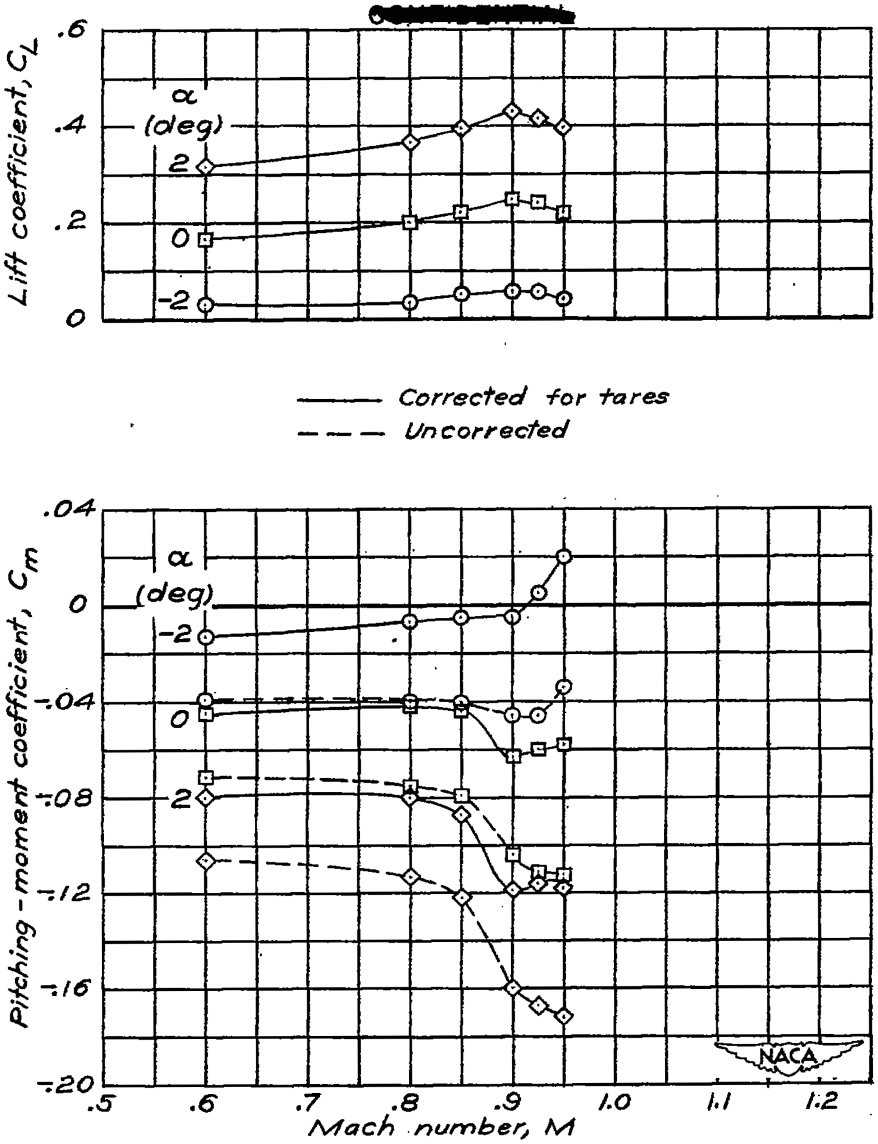

(i) Complete model; $i_t = 1.9^\circ$; $\delta_e = 2^\circ$.

Figure 10.– Continued.

[redacted]

[redacted]

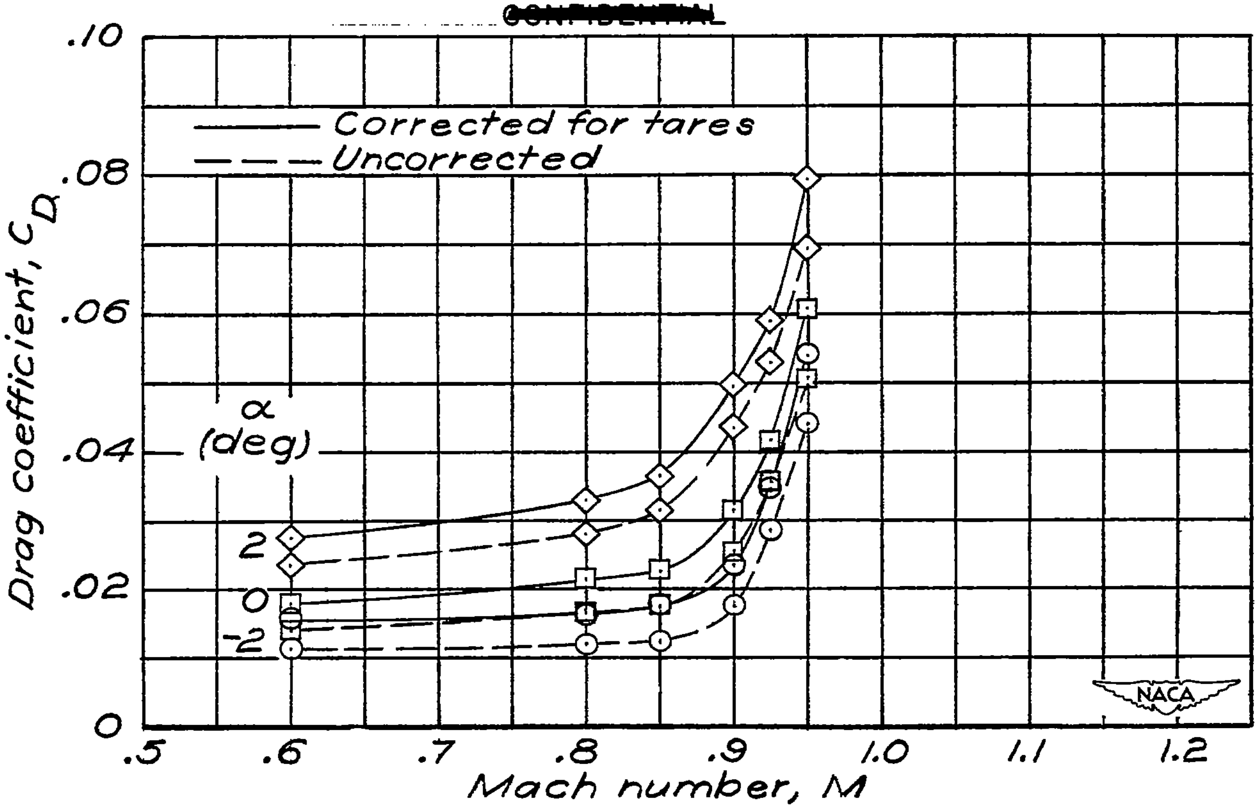

(i) Complete model; $i_t = 1.9^\circ$; $\delta_e = 2^\circ$. Concluded.

Figure 10.– Continued.

[redacted]

[redacted]

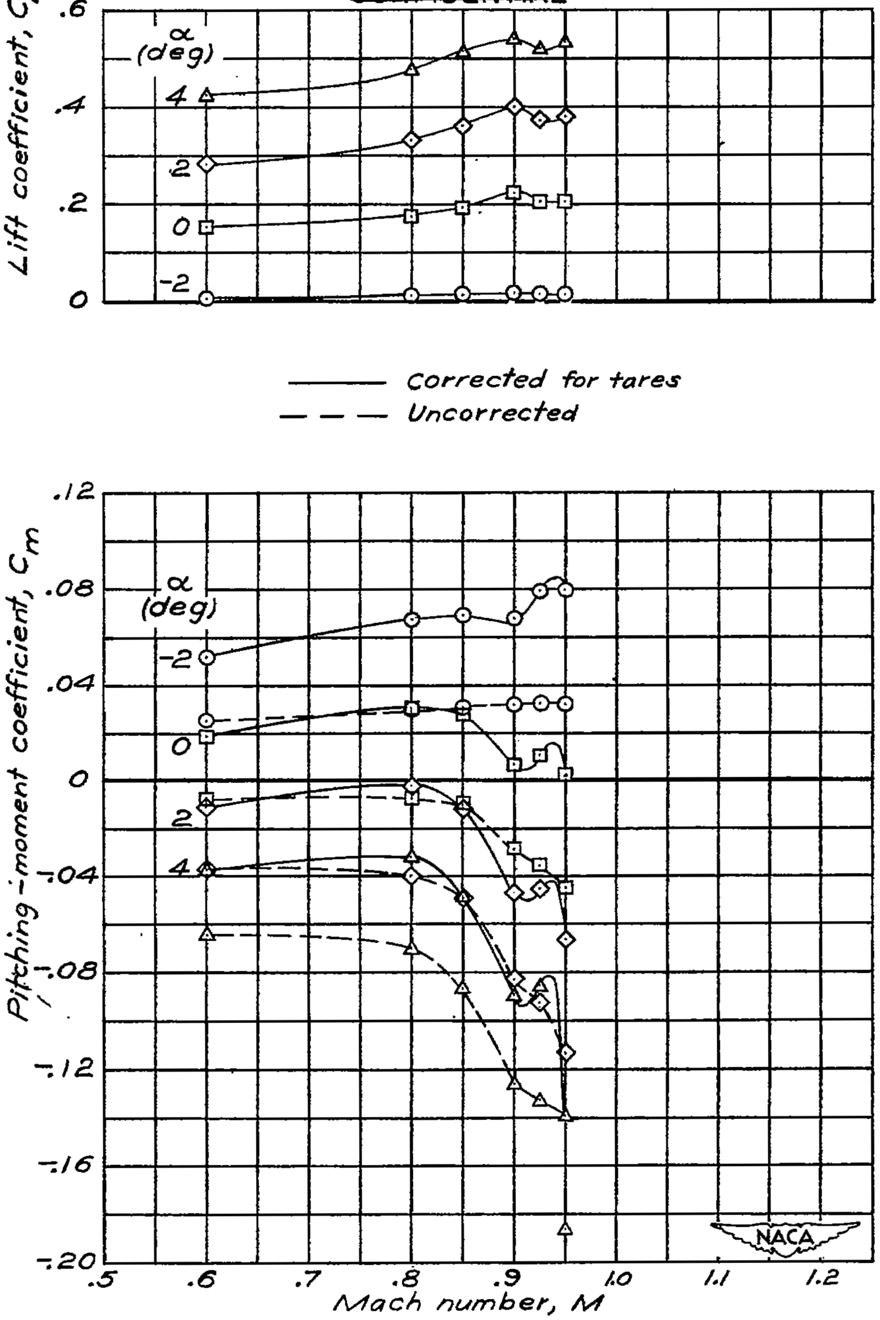

(j) Complete model; $i_t = 1.9^\circ$; $\delta_e = -2^\circ$.

Figure 10.– Continued.

[redacted]

[redacted]AL

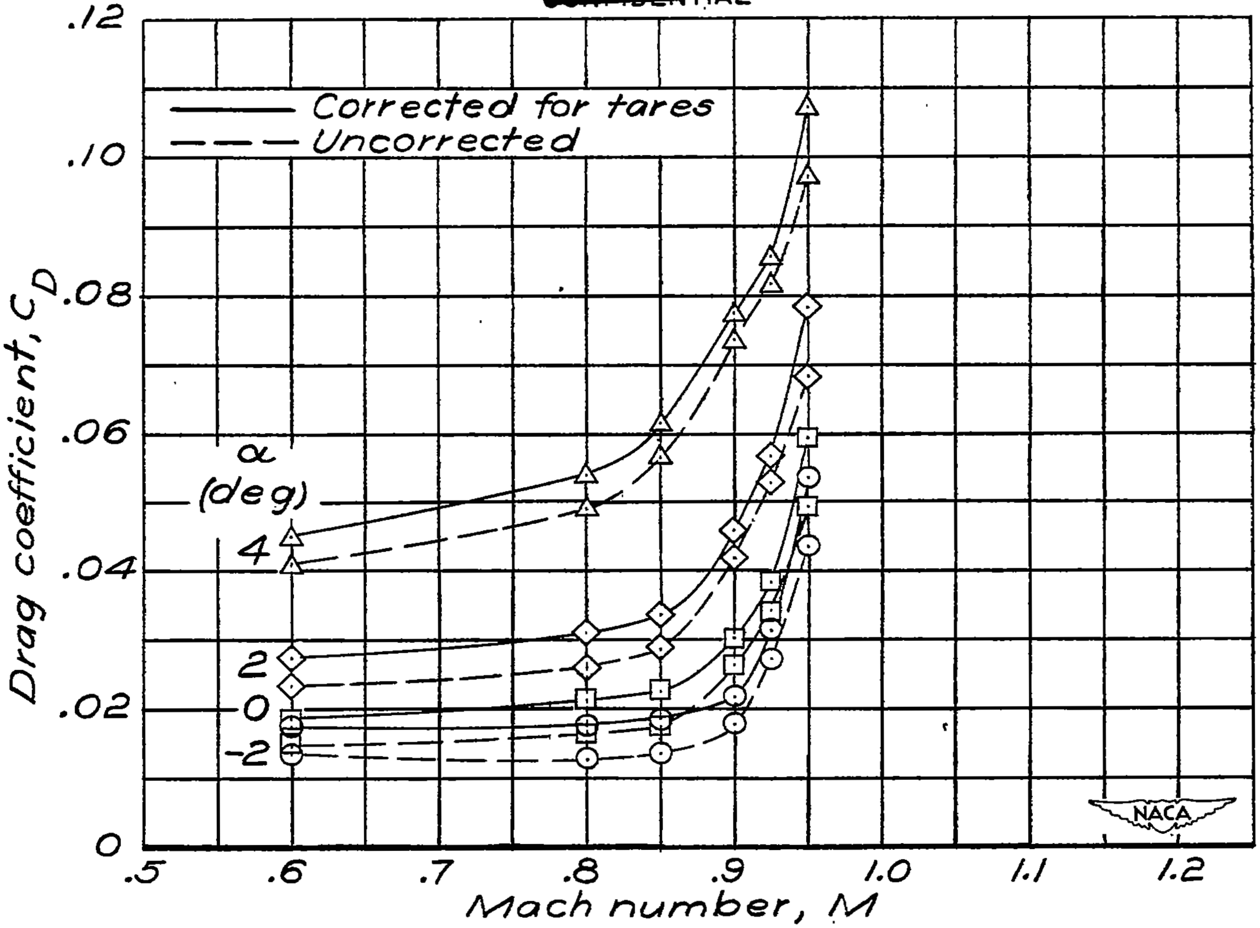

(j) Complete model; $i_t = 1.9^\circ$; $\delta_e = -2^\circ$. Concluded.

Figure 10.– Continued.

[redacted]

[redacted]

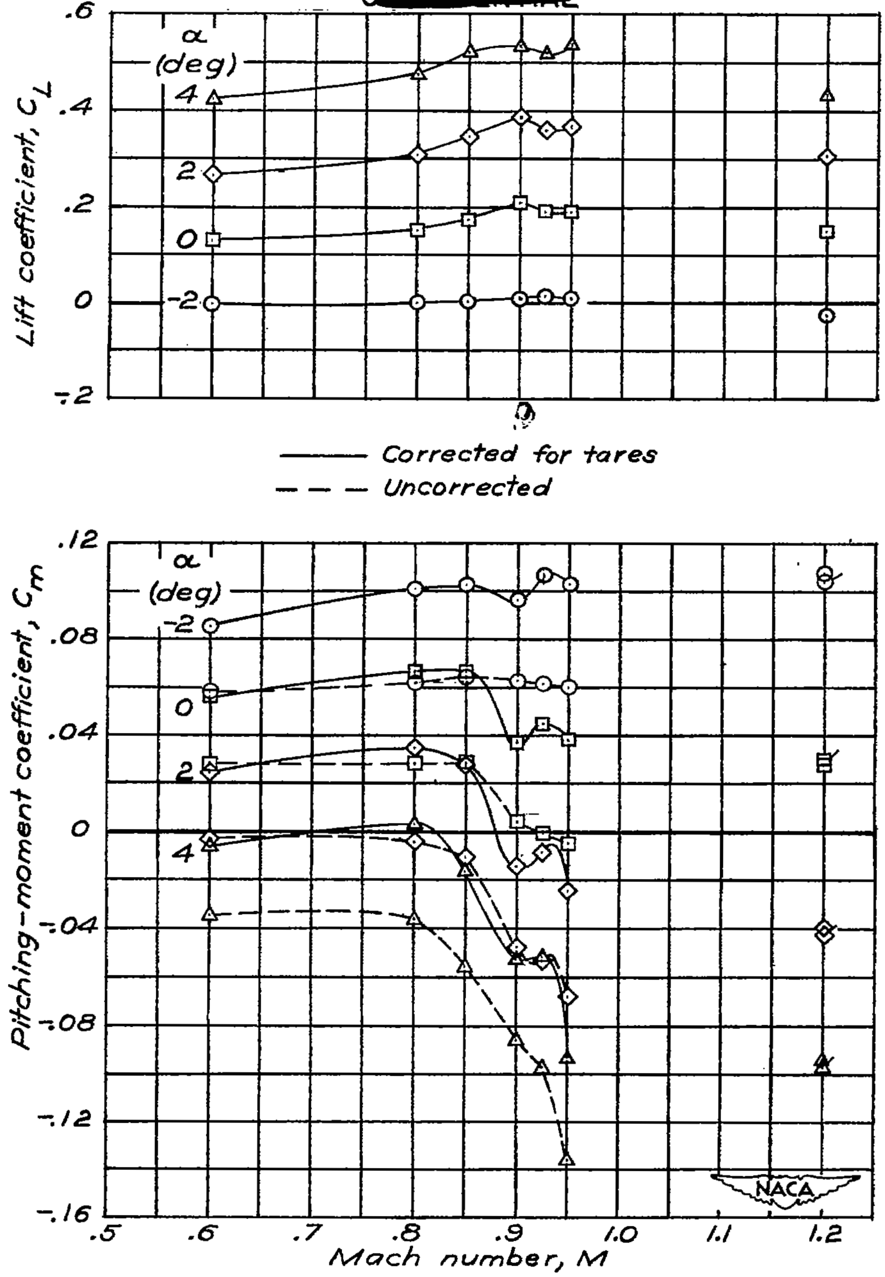

(k) Complete model; $i_t = 1.9^{\circ}$; $\delta_e = -4^{\circ}$.

Figure 10.– Continued.

[redacted]

~~CONFIDENTIAL~~

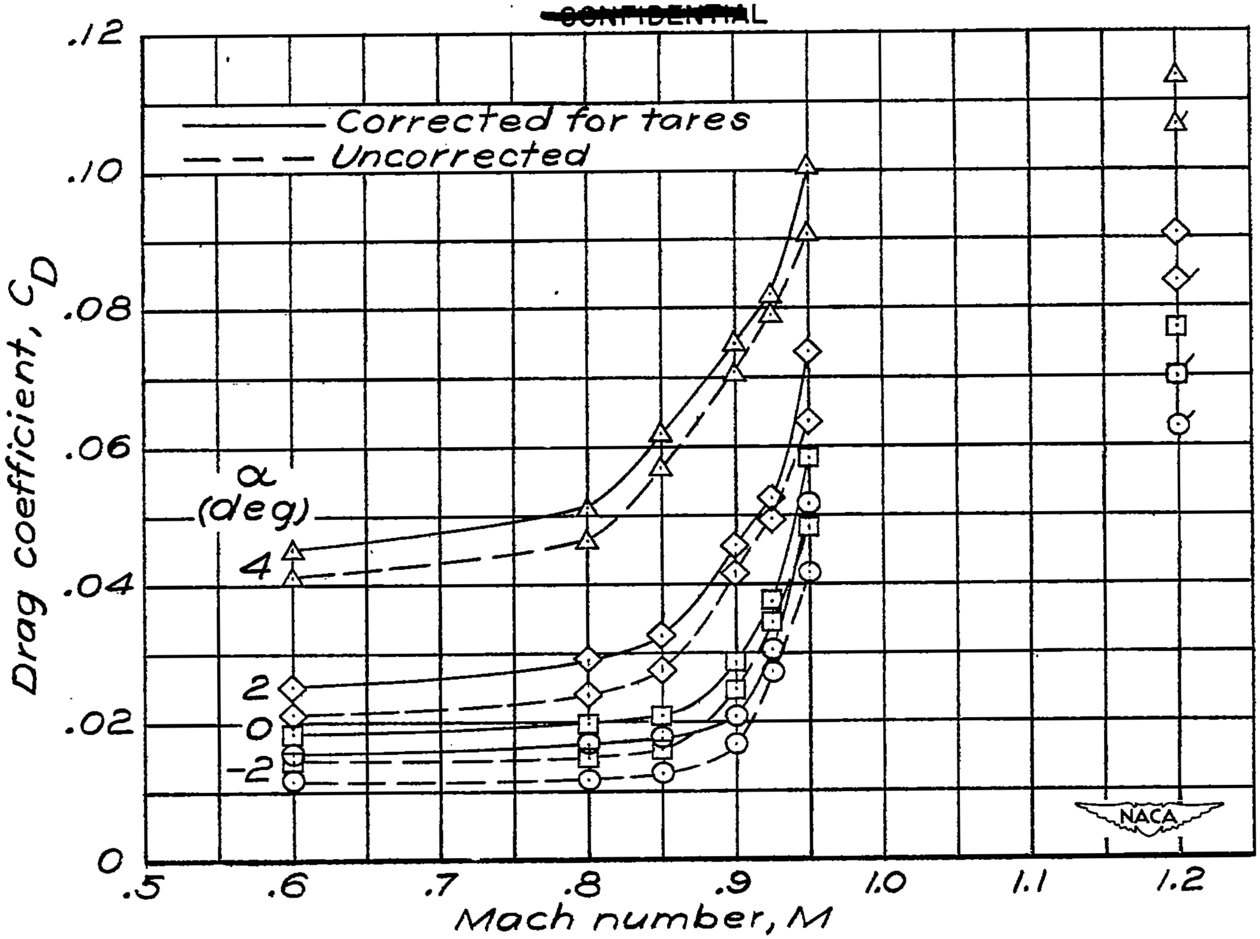

(k) Complete model; $i_t = 1.9^\circ$; $\delta_e = -4^\circ$. Concluded.

Figure 10.– Continued.

[redacted]

[redacted]

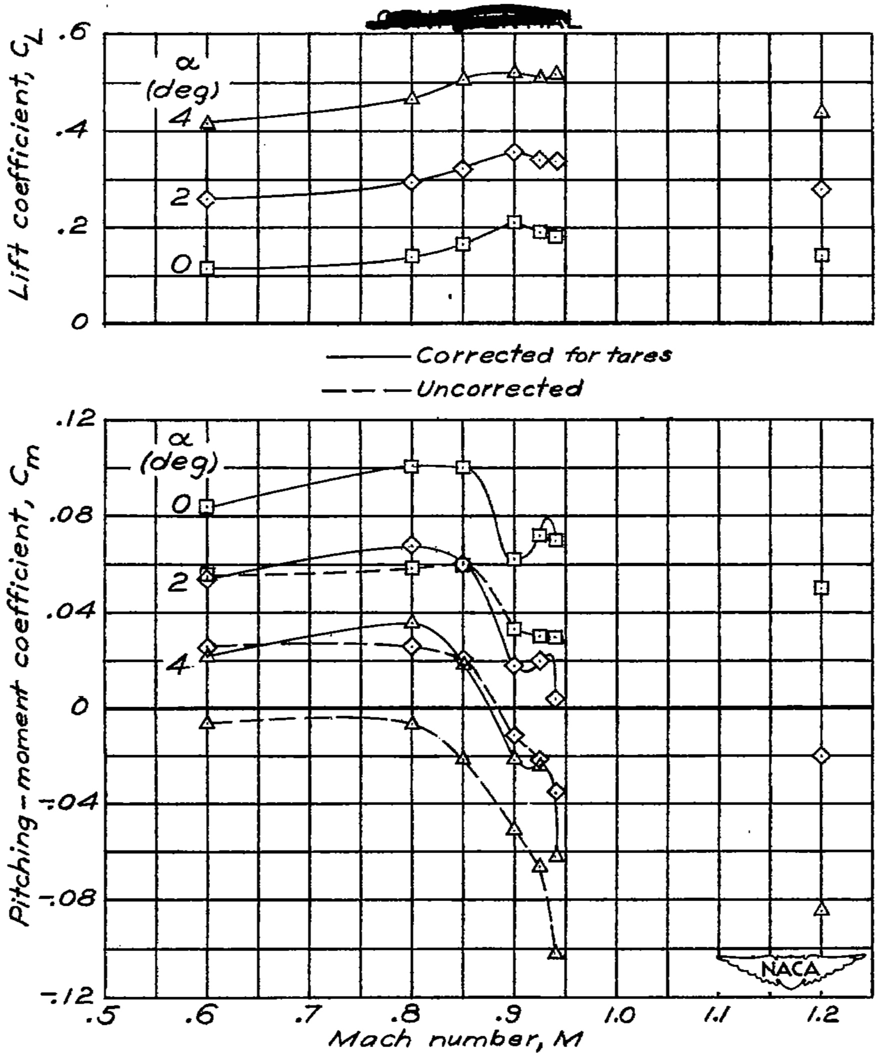

(l) Complete model; $i_t = 1.9^{\circ}$; $\delta_e = -6^{\circ}$.

Figure 10.– Continued.

[redacted]

[redacted]

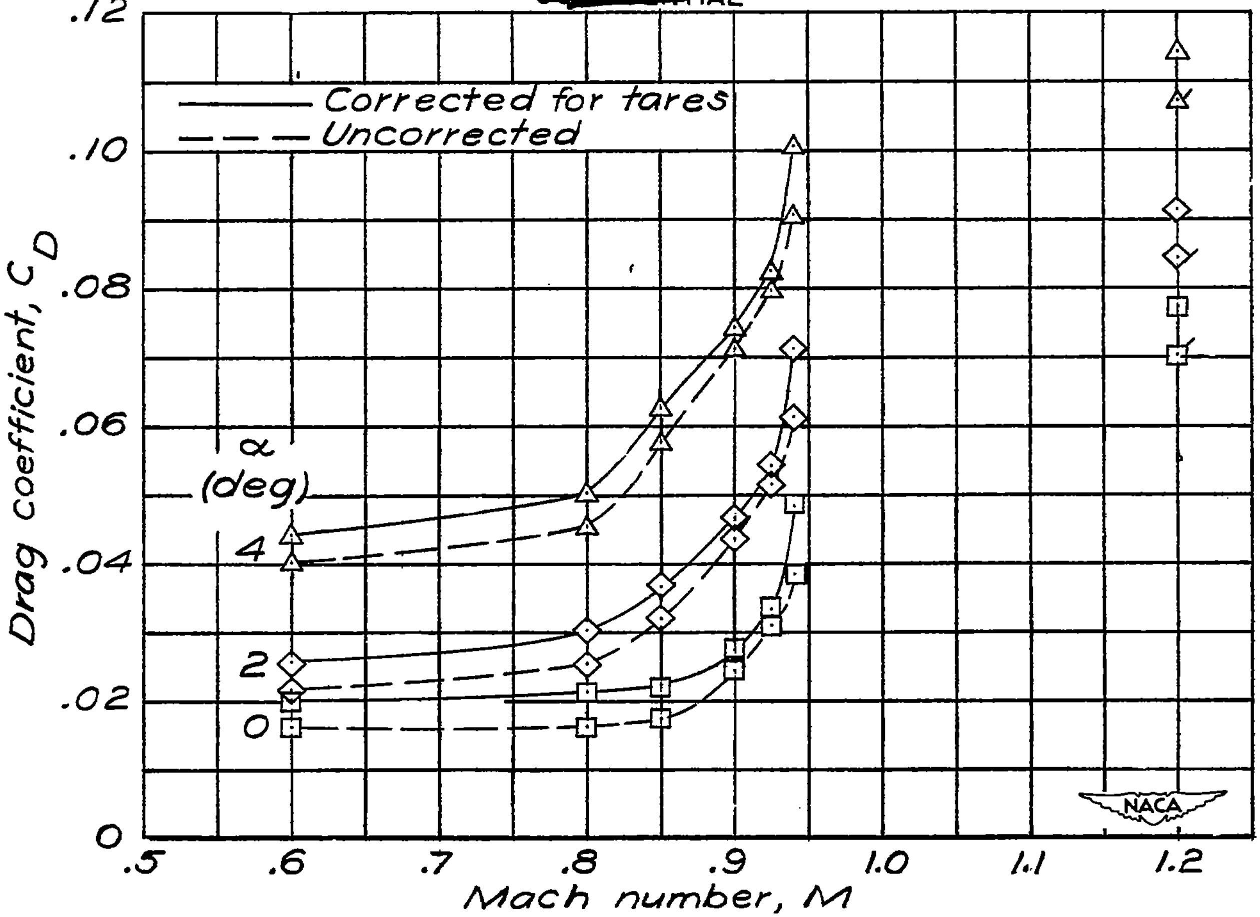

(*l*) Complete model; $i_t = 1.9^\circ$; $\delta_e = -6^\circ$. Concluded.

Figure 10.– Continued.

[redacted]

[redacted]

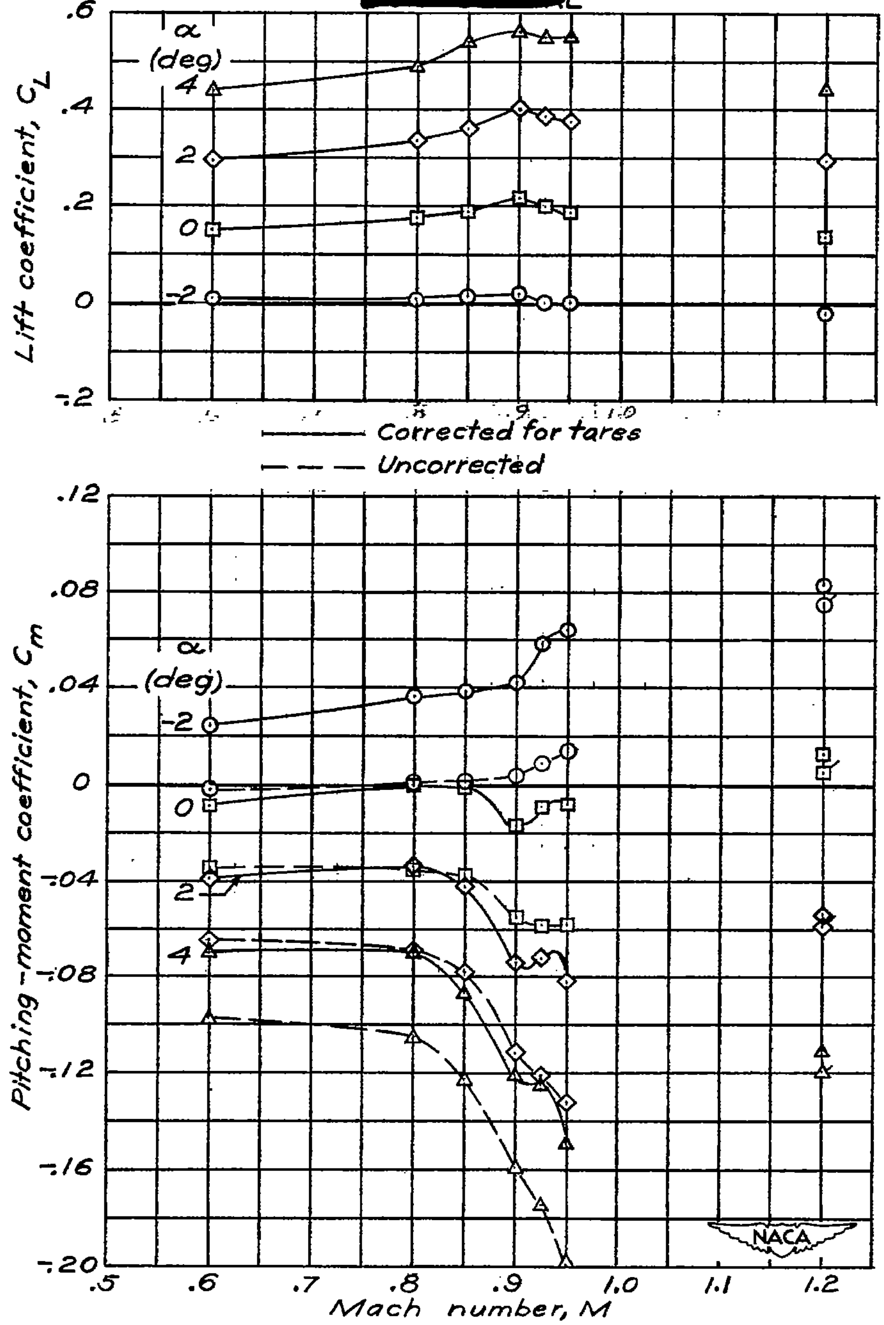

(m) Complete model and 0.68c fences; $i_t = 1.9^\circ$; $\delta_e = 0^\circ$.

Figure 10.– Continued.

[redacted]

[redacted]

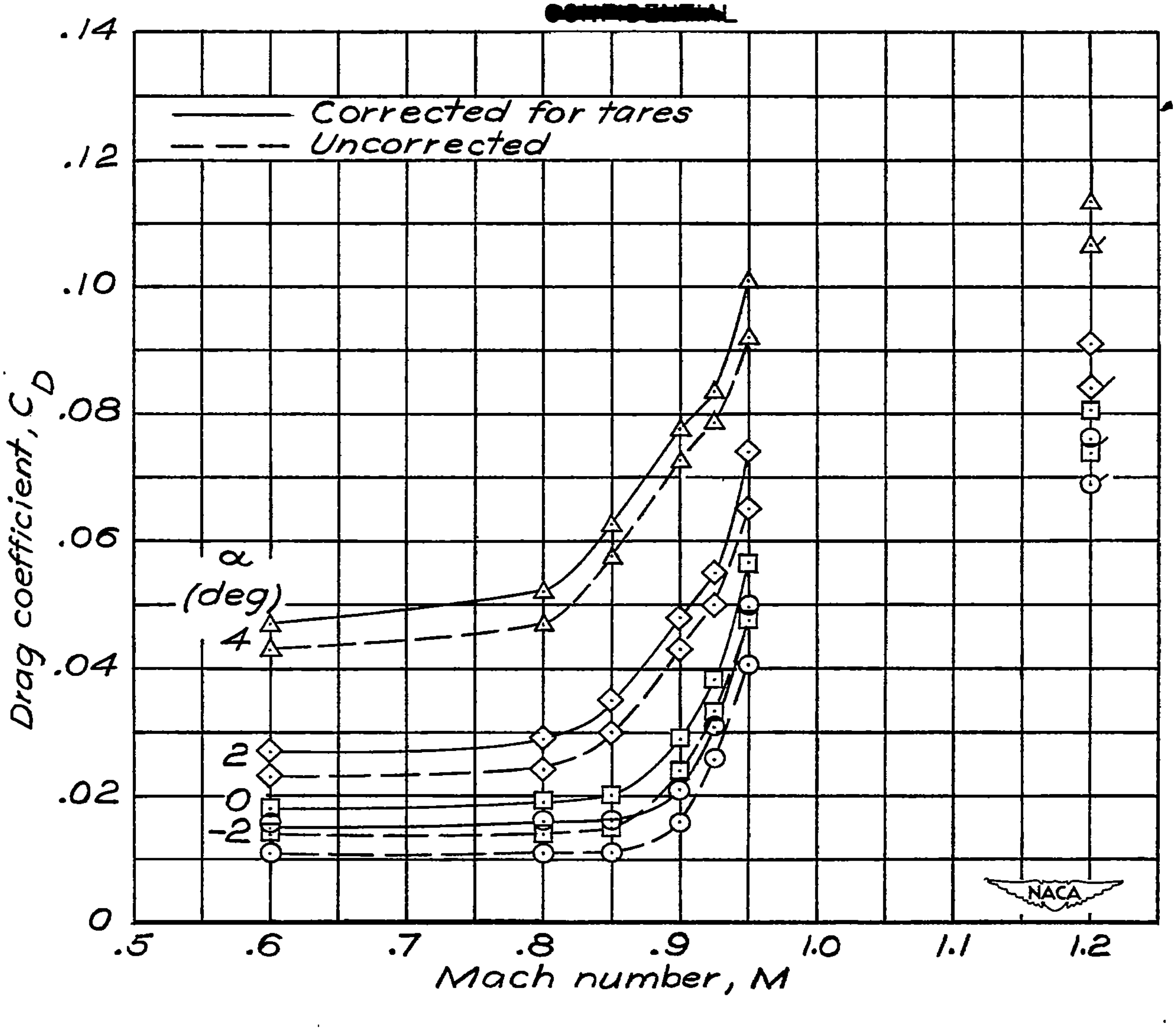

(m) Complete model and 0.68c fences; i_t = 1.9°; δ_e = 0°. Concluded.

Figure 10.– Continued.

[redacted]

[redacted]

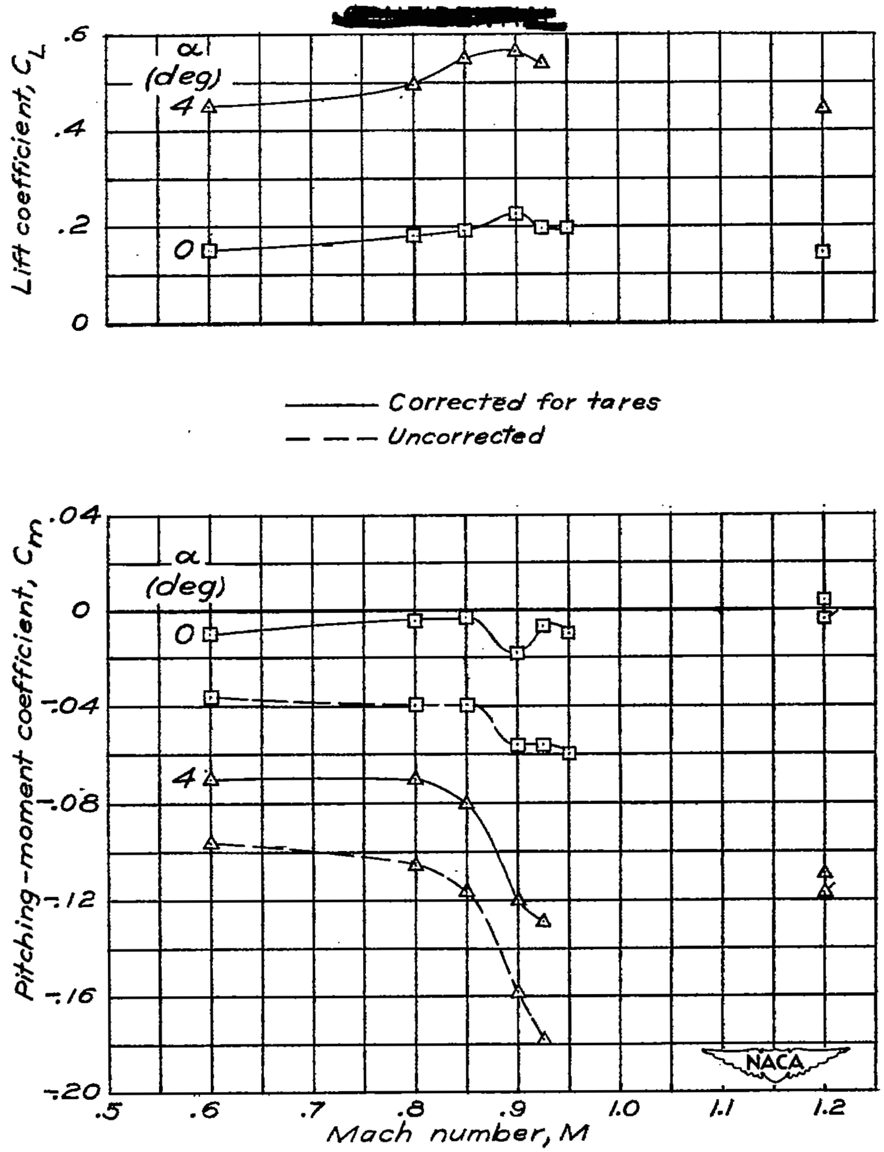

(n) Complete model and 0.95c fences; i_t = 1.9°; δ_e = 0°.

Figure 10.– Continued.

[redacted]

[redacted]

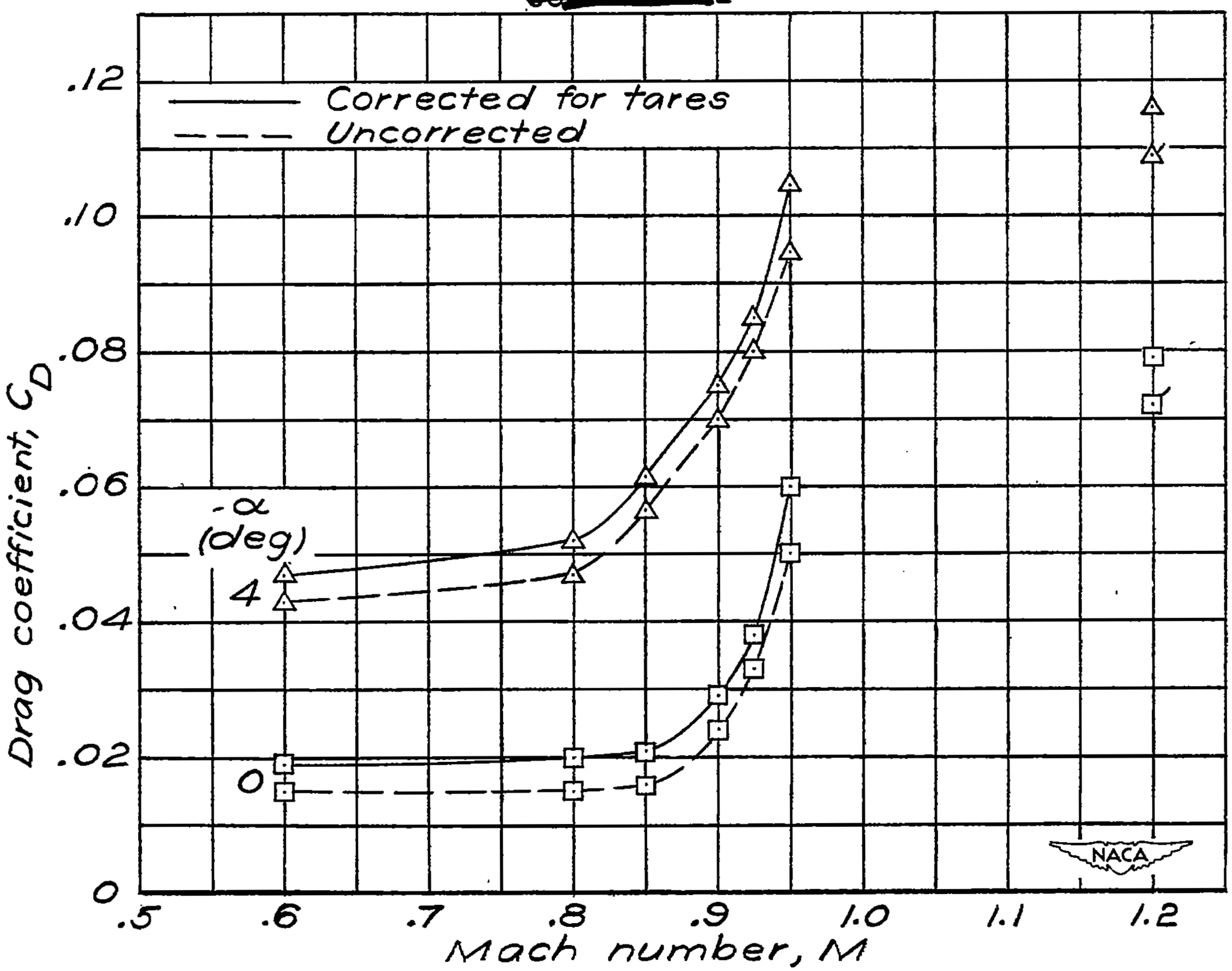

(n) Complete model and 0.95c fences; i_t = 1.9°; δ_e = 0°. Concluded.

Figure 10.— Concluded.

[redacted]

[redacted]

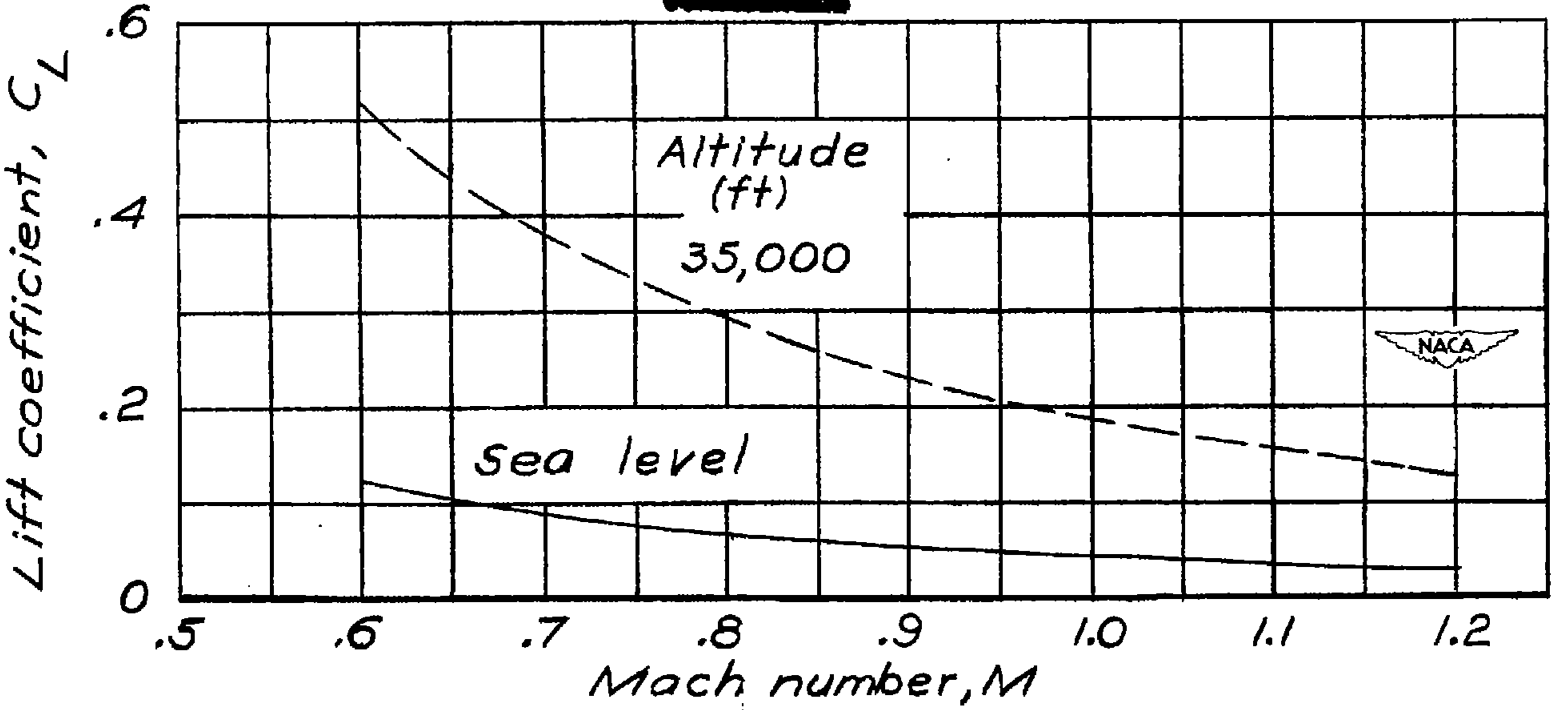

Figure 11.– Variation of lift coefficient required for level flight with Mach number for two altitude conditions with a wing loading of 65 pounds per square foot.

[redacted]

[redacted]

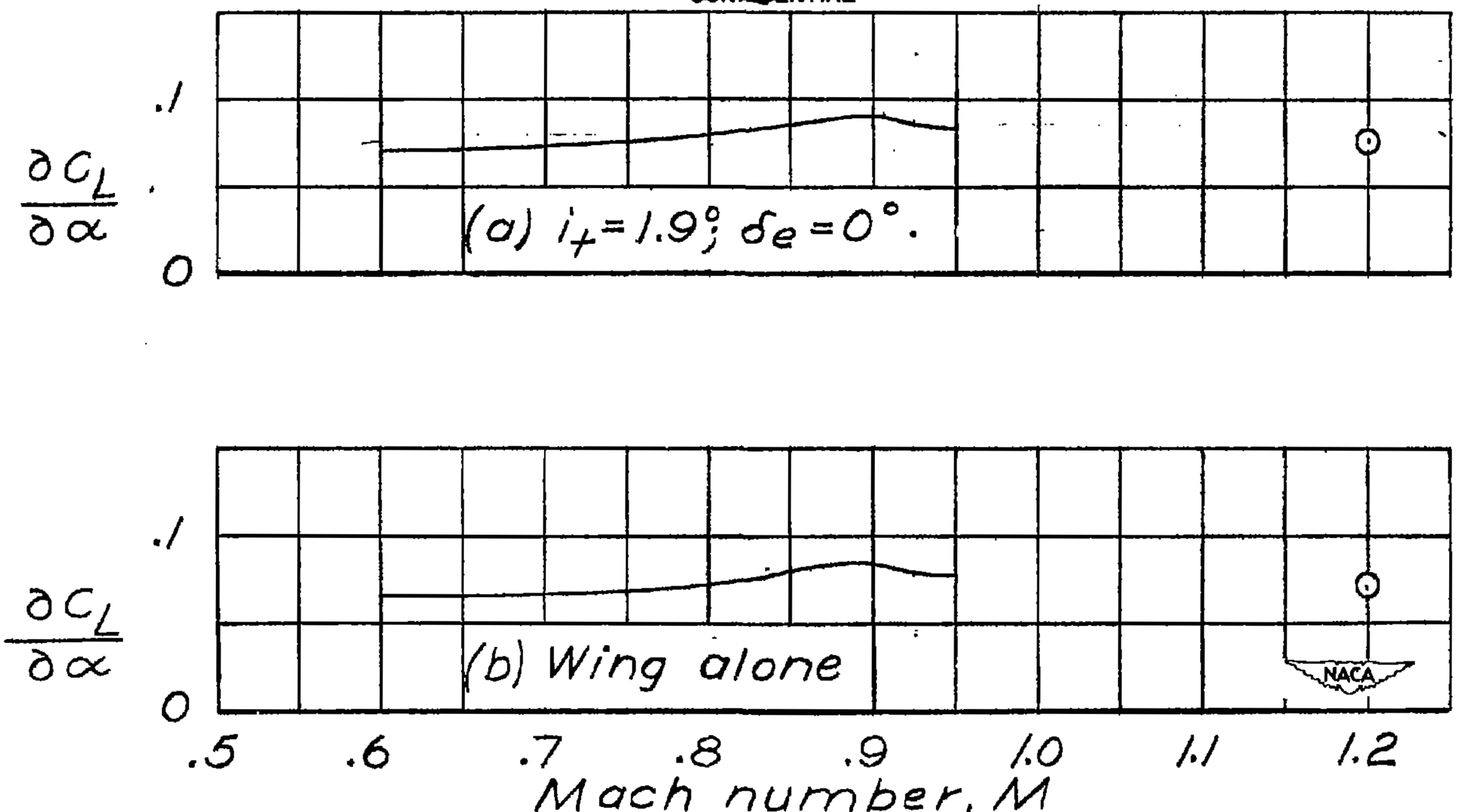

Figure 12.– Variation of slope of the lift curve $\partial C_L/\partial \alpha$ with Mach number. Complete model and wing alone.

[redacted]

[redacted]

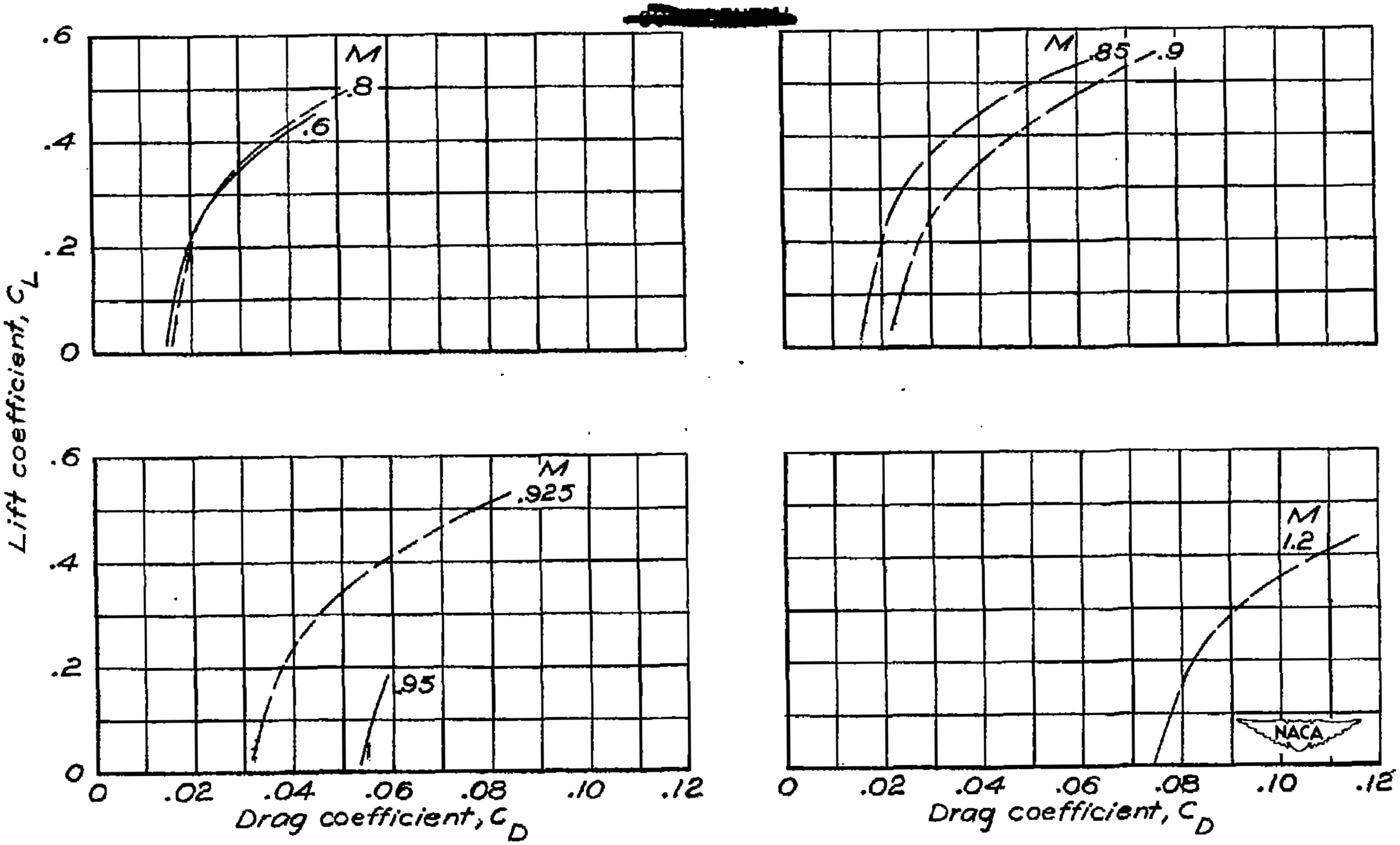

Figure 13.– Variation of lift coefficient with drag coefficient. Complete model; $i_t = 1.9^{\circ}$; $\delta_e = 0^{\circ}$.

[redacted]

[redacted]

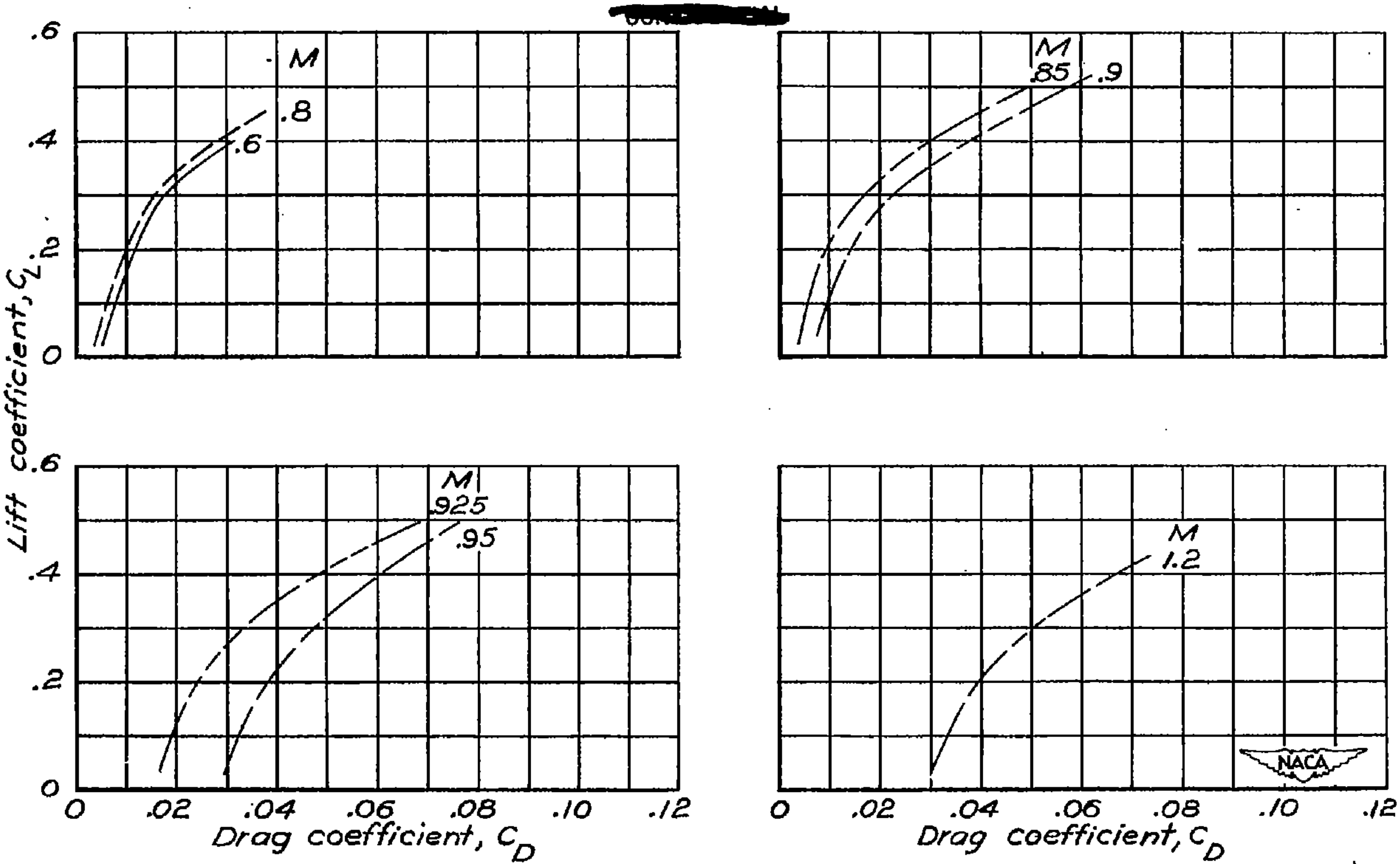

04

Figure 14.– Variation of lift coefficient with drag coefficient. Wing alone.

[redacted]

[redacted]

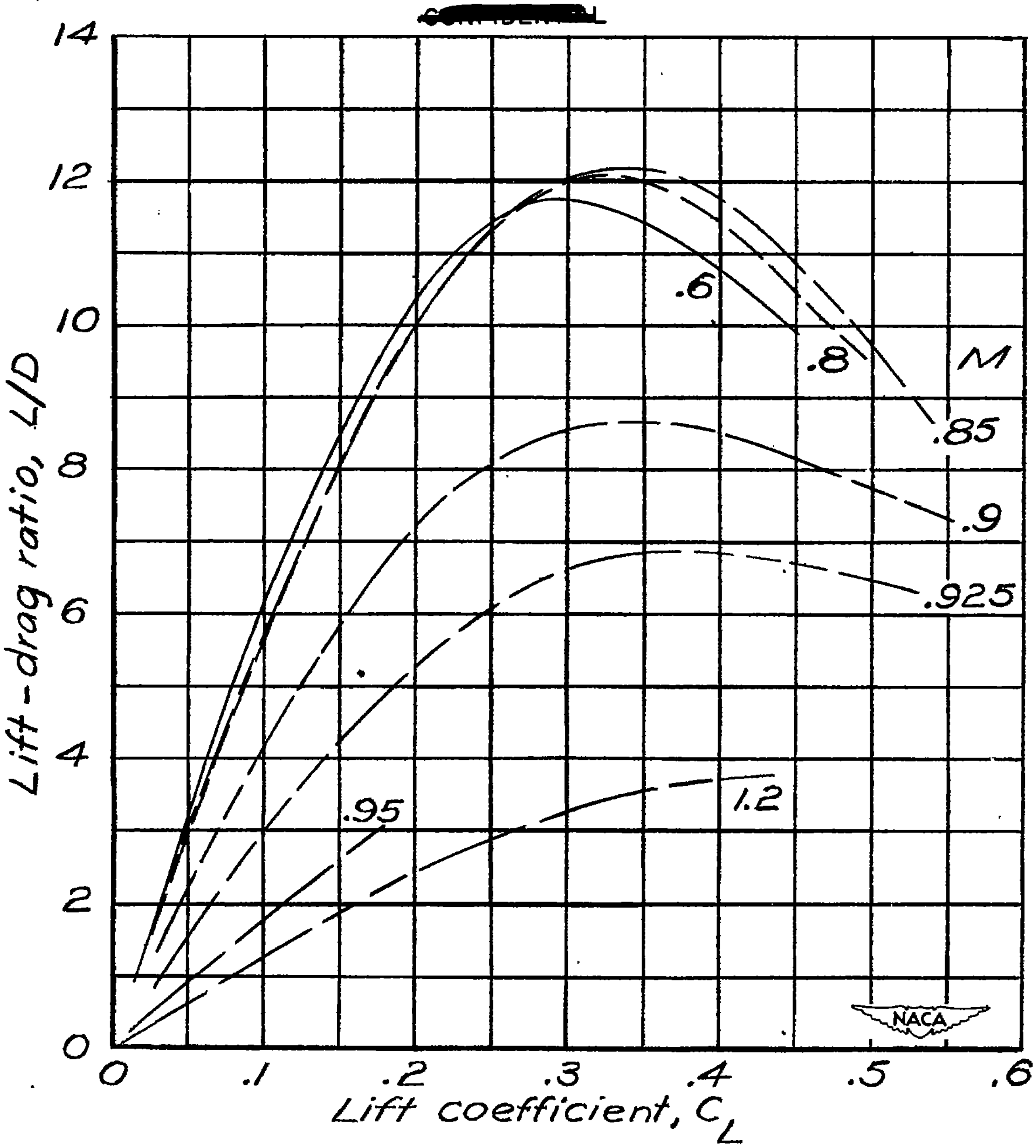

Figure 15.– Variation of lift-drag ratio with lift coefficient. Complete model; $i_t = 1.9^{\circ}$; $\delta_e = 0^{\circ}$.

[redacted]

[redacted]

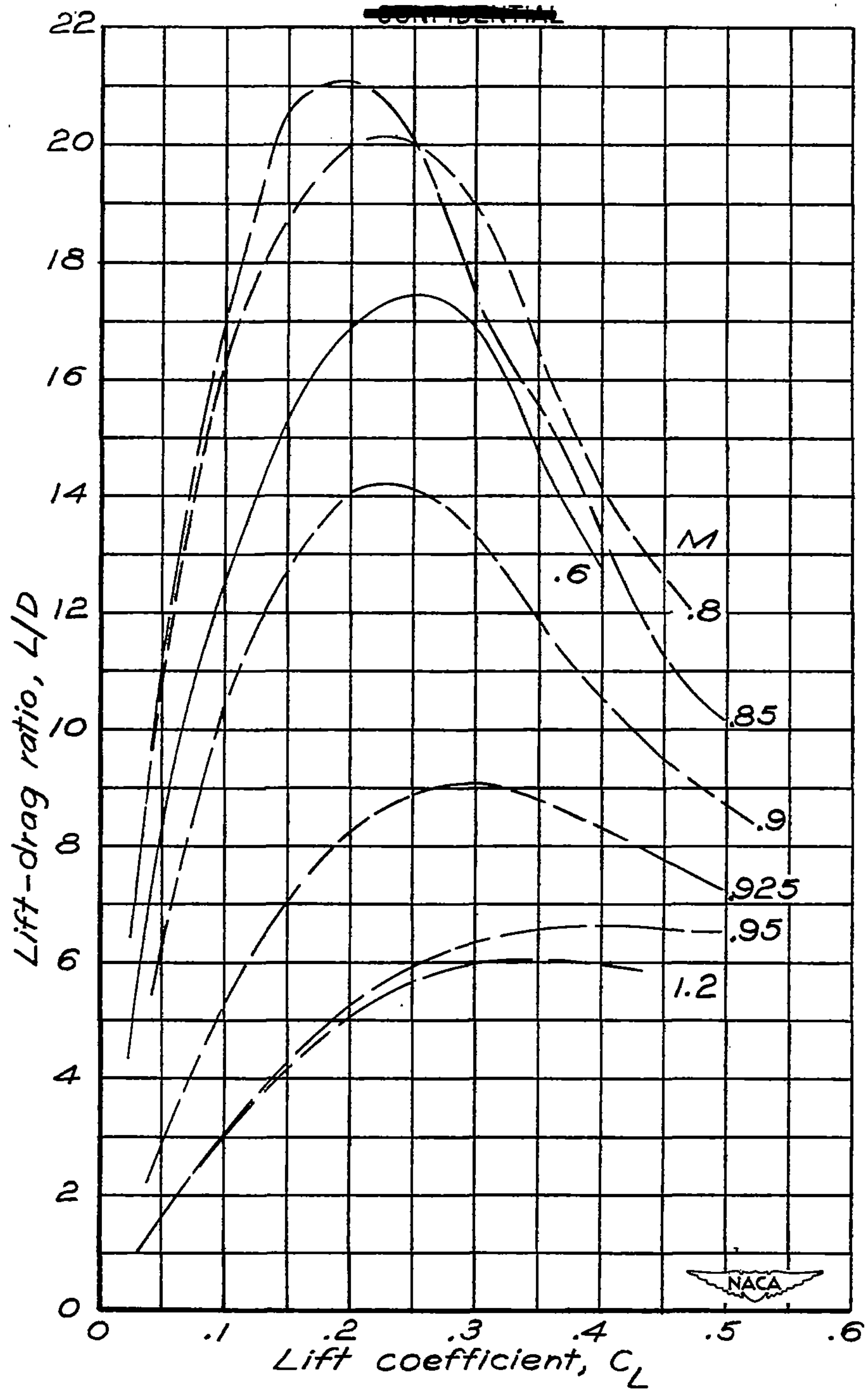

Figure 16.– Variation of lift-drag ratio with lift coefficient.
Wing alone.

[redacted]

[redacted]

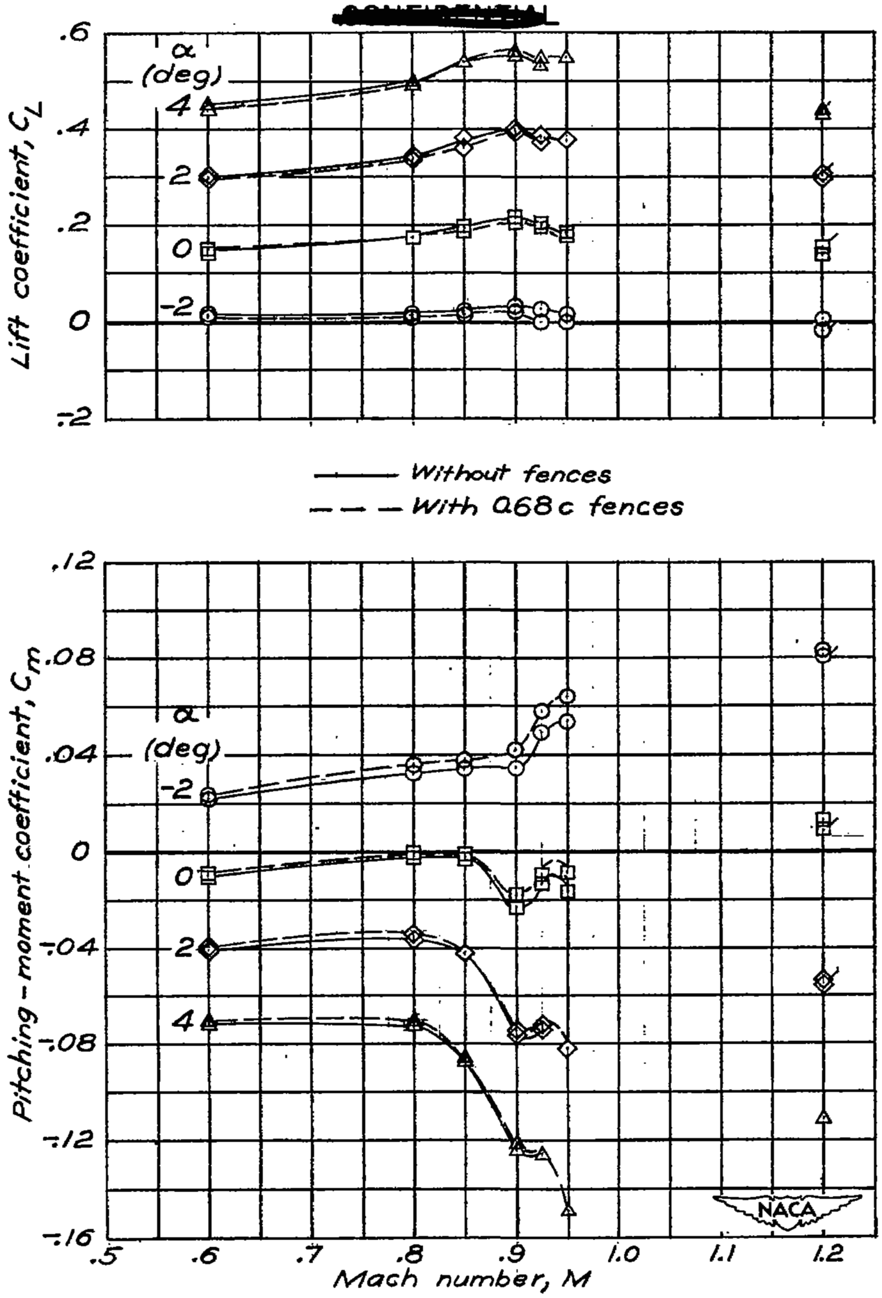

Figure 17.– Comparison of the variation of lift coefficient, pitching-moment coefficient, and drag coefficient with Mach number. With and without 0.68c fences; $i_t = 1.9^{\circ}$; $\delta_e = 0^{\circ}$. (Plain symbols at M = 1.2 refer to data without fences, and flagged symbols refer to data with fences.)

[redacted]

~~CONFIDENTIAL~~

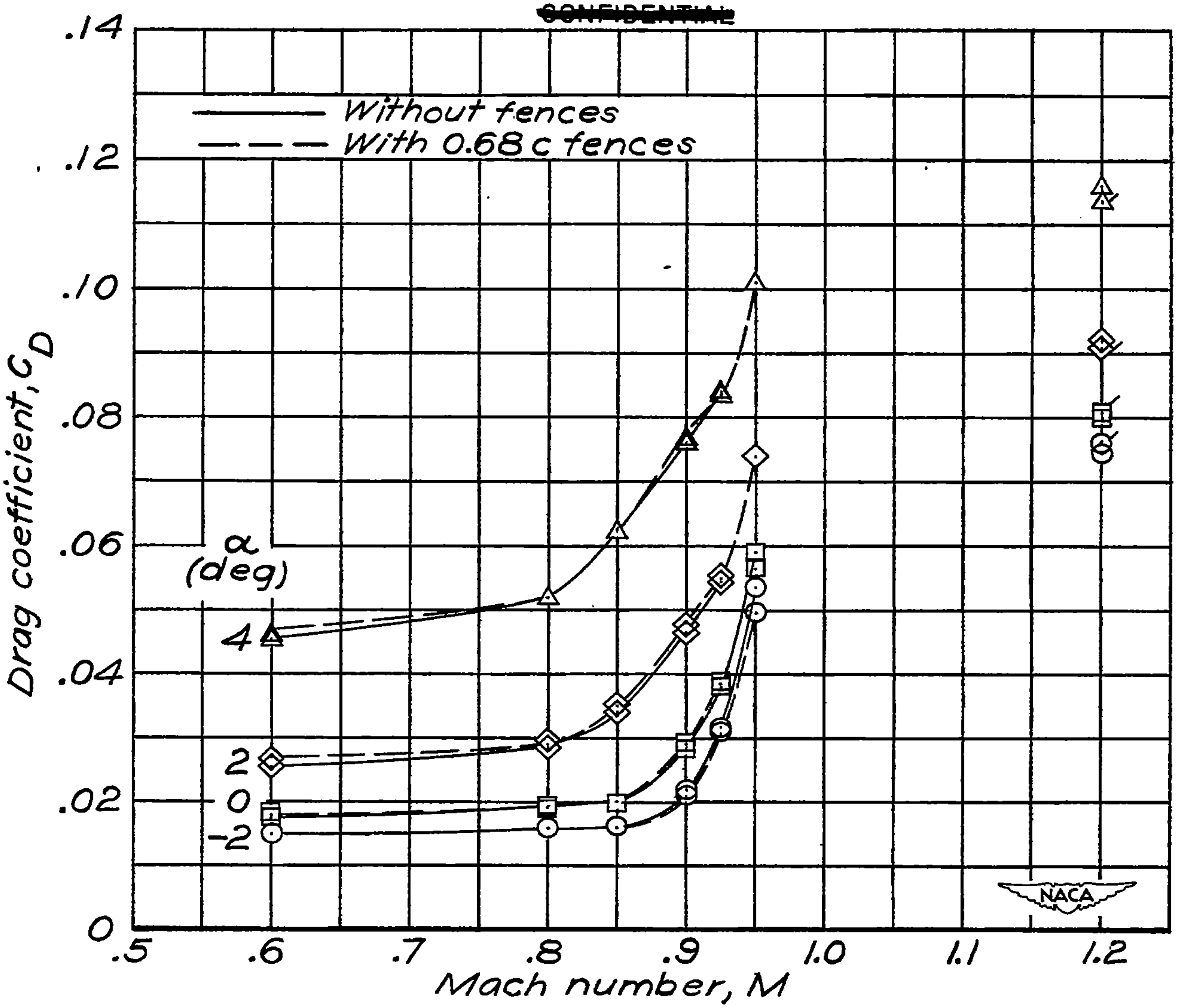

Figure 17.– Concluded.

[redacted]

[redacted]

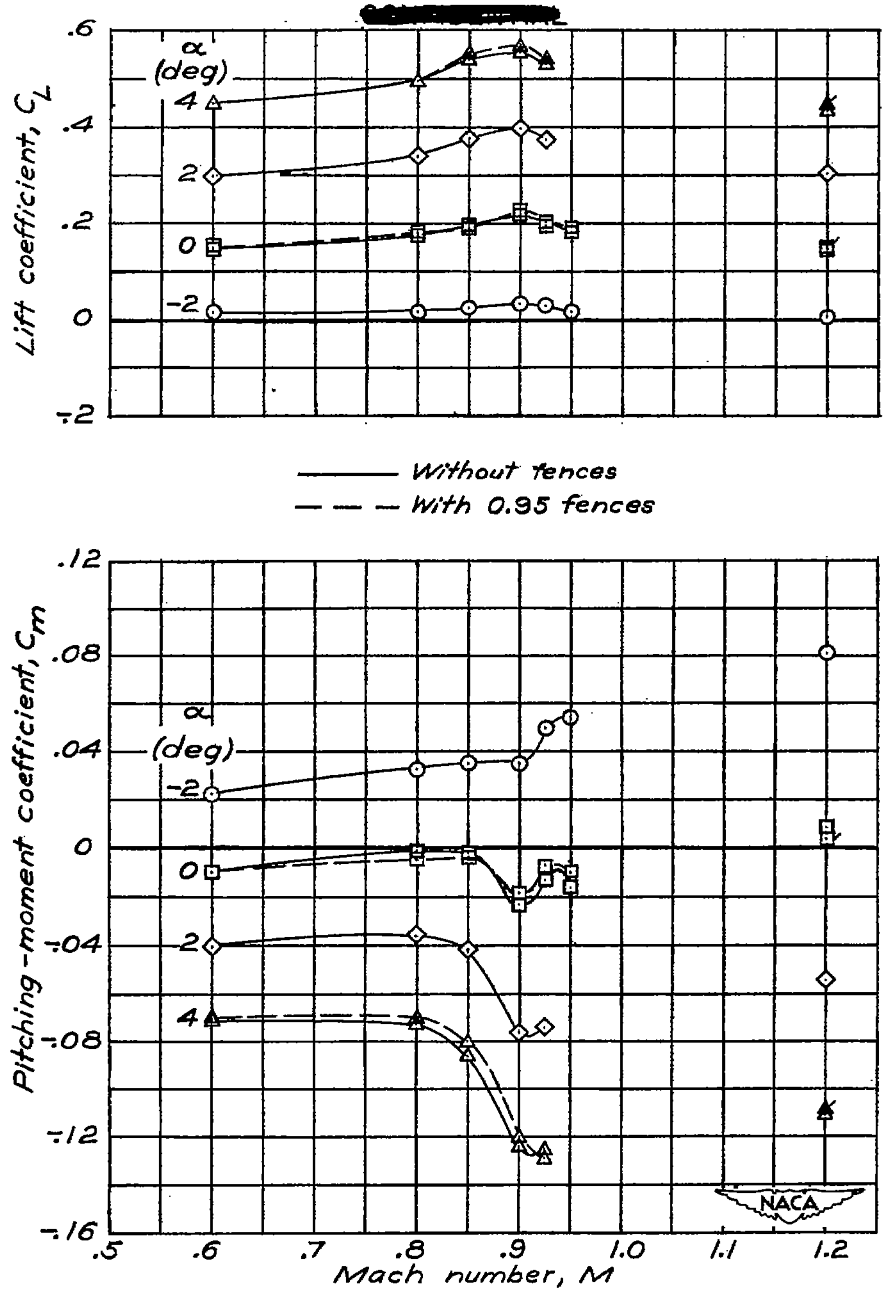

Figure 18.– Comparison of the variation of lift coefficient, pitching-moment coefficient, and drag coefficient with Mach number. With and without 0.95c fences; $i_t = 1.9^\circ$; $\delta_e = 0^\circ$. (Plain symbols at M = 1.2 refer to data without fences, and flagged symbols refer to data with fences.) [redacted]

[redacted]

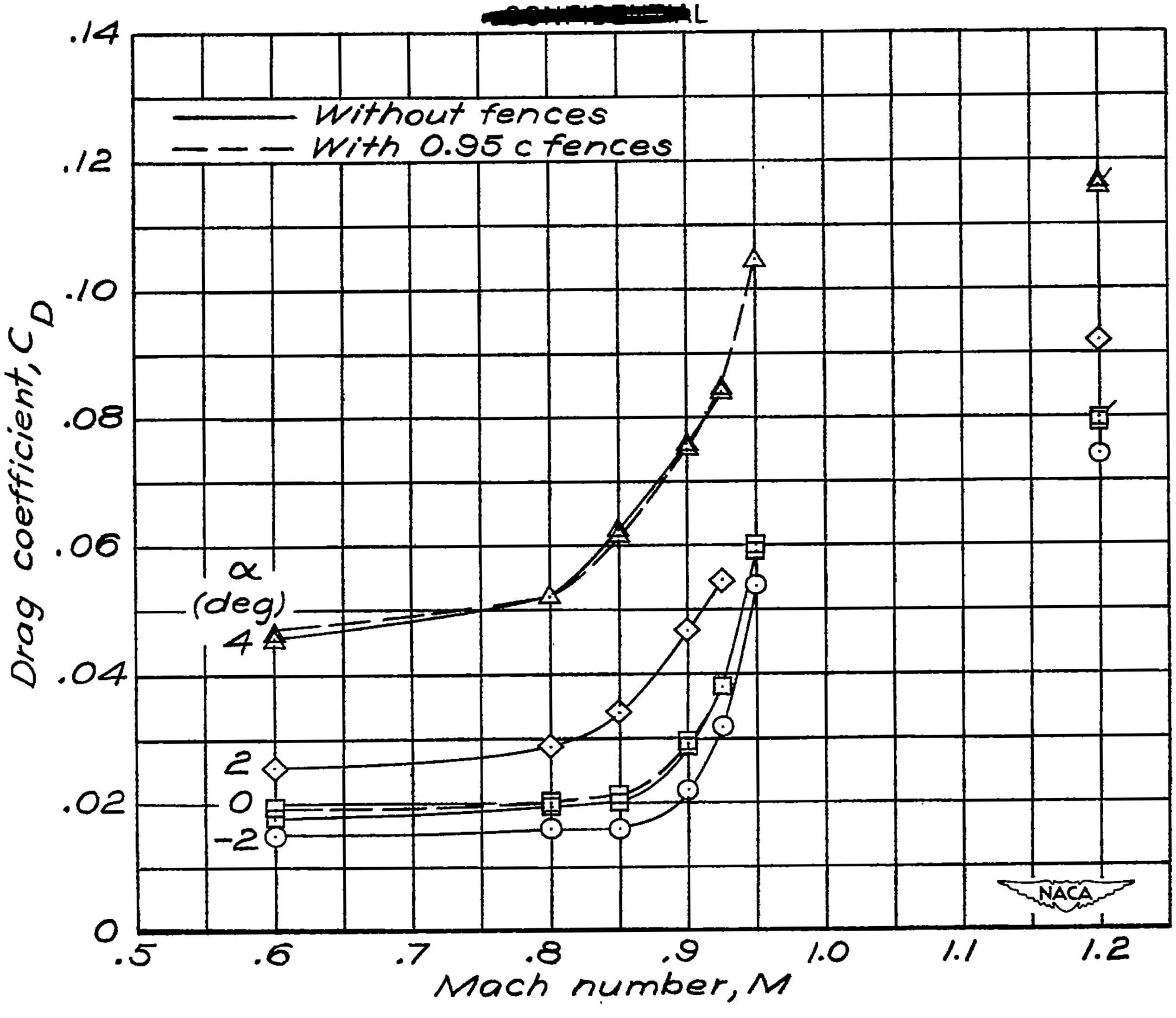

Figure 18.– Concluded.

[redacted]

[redacted]

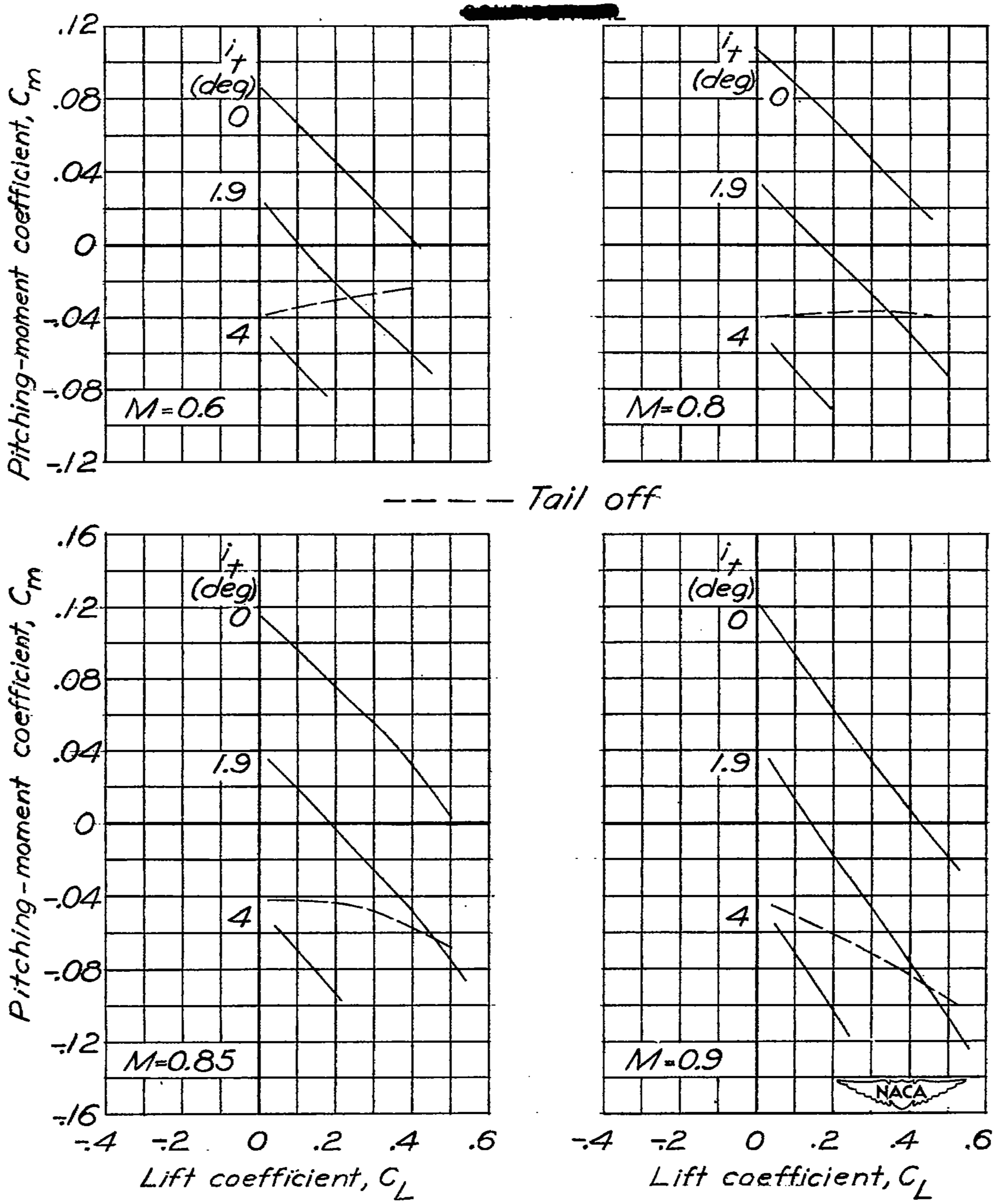

Figure 19.– Variation of pitching-moment coefficient with lift coefficient for various horizontal stabilizer angles. Complete model; $\delta_e = 0^\circ$.

[redacted]

[redacted]

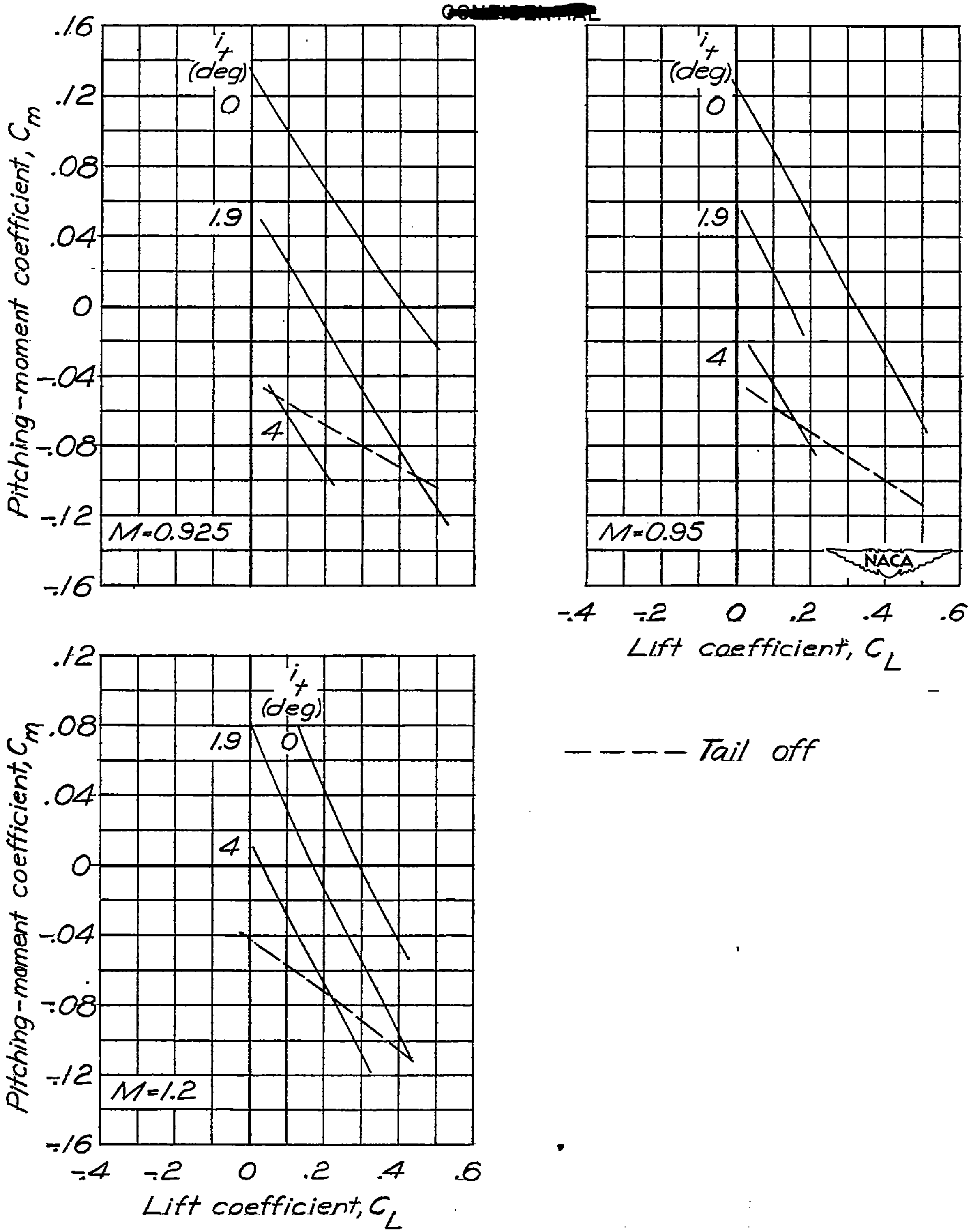

Figure 19.– Concluded.

[redacted]

[redacted]

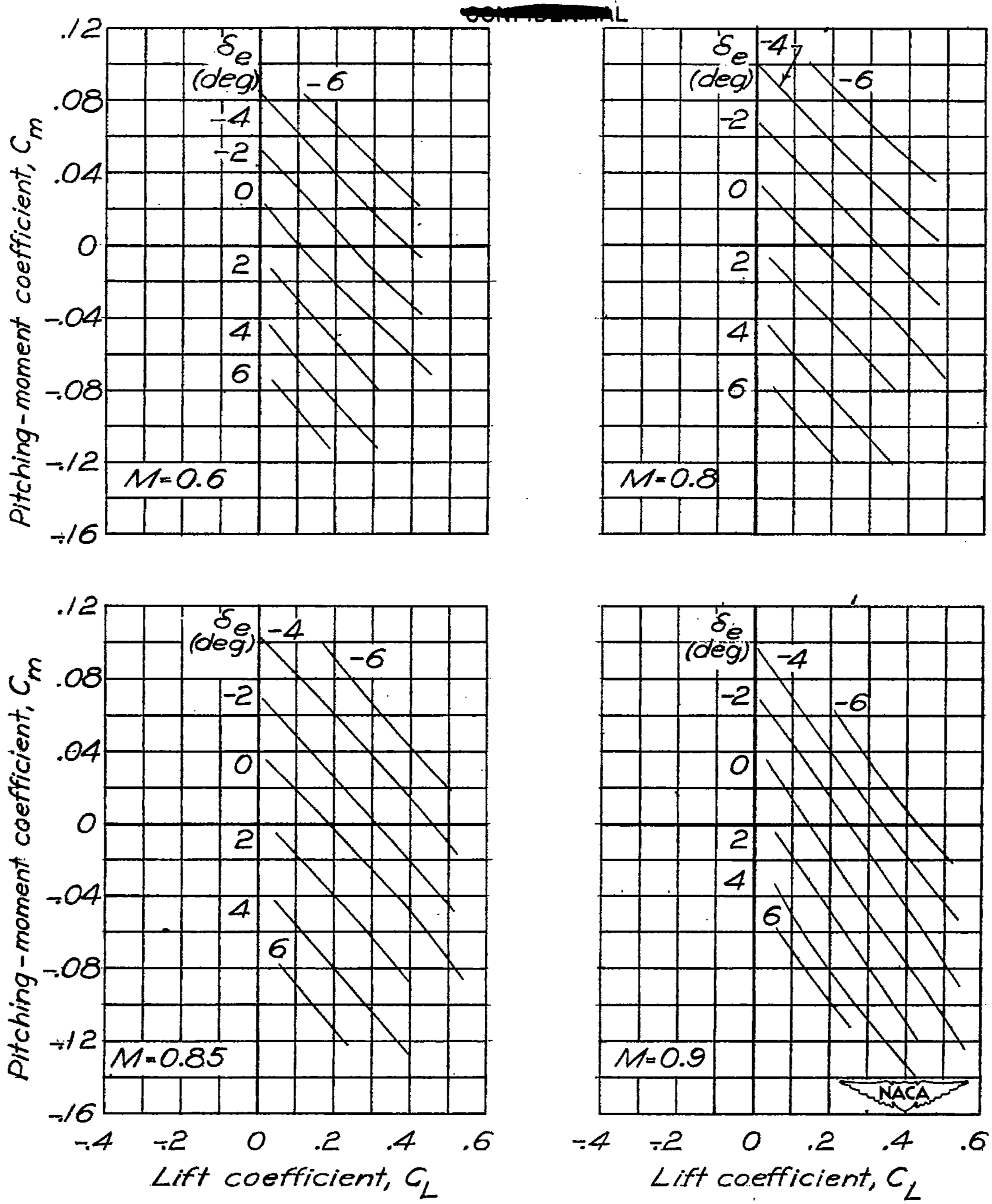

Figure 20.– Variation of pitching-moment coefficient with lift coefficient for various elevator angles. Complete model; $i_t = 1.9^\circ$.

[redacted]

[redacted]

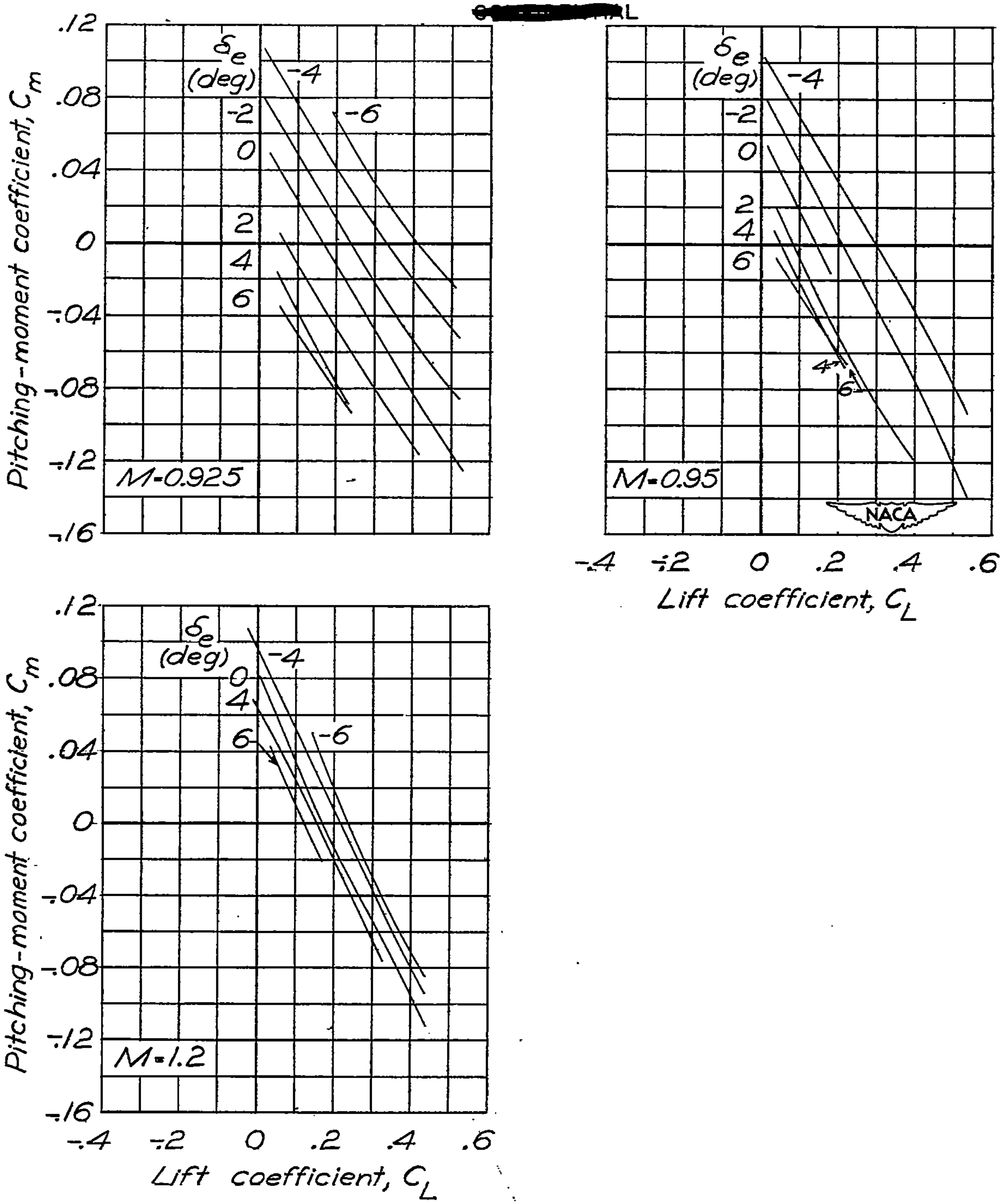

Figure 20.- Concluded.

~~CONFIDENTIAL~~

Cg. 20.2
21
41.2=8

[redacted]

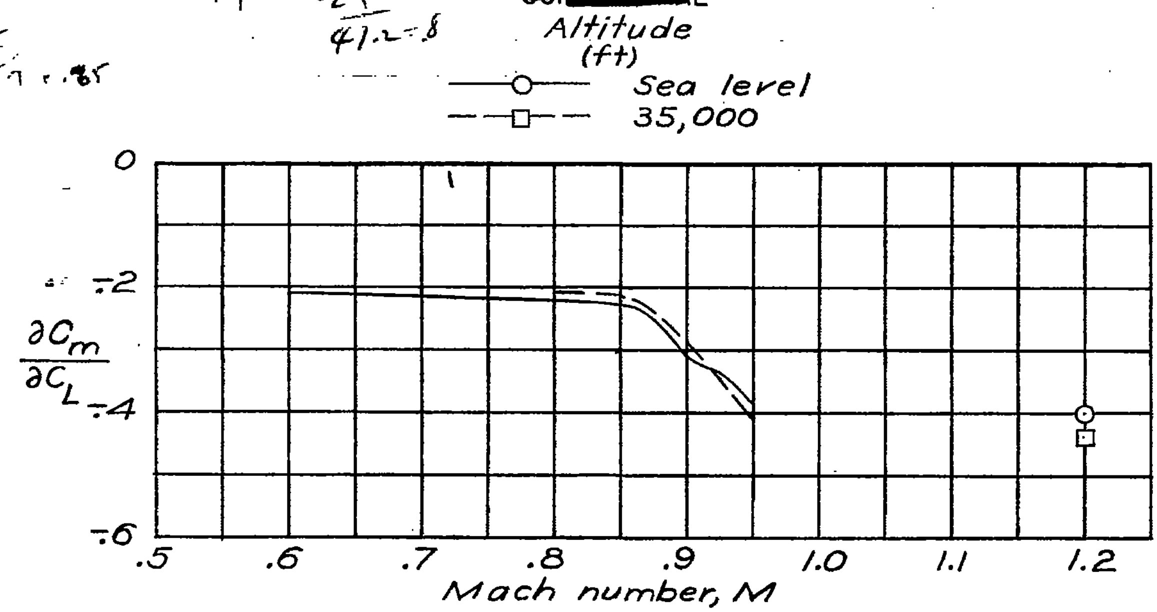

(a) Complete model at trim conditions; $\delta_e = 0^{\circ}$.

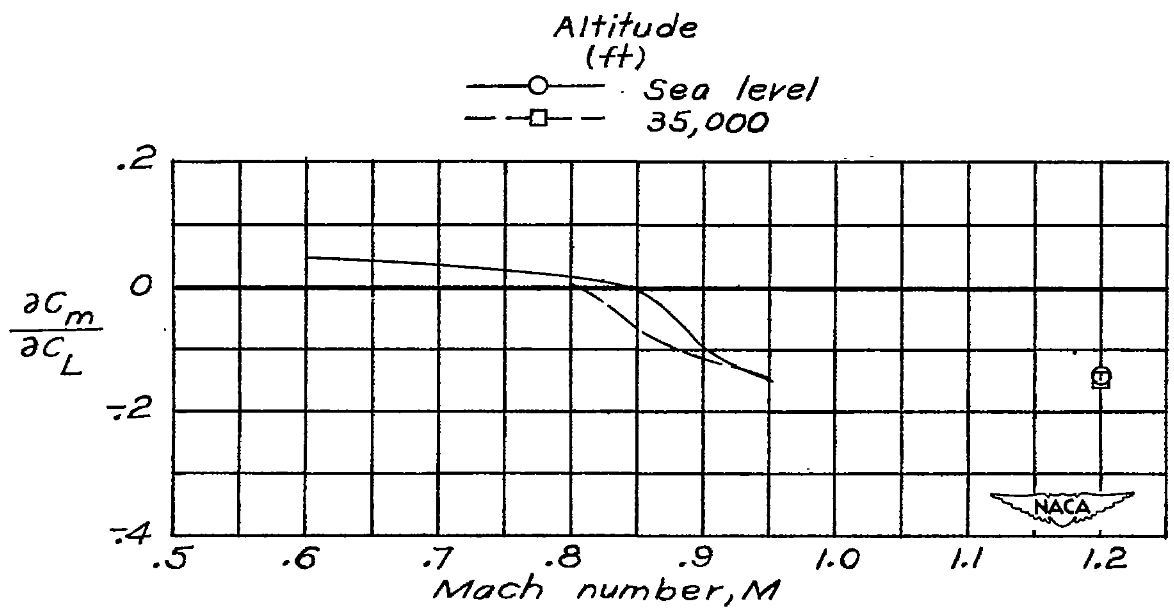

(b) Fuselage, fin, and wing.

Figure 21.- Variation of static-longitudinal-stability parameter $\frac{\partial C_m}{\partial C_L}$ with Mach number for level flight at two altitudes.

[redacted]

[redacted]

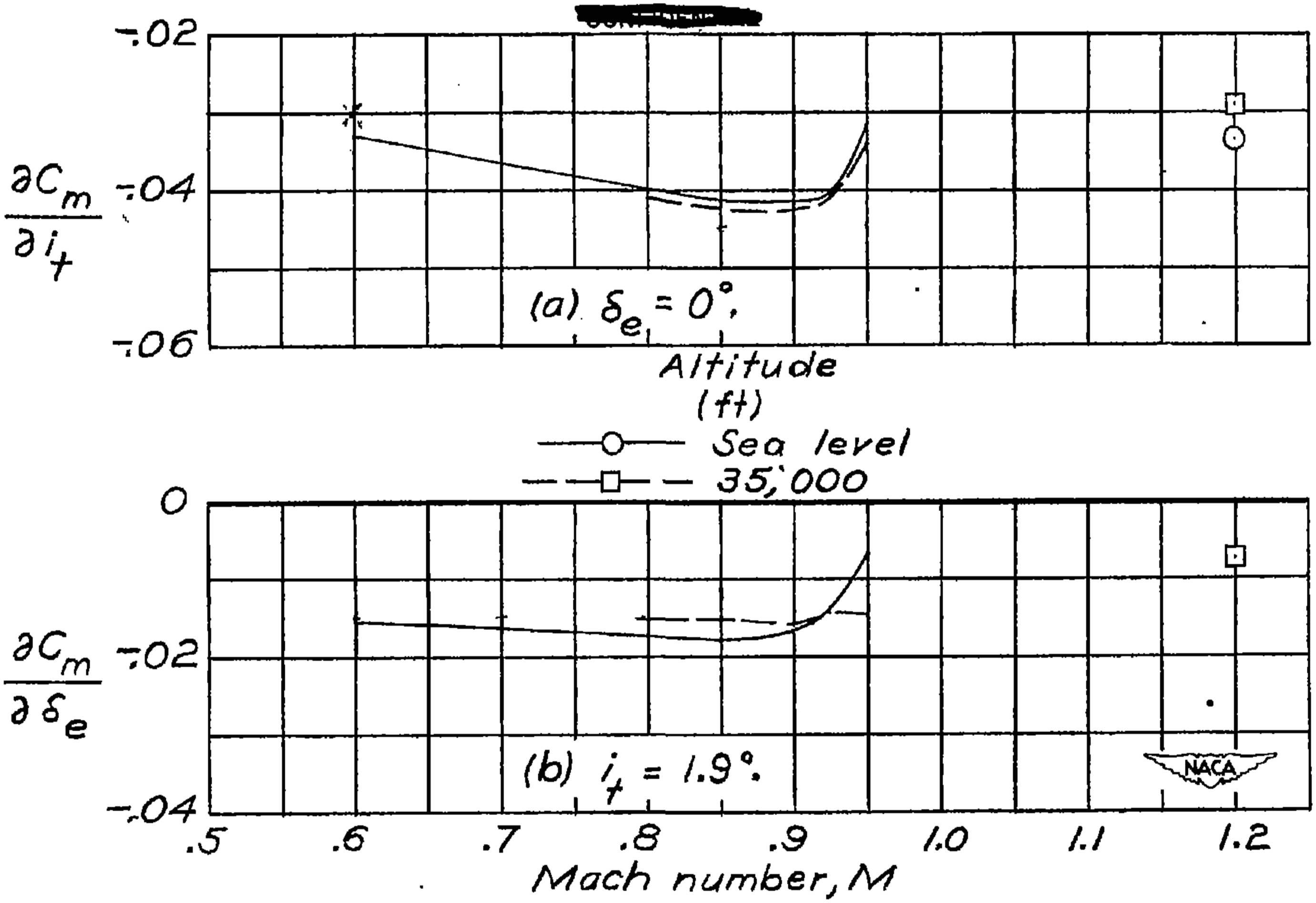

Figure 22.- Variation of horizontal-stabilizer effectiveness $\frac{\partial C_m}{\partial i_t}$ and elevator effectiveness $\frac{\partial C_m}{\partial \delta_e}$ with Mach number for level-flight trim conditions at two altitudes. Complete model.

[redacted]

[redacted]

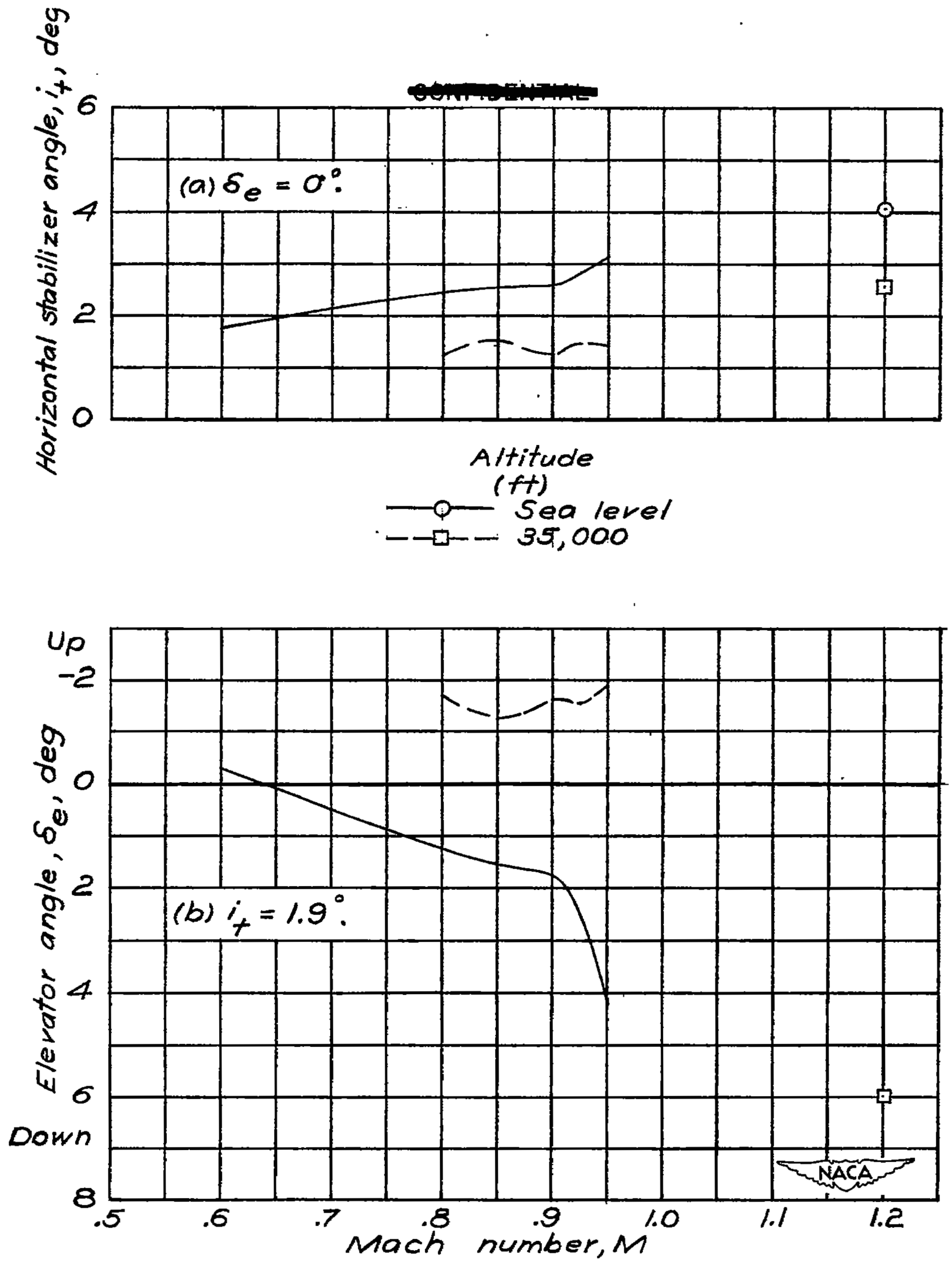

Figure 23.– Variation of the horizontal stabilizer and elevator settings required with Mach number for level-flight trim conditions at two altitudes. Complete model.

[redacted]

[redacted]

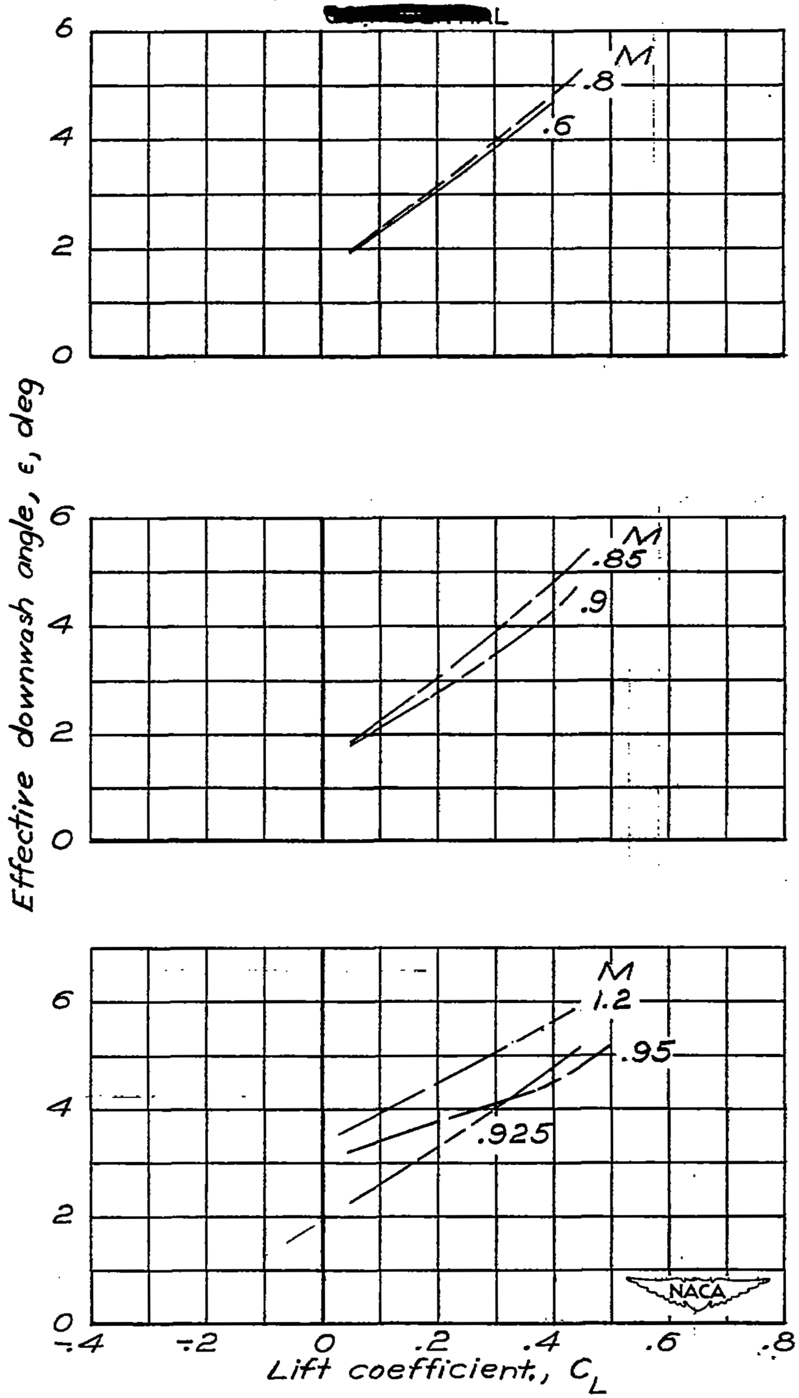

Figure 24.- Variation of effective downwash angle with lift coefficient. Complete model; $\delta_e = 0^{\circ}$.

[redacted]

[redacted]

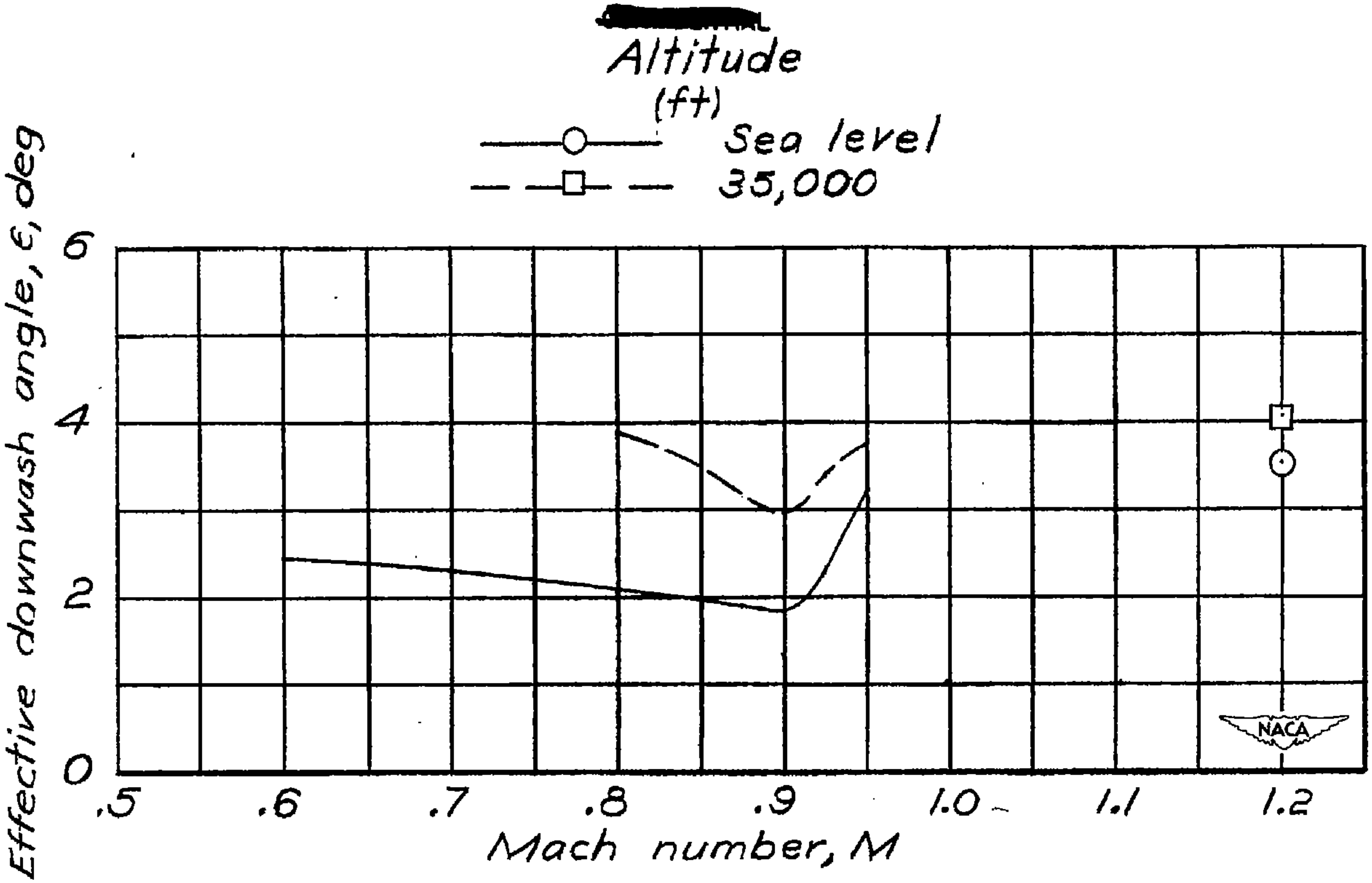

Figure 25.– Variation of effective downwash angle with Mach number for level flight at two altitudes. Complete model; $\delta_e = 0^\circ$.

[redacted]

[redacted]

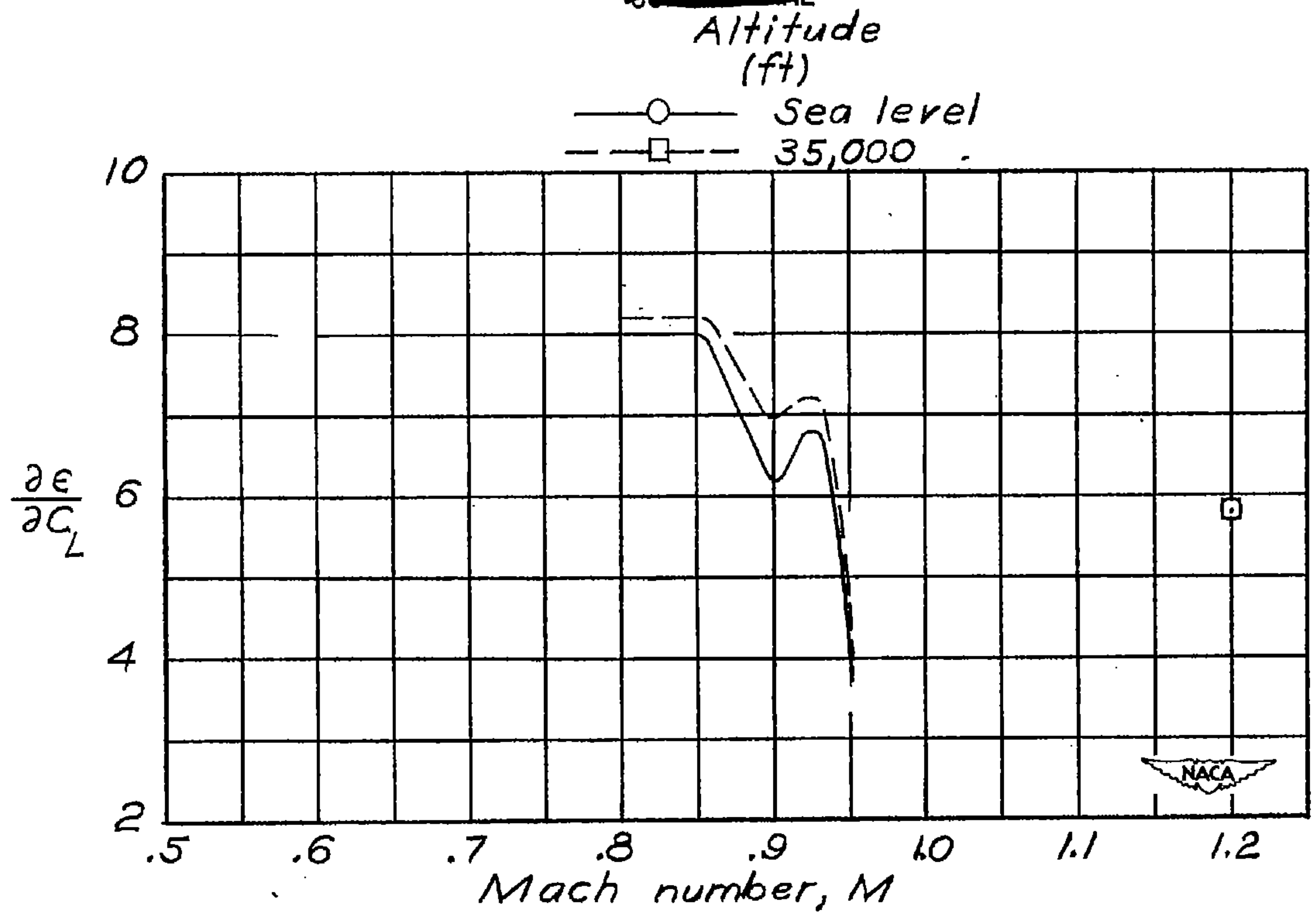

Figure 26.– Variation with Mach number of the rate of change of effective downwash angle with lift coefficient $\frac{\partial \epsilon}{\partial C_L}$ for level flight at two altitudes. Complete model; $\delta_e = 0^{\circ}$.

[redacted]